

**DYNAMIC PHASOR MODELING OF DOUBLY-FED INDUCTION MACHINES
INCLUDING SATURATION EFFECTS OF MAIN FLUX LINKAGE**

by

Benjamin Braconnier

B.Sc., The University of Alberta, 2009

A THESIS SUBMITTED IN PARTIAL FULFILLMENT OF
THE REQUIREMENTS FOR THE DEGREE OF

MASTER OF APPLIED SCIENCE

in

THE FACULTY OF GRADUATE STUDIES

(Electrical and Computer Engineering)

THE UNIVERSITY OF BRITISH COLUMBIA

(Vancouver)

September 2012

© Benjamin Braconnier, 2012

Abstract

Power system simulation has become an integral part of power system planning, design and study today. Due to the vast array of power system disturbances that occur and the speed of their respective dynamics, simulation tools have traditionally been split into two types; Transient Stability type programs (TSP) which generally make simplifying assumptions to simulate longer electromechanical transients and Electromagnetic Transient type programs (EMTP) which require much greater detail in their models as they are generally used to simulate much faster transients that occur during electromagnetic disturbances. Several papers have been written and solutions have been proposed to come up with a solution that would combine these two different types of programs into one simulation tool that can be used to simulate both the slow electromechanical transients and fast electromagnetic transients that occur on power systems. One such method that has been proposed and is being thoroughly studied and showing promising potential for unified power system simulation is the concept of dynamic phasors. The dynamic phasor concept extends the traditional concept of steady state phasor representation used extensively in TSP programs by allowing these phasor quantities to change with time during transient events.

This thesis focuses on the modeling of induction machines using the dynamic phasor concept. The induction machine is chosen as it represents a significant portion of power system loads and therefore plays an important role in power system stability and behavior. Several induction machine models have already been proposed using the dynamic phasor concept however none of which take into account the effects of saturation that often occurs

during induction machine operation. This thesis therefore focuses specifically on modeling the effects of main flux linkage saturation in induction machines using the concept of dynamic phasors. The proposed model is based on the flux correction method and extends this concept to representation in dynamic phasor quantities. This is done by first verifying the consistency of the unsaturated dynamic phasor induction machine model against well known conventional models and then implementing the proposed dynamic phasor saturation model and again verifying it's consistency with conventional saturation model of the induction machine. The results obtained in this thesis show that the proposed saturation model using the dynamic phasor concept is consistent with conventional saturation models with reasonable accuracy and efficiency and therefore provides a good starting point for further research in machine saturation modeling using the dynamic phasor concept.

Table of Contents

Abstract.....	ii
Table of Contents	iv
List of Tables	vi
List of Figures.....	vii
Acknowledgements	x
Dedication	xi
Chapter 1: Introduction	1
1.1 Background	1
1.2 Thesis Motivation	6
1.3 Thesis Outline	8
Chapter 2: Dynamic Phasor Analysis	10
2.1 Concept and Definition	10
2.1.1 Single Phase Systems.....	10
2.1.2 Polyphase Systems.....	13
2.2 Dynamic Phasors and Complex Space Vectors	17
2.2.1 Complex Space Vector Representation of 3-Phase Variables	17
2.2.2 Dynamic Phasor Representation of Complex Space Vectors	20
Chapter 3: Induction Machine Modeling Based on Dynamic Phasors.....	22
3.1 Time Domain Model of Doubly-Fed Induction Machine.....	22
3.1.1 abc Phase Model of Doubly-Fed Induction Machine	22
3.1.2 $qd0$ Model of Doubly-Fed Induction Machine	25

3.1.3	Complex Vector Model of Doubly-Fed Induction Machine.....	31
3.2	Dynamic Phasor Model of Doubly-Fed Induction Machine.....	34
3.3	Model Verification.....	40
3.3.1	Free Acceleration of Induction Machine	41
3.3.2	Mechanical Torque Change	43
3.3.3	Balanced 3-phase Voltage Dip.....	46
3.3.4	Unbalanced Single Line-to-Ground Fault.....	48
Chapter 4:	Modeling of Saturation in Induction Machines.....	56
4.1	Time Domain Modeling of Induction Machine Saturation.....	56
4.2	Dynamic Phasors Model of Induction Machine Saturation.....	59
4.3	Saturation Model Verification	62
Chapter 5:	Induction Machine Dynamic Phasor Model Performance	70
5.1	Fixed Time-Step Model Performance	70
5.2	Variable Time-Step Model Performance	83
Chapter 6:	Conclusion.....	89
6.1	Summary of Contributions.....	89
6.2	Future Research	90
References.....		94
Appendices.....		102
Appendix A -	500 HP Induction Machine Parameters	102
Appendix B -	Saturation Data of 500 HP Induction Machine	103

List of Tables

Table 3.1	Maximum error introduced by dynamic phasor model	55
Table 4.1	Maximum error introduced by saturated dynamic phasor model	67
Table 5.1	CPU times for test case simulation	82
Table 5.2	Model performance using variable time-step solver.....	88
Table A.1	500hp induction machine parameters [49].....	102
Table B.1	Saturation data for 500hp induction machine [59].....	103

List of Figures

Figure 1.1 General time-frame for power system disturbances	2
Figure 2.1 Illustration of “sliding” window of periodicity	11
Figure 2.2 Resolution of unbalanced 3-phase quantities into balanced sequence components	14
Figure 2.3 Illustration of the rotating complex space vector	18
Figure 2.4 Representation of rotating complex phasor	21
Figure 3.1 Illustration of the magnetic axis of a 2-pole induction machine	22
Figure 3.2 $qd0$ magnetic axis	26
Figure 3.3 $qd0$ equivalent circuit of three phase induction machine	29
Figure 3.4 Y-connection of stator and rotor circuits of doubly-fed induction machine	30
Figure 3.5 Complex Space Vector equivalent circuit of 3-phase induction machine	33
Figure 3.6 Torque and speed ripple during unbalanced machine operation	36
Figure 3.7 Dynamic phasor equivalent circuit of 3-phase induction machine	38
Figure 3.8 Stator current during free acceleration ($\Delta t=50\mu s$)	41
Figure 3.9 Electrical torque during free acceleration ($\Delta t=50\mu s$)	42
Figure 3.10 Rotor speed during free acceleration ($\Delta t=50\mu s$)	43
Figure 3.11 Stator current during mechanical torque change ($\Delta t=50\mu s$)	44
Figure 3.12 Electrical torque during mechanical torque change ($\Delta t=50\mu s$)	45
Figure 3.13 Rotor speed during mechanical torque change ($\Delta t=50\mu s$)	45
Figure 3.14 Stator current during balanced 3-phase voltage dip ($\Delta t=50\mu s$)	46
Figure 3.15 Electrical torque during balanced 3-phase voltage dip ($\Delta t=50\mu s$)	47

Figure 3.16 Rotor speed during balanced 3-phase voltage dip ($\Delta t=50\mu s$)	47
Figure 3.17 Real and imaginary parts of positive sequence stator current dynamic phasor..	48
Figure 3.18 Real and imaginary parts of negative sequence stator current dynamic phasor.	49
Figure 3.19 Stator current during unbalanced fault ($\Delta t=50\mu s$).....	50
Figure 3.20 DC component of electrical torque dynamic phasor	51
Figure 3.21 2 nd harmonic component of electrical torque dynamic phasor	52
Figure 3.22 Electrical torque during unbalanced fault ($\Delta t=50\mu s$)	52
Figure 3.23 DC component of rotor speed dynamic phasor	53
Figure 3.24 2 nd harmonic component of rotor speed dynamic phasor	54
Figure 3.25 Rotor speed during unbalanced fault ($\Delta t=50\mu s$)	54
Figure 4.1 Typical magnetization curve of an induction machine.....	57
Figure 4.2 qd decomposition of flux correction term	58
Figure 4.3 Saturation of main magnetizing flux linkage in terms of dynamic phasors	61
Figure 4.4 Stator current in saturation region	63
Figure 4.5 Magnetizing flux linkage in saturation region.....	64
Figure 4.6 Zoomed view of stator current in saturation region	65
Figure 4.7 Zoomed view of magnetizing flux linkage in saturation region.....	65
Figure 4.8 Stator current in saturation region during unbalanced fault	66
Figure 4.9 Magnetizing flux linkage in saturation region during unbalanced fault.....	67
Figure 4.10 Zoomed view of stator current in saturation region during unbalanced fault	68
Figure 4.11 Zoomed view of magnetizing flux in saturation region during unbalanced fault	68
Figure 5.1 Stator current during start-up for fixed Δt studies	71

Figure 5.2 Stator current during load torque change for fixed Δt studies.....	72
Figure 5.3 Stator current during balanced 3-phase fault for fixed Δt studies	73
Figure 5.4 Stator current during unbalanced fault for fixed Δt studies.....	74
Figure 5.5 Positive sequence stator current dynamic phasor using different Δt	75
Figure 5.6 Negative sequence stator current dynamic phasor using different Δt	76
Figure 5.7 Electrical torque using different Δt	77
Figure 5.8 DC component of electrical torque dynamic phasor using different Δt	77
Figure 5.9 2 nd harmonic component of electrical torque dynamic phasor using different Δt	78
Figure 5.10 Rotor speed using different Δt	79
Figure 5.11 DC component of rotor speed dynamic phasor using different Δt	80
Figure 5.12 2 nd harmonic component of rotor speed dynamic phasor using different Δt	80
Figure 5.13 Load change results using dynamic phasor model	82
Figure 5.14 Stator current during free acceleration using variable Δt solver	84
Figure 5.15 Time-step results during free acceleration using variable Δt solver	84
Figure 5.16 Stator current during load torque change using variable Δt solver	85
Figure 5.17 Time-step results during load torque change using variable Δt solver.....	85
Figure 5.18 Stator current during balanced fault using variable Δt solver	86
Figure 5.19 Time-step results during balanced fault using variable Δt solver	86

Acknowledgements

For their patience, knowledge and probing questions that encouraged me to look deeper and gain a better understanding of my research topic I would like to thank my supervisors Dr. José Marti and Dr. Hermann Dommel. I would like to express my deep gratitude to Dr. Hermann Dommel for his continuous financial support throughout my research and for taking a chance on me and opening a spot in the M.A.Sc. program; allowing me to transfer to UBC. I would also like to thank Dr. Juri Jatskevich; who was not my supervisor but at times I'm sure felt like he was, for his expertise and insight into electric machine theory and modeling. I would also like to sincerely thank all of the friends and colleagues that I have gained throughout my studies here at the University of British Columbia; I hope the relationships that we have developed will stay with me for the rest of my life.

Finally, I would like to express my deepest gratitude to my loving wife and our families who have been extremely patient and provided so much support and encouragement to me throughout my post-secondary education. I will be forever grateful to them and I find it difficult to express in words how much their ongoing support has meant to me throughout the years; from the bottom of my heart, thank you.

Dedication

The work done in this thesis is dedicated to my loving wife Blair. Her ongoing support in all aspects has meant more to me than I would ever be able to express in words. I can only hope that one day I will be able to repay her by providing that same support to her. She has been my rock, my confidant and sounding board but most importantly, she has been my best friend. I will always be grateful to you Blair and I love you more than words can express. From the deepest parts of my soul I thank you.

Chapter 1: Introduction

1.1 Background

The electric power system is often referred to as one of the most important infrastructure systems built by humankind. So important and fundamental in fact that many other systems that have been developed to progress the human race are dependent on electric power systems to allow them to operate. For example; communication, transportation, water supply and many other infrastructure systems are completely dependent upon the continuous reliable operation of the electric power system. Due to growing electricity demand and increased load and stress being added to an aging electric power system infrastructure, power system stability and security has become a major concern and area of focus for research and improvement [1]. Major blackouts in the USA, Europe and most recently in north eastern India for example; which caused an estimated 670 million people [2], or roughly 10% of the world's population to be without power, have forced researchers to look closely at ways to increase the reliability and security of electric power systems to mitigate such catastrophic failures in the future.

During planning and operation, power systems must be thoroughly analyzed and therefore be accurately modeled. Models and computer programs for power system analysis have become an essential part of power system planning and operation. Power system engineers perform a variety of system studies in order to plan effectively for system upgrades and changes and to reliably operate the power system. Some of the types of studies performed regularly are

- short circuit (or fault) analysis

- electromagnetic transient analysis
- power (or load) flow analysis, and
- voltage and transient stability studies

One of the major challenges in modeling and simulating the power system for the above studies is the fact that the dynamics of the system react at very different speeds depending on the type of disturbance to the system and the type of study being conducted. For example, Figure 1.1 illustrates the general time-frame in which many of the major power system disturbances occur. These disturbances can be generally classified into two different categories; electromagnetic transients and electromechanical transients.

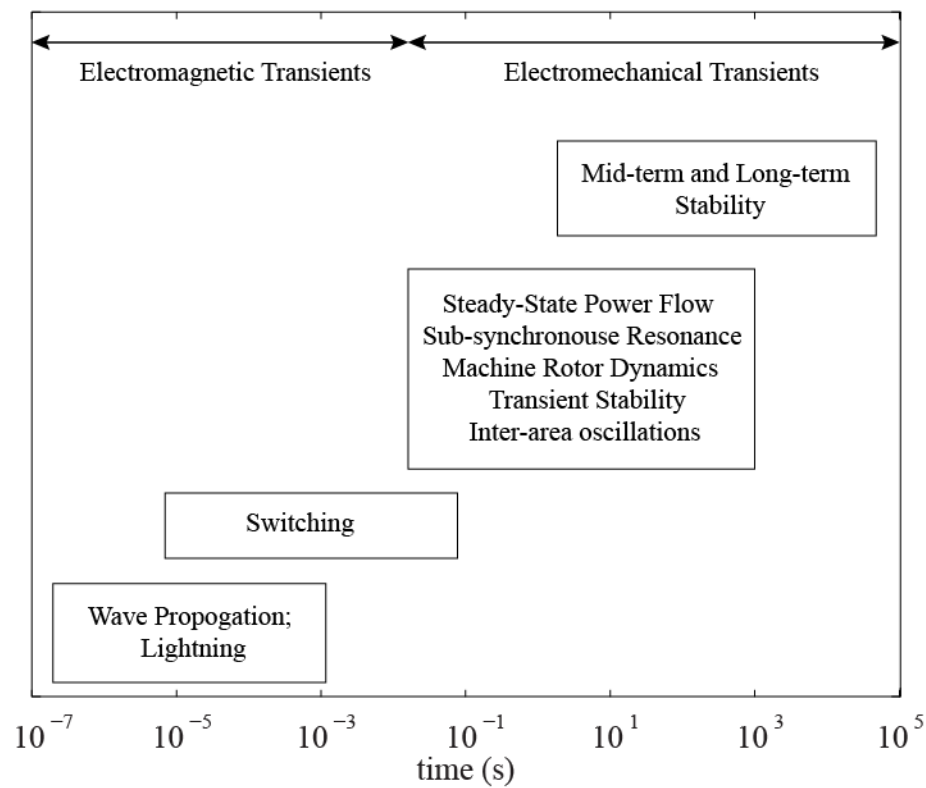


Figure 1.1 General time-frame for power system disturbances

Electromagnetic transient phenomena generally occur during sudden system topology changes. These changes can be attributed to many different types of disturbances such as lightning strokes, closing or opening of circuit breakers, high frequency switching of power electronic devices and faults that occur in the power system to name just a few. The effects of these types of disturbances are usually fairly localized in the surrounding system and usually have very fast transients associated with them. Electromagnetic transient disturbances therefore require a greater amount of detail in modeling the system components that are most affected and because of the speed of the transients require a much smaller time-step when performing simulations; usually of the order of tens of microseconds or smaller depending on the phenomena being studied.

Electromechanical transients are generally associated with much slower disturbance phenomena such as mismatches between the mechanical energy present in rotating electric machines and the electric energy present in the electrical system that it is attached to. These types of slow transients can also occur during a power imbalance that occurs between two different areas of the power system; known as inter-area oscillations. The dynamics of this type of disturbance phenomena are much slower than those that occur in electromagnetic transients and therefore many simplifying assumptions are made to increase the efficiency of the simulation of these types of transients. For one, because of the timescales associated with these types of transient studies the electromagnetic transients are generally neglected and a quasi-steady state is assumed for simulation. This is generally achieved using the concept of steady-state phasor representation of system quantities around the system operating frequency.

Due to the vast difference in dynamic transient speeds that occur in the power system, traditionally two different types of simulators have been used to simulate transients in the power system depending on which type of study was being done. For the fast electromagnetic transient simulations, *Electromagnetic Transient Program* or EMTP type programs are used. These types of programs require a great amount of detail in the system component models and very small time-steps to simulate the fast dynamics that occur in these types of studies. The much slower transient stability studies are usually performed by Transient Stability Programs which require much less detail in the system component models and make simplifying assumptions to increase the efficiency of the programs as mentioned above.

The *Electromagnetic Transients Program* (EMTP) [3] was first introduced in the late 1960's by H. W. Dommel [4] and was quickly adopted as one of the standard industry tools used for the digital simulation of power system transients. Prior to EMTP, a system known as a *Transient Network Analyzer* (TNA) was used extensively to perform load flow, short-circuit analysis and stability studies on AC power systems. The quick adoption of EMTP-type programs (PSCAD/EMTDC, ATP, MICROTRAN, etc.) [5-8] as the industry standard tools for transient analysis is partly due to several advantages that they have over the TNA. Firstly, these programs are fully digital simulators that are able to run on inexpensive desktop computers, whereas the TNA is an analog scale model of the system that is very expensive to build and requires a significant amount of space. Secondly, EMTP-type programs are able to provide much more accurate simulation results than the TNA at higher frequencies. This is

due to phenomena that are present at higher frequencies in the TNA model such as parasitic capacitances that can have significant impacts on the accuracy of the simulation results.

One drawback to these EMTP-type simulators is that they require very small integration time-steps in order to accurately recreate all of the transient variables during simulations. Therefore, these types of programs work well with transient and mid-term stability studies; which contain faster dynamic phenomena, but become inefficient for use with long term stability problems and slow dynamic simulations of large systems that occur when studying problems such as voltage stability or inter-area oscillations. Other types of methods are used in this case, that make simplifying assumptions to increase the speed and efficiency of the program during simulation [9-11].

One of the first attempts to unify the simulation of dynamic operating conditions in power systems is outlined in [12], in which the authors make use of an implicit variable-step algorithm to simulate the faster transients and slower long-term phenomena that occur in power system operation. The algorithm presented here is quite robust but is not capable of simulating the very fast electromagnetic transients. Another, more recent, attempt at unifying power system simulators using the concept of time varying phasors or dynamic phasors is presented by Venkatasubramanian in [13] and further extended in [14, 15]. The dynamic phasor concept as presented in these papers extends the concept of traditional phasor representation of sinusoidal signals; which are the standard tool for power system stability analysis and generally limited to quasi-stationary assumptions, to a time-varying phasor representation that can accommodate much faster transient speeds. The concept of dynamic

phasors allows for the efficient solution of both fast electromagnetic transients as well as slow electromechanical simulations due to the fact that their dynamics are much slower in time than the time-domain circuit quantities. During steady state dynamic phasor quantities do not change with time and reduce to the traditional phasor representation of power system quantities making them efficient for modeling longer term electromechanical transients.

Since their early applications to averaging power conversion circuit behaviour for simulations [16], dynamic phasors have been used to successfully model many power system components and simulation phenomena. For example, system components such as HVDC converters [17-19], static var compensators (SVC) [20], unified power flow controllers (UPFC) [21] and synchronous machines [22] among others. The dynamic phasor concept has also been used to perform various system studies including analysis of balanced power system transients [13-15, 23] as well as unbalanced transients [24]. The concept of dynamic phasor estimates have also been applied to studying power system oscillations in [25-28].

1.2 Thesis Motivation

Electric motors typically consume 60 to 70% of the energy supplied by a power system and therefore encompass a major portion of power system loads. The dynamics attributed to motors are usually the most significant contribution to power system load dynamic characteristics. In particular induction motors are the workhorse of modern electrical industry. From large industrial motors used in mills and manufacturing facilities to home appliances such as refrigerators, washing machines, dishwashers etc., induction machines are extensively used throughout many power systems. Thus it is very important to be able to

accurately and efficiently model induction motors for power system simulation and stability studies.

Various dynamic phasor models of induction machines have been presented in literature. For example references [23] and [29] present a dynamic phasor model for an induction machine that is derived from dimension reduced (DR) induction machine model where the equations of stator, rotor and flux variables are reduced to those of only stator variables. The analysis in these papers however assumes only balanced machine operation and doesn't take into account unbalanced conditions that may occur in induction machine operation. Reference [30] presents a dynamic phasor model of a doubly-fed induction machine that does take into account unbalanced machine operation. The model presented is derived from the conventional $qd0$ induction machine model in a synchronous reference frame. This model contains a dc component dynamic phasor that captures the positive sequence machine quantities as well as a 2nd harmonic dynamic phasor that captures the negative sequence machine quantities during unbalanced operation. In reference [31] a dynamic phasor model for doubly-fed induction machines is derived from the complex space vector induction machine model with a stationary reference frame. This model contains a positive system frequency dynamic phasor to account for positive sequence machine quantities and balanced operation as well as a negative system frequency dynamic phasor that accounts for negative sequence quantities that arise during unbalanced machine operation.

Although induction machines have been modeled successfully several different ways using the concepts of dynamic phasors, none of the models presented in the literature mentioned

include the effects of machine saturation. The effects of machine saturation have been a topic of significant research and study [32-43]. During operation, induction machines routinely face a number of operating conditions where the effects of saturation cannot be ignored. Therefore, in order to produce more accurate and reliable results during simulations the effects of saturation must be included in the machine models. The motivation behind this thesis therefore is to extend the dynamic phasor model of the doubly-fed induction machine to include the effects of main flux-linkage saturation. The dynamic phasor saturation model developed in this thesis is intended to be a starting point for further dynamic phasor model developments and research.

1.3 Thesis Outline

Following the introduction, the concepts of dynamic phasors are introduced to the reader in Chapter 2. In particular, Section 2.1 presents the concept and definition of the dynamic phasors and how they can be used to represent circuit quantities in single phase systems (Section 2.1.1). The concept of dynamic phasors is then generalized to include polyphase systems (Section 2.1.2), particularly the three-phase system that is commonly encountered in the modern day power system. Section 2.2 describes how dynamic phasors can be used to represent complex space vector quantities by first describing the concept of complex space vectors (Section 2.2.1) and how they are used to describe three phase systems and then describing how dynamic phasors can be used to express complex space vector quantities (Section 2.2.2).

Chapter 3 first presents some conventional time domain models that are used to model induction machines. These include the three-phase *abc* induction machine model (Section 3.1.1), the two-axis *qd0* induction machine model (Section 3.1.2) and finally the complex space vector induction machine model (Section 3.1.3). The dynamic phasor induction machine model is then presented in Section 3.2, followed by a few system studies in Section 3.3 to illustrate the validity of the dynamic phasor induction machine model.

Chapter 4 presents the method used to implement the effects of main flux linkage saturation into the dynamic phasor model. First however, a conventional time domain model for implementing the effects of main flux saturation is presented in Section 4.1 followed by its extension to the dynamic phasor model in Section 4.2. Once the models have been presented the dynamic phasor model is then verified in the saturation region of operation for both balanced and unbalanced machine operation in Section 4.3.

In Chapter 5 the focus is on assessing the performance of the dynamic phasor induction machine model. Section 5.1 looks at the models performance using a fixed time-step and compares it to the performance of a conventional time domain model. Section 5.2 investigates the dynamic phasor model performance using a variable time-step solver and compares the results to those obtained using a conventional time domain model.

Finally, Chapter 6 concludes the thesis by highlighting the key contributions provided in this thesis along with recommendations for future research and model improvements.

Chapter 2: Dynamic Phasor Analysis

2.1 Concept and Definition

The concept of phasors is based on the property that a periodic (possibly complex-valued) time-domain waveform $x(\tau)$ with period T , that is $x(\tau) = x(\tau - T)$, can be expressed as a complex Fourier series [44] of the form

$$x(\tau) = \sum_{k=-\infty}^{\infty} \underline{X}_k \cdot e^{jk\omega_s\tau} \quad (2.1)$$

where $\omega_s = 2\pi/T$ and \underline{X}_k is the k^{th} Fourier coefficient in complex form. In this case, since $x(\tau)$ is periodic, the Fourier coefficients \underline{X}_k are time invariant and can be expressed as

$$\underline{X}_k = \frac{1}{T} \int_{t-T}^t x(\tau) \cdot e^{-jk\omega_s\tau} d\tau \quad (2.2)$$

In power system studies, during steady-state analysis, these coefficients \underline{X}_k are also known as phasors and are extensively used as a tool to greatly simplify the study of steady-state power flow and system behavior.

2.1.1 Single Phase Systems

In power system dynamic situations, the waveforms are generally not strictly periodic but are nearly periodic. The idea now is to generalize equations (2.1) – (2.2) to accommodate arbitrary, nearly periodic types of waveforms. This is achieved by using the approach outlined in [45], where the Fourier coefficients are allowed to vary with time. Considering a window of length T for a given waveform, and viewing that waveform to be periodic with a

duration of T , such that a Fourier analysis of the waveform $x(\tau)$ can be performed. The time evolution of the Fourier coefficients can then be calculated as the window of length T “slides” along the actual waveform. Figure 2.1 for example depicts the stator phase a current of an induction machine during and immediately following an unbalanced single phase fault along with the “sliding window” of length T .

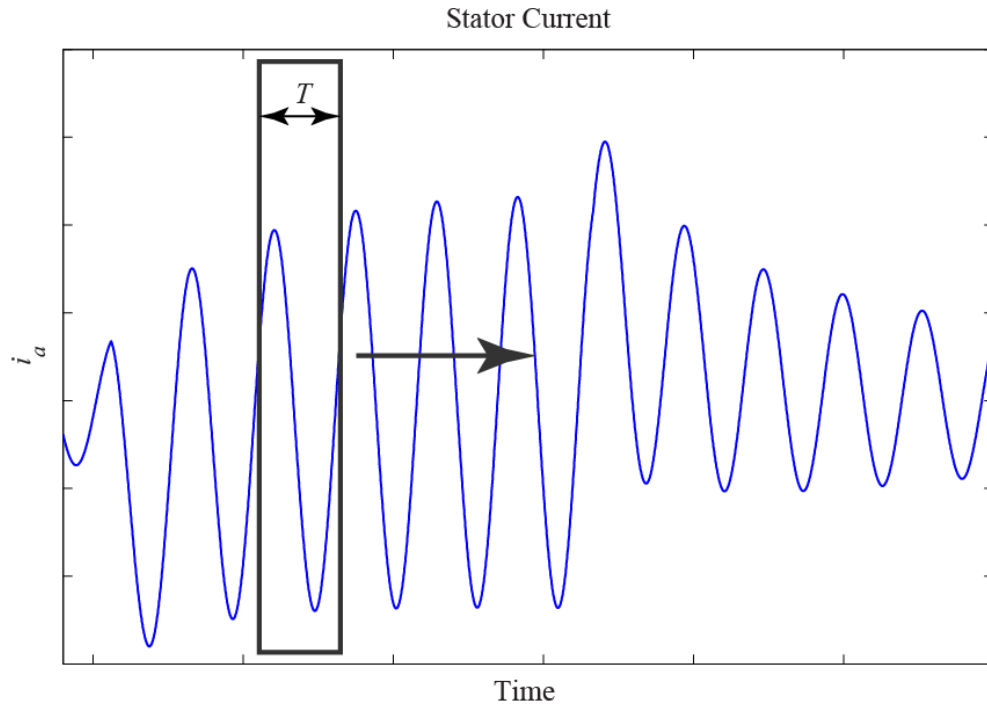


Figure 2.1 Illustration of “sliding” window of periodicity

Now, for an arbitrary, possibly complex-valued time-domain waveform $x(\tau)$ with period T , the method considers the Fourier coefficients of $x(\tau)$ on the interval $\tau \in (t - T, t]$. The Fourier series is now expressed in the form

$$x(\tau) = \sum_{k=-\infty}^{\infty} \underline{X}_k(t) \cdot e^{jk\omega_s\tau} \quad (2.3)$$

where the k^{th} Fourier coefficient $\underline{X}_k(t)$ is now time-dependent and can shift in both magnitude and phase as the window of periodicity “slides” over the waveform. These time-dependent Fourier coefficients are referred to as *dynamic phasors* in many research papers and throughout this thesis and are expressed as

$$\underline{X}_k(t) = \frac{1}{T} \int_{t-T}^t x(\tau) \cdot e^{-jk\omega_s\tau} d\tau = \langle x \rangle_k(t). \quad (2.4)$$

In many cases, a reasonable approximation of the waveform $x(\tau)$ can be achieved by considering only the Fourier coefficients $\underline{X}_k(t)$ that are dominant in equation (2.3). That is, if we consider a subset $\{K\}$ containing only the dominant Fourier coefficients, we can approximate (2.3) as

$$x(\tau) \approx \sum_{k \in \{K\}} \underline{X}_k(t) \cdot e^{jk\omega_s\tau} \quad (2.5)$$

For the purposes of this thesis, we will only be considering the subset $\{K\} = \{1, -1\}$; which corresponds to plus and minus the system frequency. For the system that is studied in this thesis, the system frequency is assumed to be 60 Hz and the above approximation looks only at the +60 Hz and -60 Hz components that are present in the system operation.

Some useful properties of the Fourier coefficients that will be used in later chapters of this thesis will now be outlined. For example, the time derivative for the k^{th} Fourier coefficient, as expressed in equation (2.6), is obtained by differentiating equation (2.3) with respect to

time. This property is used extensively in the dynamic model of the doubly-fed induction machine model.

$$\frac{d\underline{X}_k}{dt} = \left\langle \frac{dx}{dt} \right\rangle_k - jk\omega_s \underline{X}_k. \quad (2.6)$$

Another important property is shown in equation (2.7) which illustrates that a product of two time domain signals is equivalent to a discrete time convolution of the two signals' sets of dynamic phasors.

$$\langle xy \rangle_k = \sum_{i=-\infty}^{\infty} (\underline{X}_{k-i} \underline{Y}_i) \quad (2.7)$$

If the signal $x(\tau)$ is complex valued, the relationship between \underline{X}_{-k} and $\langle x \rangle_k$ is given below in equation (2.8).

$$\underline{X}_{-k} = \langle x \rangle_{-k} = \langle x^* \rangle_k^* \quad (2.8)$$

where x^* represents the complex conjugate of x . In the case where $x(\tau)$ is real valued, equation (2.8) reduces to the form shown below in equation (2.9).

$$\underline{X}_{-k} = \underline{X}_k^* \quad (2.9)$$

2.1.2 Polyphase Systems

Our goal now is to extend the dynamic phasor concept to include polyphase systems. We begin by using the method of symmetrical components [46] which allows a set of n unbalanced phasors to be expressed as the sum of n symmetrical sets of balanced phasors. Therefore, in the common three-phase (abc) power system, a set of three unbalanced phasors can be broken down into three sets of balanced symmetrical phasors which consist of;

- *Positive-sequence* components which are equal in magnitude, have an angular displacement of 120° from each other and have the same phase sequence as the original unbalanced set;
- *Negative-sequence* components which are equal in magnitude, have an angular displacement of 120° from each other and have a phase sequence that is opposite to that of the original unbalanced set;
- *Zero-sequence* components which are equal in both magnitude and phase.

Figure 2.2 illustrates the three sets of balanced sequence components that add up to form the original unbalanced set.

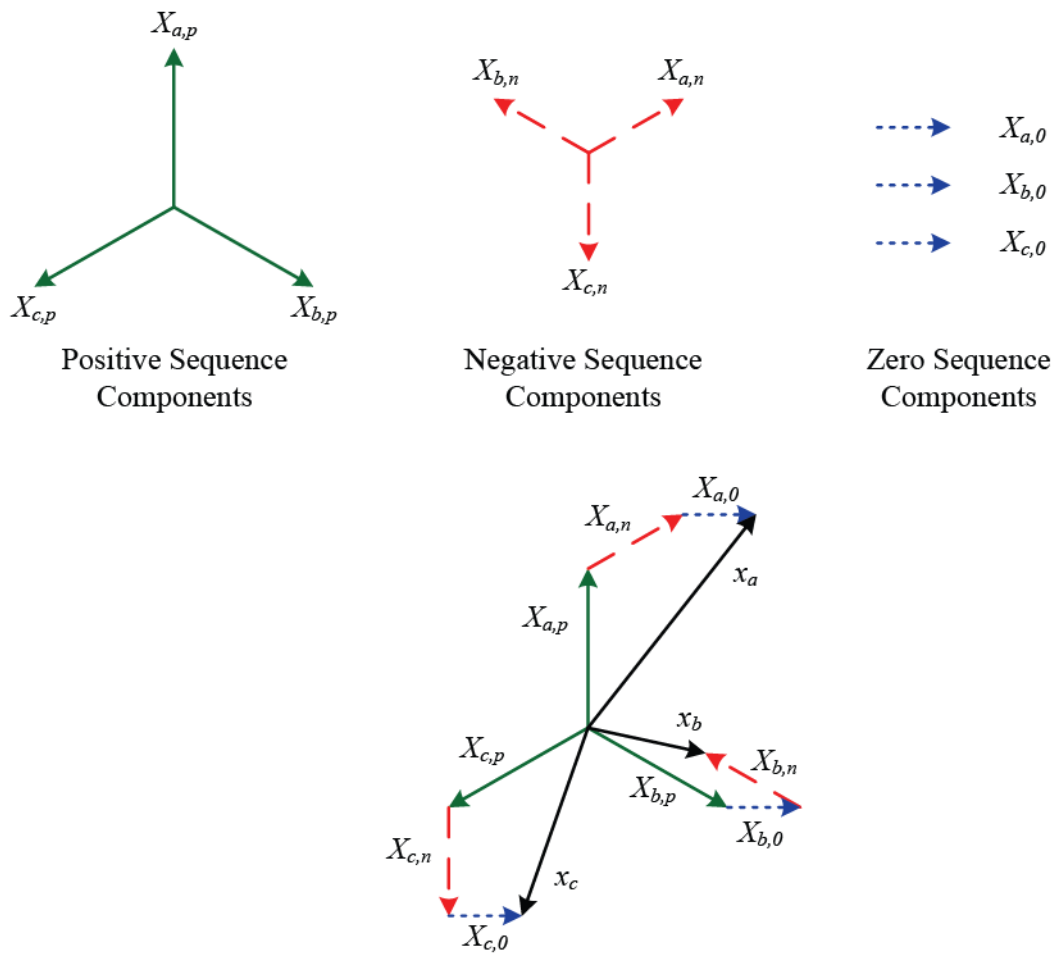


Figure 2.2 Resolution of unbalanced 3-phase quantities into balanced sequence components

The transformation from an unbalanced set of phasors to the sequence components is achieved by introducing the common operator $\alpha = e^{j(2\pi/3)}$ which represents a phase of $2\pi/3$ in the complex plane. Using the operator α , we can express the phase quantities as shown in equation (2.10).

$$\begin{bmatrix} x_a \\ x_b \\ x_c \end{bmatrix} = \underbrace{\begin{bmatrix} 1 & 1 & 1 \\ \alpha^2 & \alpha & 1 \\ \alpha & \alpha^2 & 1 \end{bmatrix}}_{\mathcal{A}} \begin{bmatrix} X_{a,p} \\ X_{a,n} \\ X_{a,0} \end{bmatrix} \quad (2.10)$$

Where $\alpha^2 = e^{j(4\pi/3)} = e^{-j(2\pi/3)}$.

The inverse transformation is given as follows

$$\begin{bmatrix} X_{a,p} \\ X_{a,n} \\ X_{a,0} \end{bmatrix} = \underbrace{\frac{1}{3} \begin{bmatrix} 1 & \alpha & \alpha^2 \\ 1 & \alpha^2 & \alpha \\ 1 & 1 & 1 \end{bmatrix}}_{\mathcal{A}^{-1}} \begin{bmatrix} x_a \\ x_b \\ x_c \end{bmatrix} \quad (2.11)$$

Using the transformation in equation (2.10) and extending the single phase dynamic phasor principles outlined in Section 2.1.1 to the poly-phase system, we can express three phase time domain quantities in dynamic phasor form as shown in equation (2.12).

$$\begin{bmatrix} x_a \\ x_b \\ x_c \end{bmatrix}(\tau) = \sum_{k=-\infty}^{\infty} e^{jk\omega_s\tau} \mathcal{A} \begin{bmatrix} \underline{X}_{p,k} \\ \underline{X}_{n,k} \\ \underline{X}_{0,k} \end{bmatrix}(t) \quad (2.12)$$

Note here that the subscript a has been dropped from the Fourier coefficients on the right hand side of equation (2.12) to avoid clutter. Similar to the single phase case, the Fourier coefficients in equation (2.12) can be expressed as

$$\begin{bmatrix} \underline{X}_{p,k} \\ \underline{X}_{n,k} \\ \underline{X}_{0,k} \end{bmatrix} (t) = \frac{1}{T} \int_{t-T}^t e^{-jk\omega_s \tau} \mathcal{A}^{-1} \begin{bmatrix} x_a \\ x_b \\ x_c \end{bmatrix} (\tau) d\tau = \begin{bmatrix} \langle x \rangle_{p,k} \\ \langle x \rangle_{n,k} \\ \langle x \rangle_{0,k} \end{bmatrix} (t) \quad (2.13)$$

The Fourier coefficients in equation (2.13) represent the *dynamic phasors* of the positive $\underline{X}_{p,k}$, negative $\underline{X}_{n,k}$ and zero-sequence $\underline{X}_{0,k}$ components of the time varying signals represented in equation (2.12) at a frequency of $k\omega_s$.

The same properties as those outlined in Section 2.1.1 for the single phase *dynamic phasors* can also be applied here to the poly-phase case since equation (2.12) is just a vector generalization of equation (2.3) for the three-phase case [31]. For example the time derivative of the time varying Fourier coefficients for the positive, negative and zero sequence components can be expressed in vector form as

$$\frac{d}{dt} \begin{bmatrix} \underline{X}_{p,k} \\ \underline{X}_{n,k} \\ \underline{X}_{0,k} \end{bmatrix} (t) = \mathcal{A}^{-1} \begin{bmatrix} \left\langle \frac{d}{dt} x_a(\tau) \right\rangle_k \\ \left\langle \frac{d}{dt} x_b(\tau) \right\rangle_k \\ \left\langle \frac{d}{dt} x_c(\tau) \right\rangle_k \end{bmatrix} (t) - jk\omega_s \begin{bmatrix} \underline{X}_{p,k} \\ \underline{X}_{n,k} \\ \underline{X}_{0,k} \end{bmatrix} (t) \quad (2.14)$$

Also, for a complex valued signal we have the relationship between balanced sequence components as

$$\begin{bmatrix} \langle x \rangle_{p,k} \\ \langle x \rangle_{n,k} \\ \langle x \rangle_{0,k} \end{bmatrix} = \begin{bmatrix} \langle x^* \rangle_{n,-k}^* \\ \langle x^* \rangle_{p,-k}^* \\ \langle x^* \rangle_{0,-k}^* \end{bmatrix} \quad (2.15)$$

In the case of real valued signals equation (2.15) can be expressed as

$$\begin{bmatrix} \underline{X}_{p,k} \\ \underline{X}_{n,k} \\ \underline{X}_{0,k} \end{bmatrix} = \begin{bmatrix} X_{n,-k}^* \\ X_{p,-k}^* \\ X_{0,-k}^* \end{bmatrix} \quad (2.16)$$

2.2 Dynamic Phasors and Complex Space Vectors

2.2.1 Complex Space Vector Representation of 3-Phase Variables

In modern literature on electric machines and drive systems it is common to represent three phase variables as what are known as *complex space vectors* [47, 48]. The concept of *complex space vectors* involves a transformation of the three phase variables to a stationary complex reference frame. This transformation is almost identical to the common *qd0* reference frame transformation that is used extensively in rotating machine modeling [46, 49], with the added abstraction that the variables are represented as complex vectors in the *q*- and *d*-axis. That is, the *q*-axis quantities represent the real part of the complex space vector and the *d*-axis quantities representing the negative imaginary part of the vector.

To illustrate the concept of complex space vectors, Figure 2.3 depicts a simplified representation of a three-phase rotating machine. The stator consists of three windings that are sinusoidally distributed around the stator of the machine such that they are 120° apart spatially from one another. When a three phase sinusoidal current is supplied to the stator windings in the machine with positive current flowing into the crossed terminals and out of the dotted terminals, each phase will produce its own magneto-motive force (*mmf*) which lies on the magnetic axis of that particular phase. If we consider the *mmf* produced by each particular phase as a vector in space, they can be added up to produce the resultant total *mmf*

that is produced within the machine which rotates inside the machine at a frequency equal to the supply frequency of the currents.

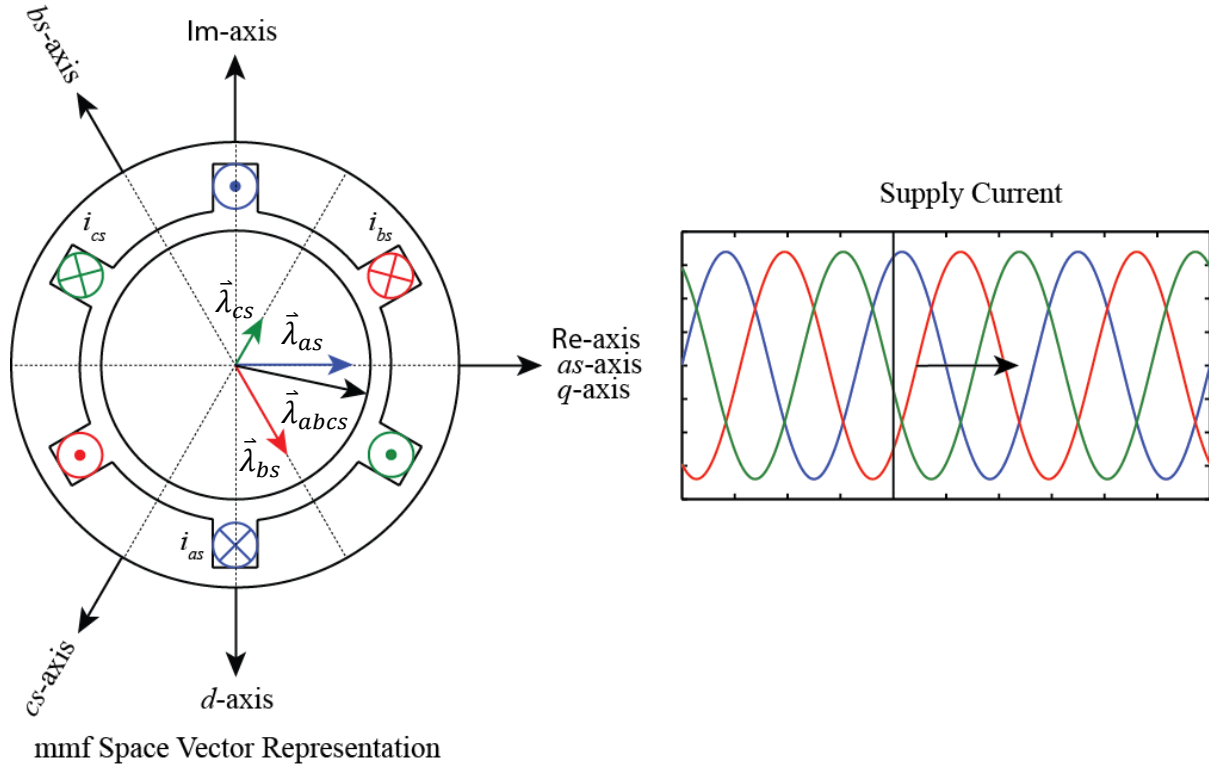


Figure 2.3 Illustration of the rotating complex space vector

We can define space vectors for the currents in each phase in a similar manner to lie on their respective magnetic axis as depicted for fluxes in Figure 2.3; from which we get

$$\begin{aligned}
 \vec{i}_{as} &= i_{as} \\
 \vec{i}_{bs} &= \alpha i_{bs} \\
 \vec{i}_{cs} &= \alpha^2 i_{cs}
 \end{aligned} \tag{2.17}$$

Note here that α in equation (2.17) is the same as that defined previously in section 2.1.2 of this thesis, that is $\alpha = e^{j(2\pi/3)}$.

Now, adding these currents and introducing a scaling factor of $2/3$, we get the total current space vector that results from the three phase currents as follows.

$$\vec{i}_{abcs} = \frac{2}{3}(i_{as} + \alpha i_{bs} + \alpha^2 i_{cs}) \quad (2.18)$$

It is not difficult to see that if a balanced set of sinusoidal currents is applied to the terminals of the machine that equation (2.18) describes a phasor of constant magnitude that rotates in the complex plane with the same frequency as the supply frequency.

It is important to note that the coefficient of $2/3$ is introduced here to conserve the magnitudes between the supply currents and the resultant space vector. Other scaling factors are also used for different purposes. For example, the scaling factor of $\sqrt{2/3}$ is sometimes used which will equate power quantities between the two representations of the system [48].

There is an easy way to retrieve the phase currents from the space vector in the case where the sum of the phase currents is equal to zero.

$$i_{as} + i_{bs} + i_{cs} = 0 \quad (2.19)$$

In this case there will be no zero-sequence currents and the phase currents can be retrieved from the complex space vector by expanding it out into its complex form as follows.

$$\begin{aligned} \vec{i}_{abcs} &= \frac{2}{3} \left[i_{as} - \frac{1}{2}(i_{bs} + i_{cs}) + j \frac{\sqrt{3}}{2}(i_{bs} - i_{cs}) \right] \\ &= i_{as} + j \frac{\sqrt{3}}{2}(i_{bs} - i_{cs}) \end{aligned} \quad (2.20)$$

From equation (2.20) it can be seen that the phase a current can be retrieved by considering only the real part of the complex space vector, \vec{i}_{abcs} . So we have

$$i_{as} = \mathcal{Re}\{ \vec{i}_{abcs} \} \quad (2.21)$$

Similarly, we can retrieve the phase b and phase c currents by considering the real part of the complex space vector after it has been multiplied by α^2 and by α , respectively. So we get

$$i_{bs} = \mathcal{Re}\{ \alpha^2 \vec{i}_{abcs} \} \quad (2.22)$$

and

$$i_{cs} = \mathcal{Re}\{ \alpha \vec{i}_{abcs} \} \quad (2.23)$$

It is important to note here that when zero sequence currents are present there will be an extra term that needs to be added to equations (2.21) through (2.23).

2.2.2 Dynamic Phasor Representation of Complex Space Vectors

We are now at a point where we can extend the dynamic phasor concept to represent quantities expressed in terms of complex space vectors as dynamic phasors. Using a similar procedure as that outlined by A. Stankovik [31], we utilize equations (2.12) and (2.18) from which we get

$$\vec{x}(\tau) = \sum_{k=-\infty}^{\infty} e^{jk\omega_s\tau} \underline{x}_{p,k}(\tau) \quad (2.24)$$

Note here that equation (2.18) has been generalized from current quantities (\vec{i}) to general quantities (\vec{x}) in order to include other circuit quantities such as voltage or flux. We also

note here that equation (2.24) contains all of the information for positive and negative sequence components since all phase quantities are real valued quantities and we have $\underline{X}_{p,-k} = \underline{X}_{n,k}^*$ as outlined in section 2.1.2 of this thesis. In the special case when there are only positive and negative sequence components ($k = \pm 1$) and there are no zero sequence components present, equation (2.24) reduces to

$$\vec{\bar{x}}(\tau) = \underline{X}_{p,1}(\tau)e^{j\omega_s\tau} + \underline{X}_{n,1}^*(\tau)e^{-j\omega_s\tau} \quad (2.25)$$

The space vector in equation (2.25) is illustrated conceptually in Figure 2.4 which shows that it can be broken down into a positive sequence space vector rotating in the anti-clockwise direction at an angular speed of ω_s rad/s and a negative sequence space vector that rotates in the clockwise direction at an angular speed ω_s rad/s.

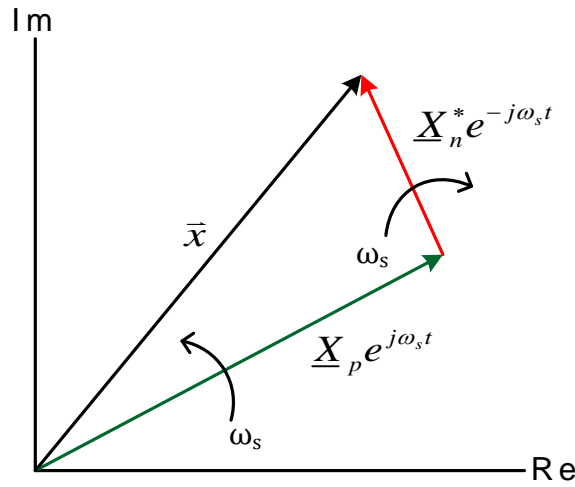


Figure 2.4 Representation of rotating complex phasor

Chapter 3: Induction Machine Modeling Based on Dynamic Phasors

3.1 Time Domain Model of Doubly-Fed Induction Machine

3.1.1 *abc* Phase Model of Doubly-Fed Induction Machine

An induction machine is comprised of two three-phase circuits; a stationary stator circuit and a rotating rotor circuit that rotates at an angular velocity of ω_r rad/s with respect to the stator circuit as illustrated in Figure 3.1. In this analysis, θ_r is defined as the angle by which the phase *a* axis of the rotor circuit leads that of the stator circuit in radians and is represented by equation (3.1).

$$\theta_r = \omega_r t \quad (3.1)$$

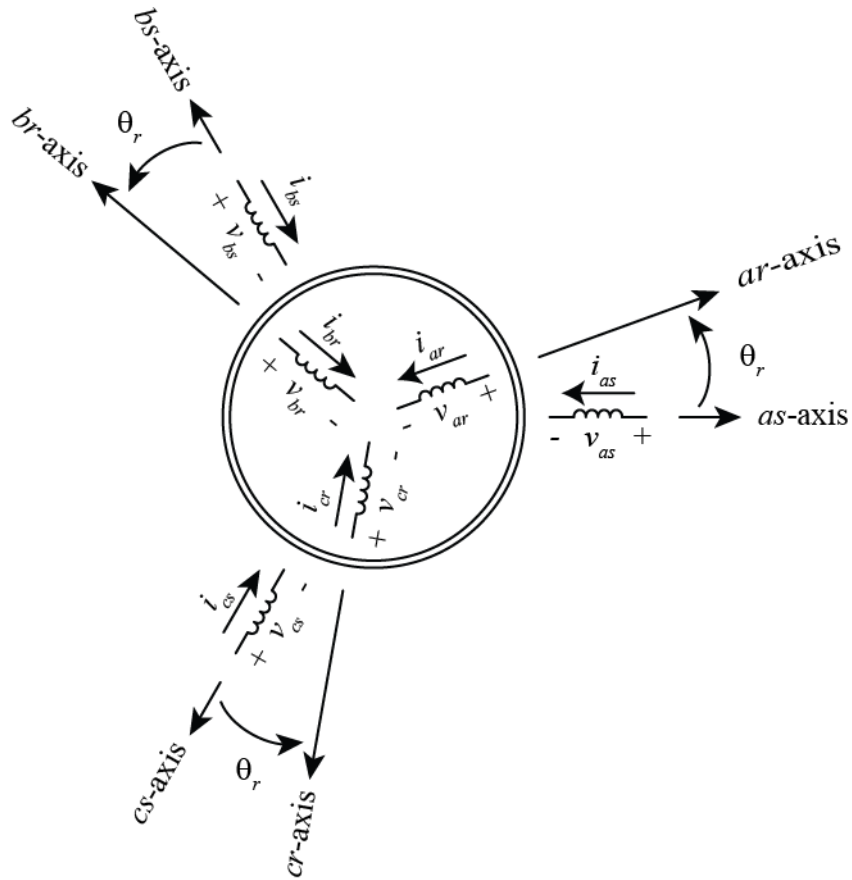


Figure 3.1 Illustration of the magnetic axis of a 2-pole induction machine

The voltage equations for both the stator circuit and the rotor circuit can be defined as follows;

Stator voltage equations:

$$\begin{aligned} v_{as} &= r_s i_{as} + \frac{d}{dt} \lambda_{as} \\ v_{bs} &= r_s i_{bs} + \frac{d}{dt} \lambda_{bs} \\ v_{cs} &= r_s i_{cs} + \frac{d}{dt} \lambda_{cs} \end{aligned} \quad (3.2)$$

Rotor voltage equations:

$$\begin{aligned} v'_{ar} &= r'_r i'_{ar} + \frac{d}{dt} \lambda'_{ar} \\ v'_{br} &= r'_r i'_{br} + \frac{d}{dt} \lambda'_{br} \\ v'_{cr} &= r'_r i'_{cr} + \frac{d}{dt} \lambda'_{cr} \end{aligned} \quad (3.3)$$

In equations (3.2) and (3.3), λ represents the flux linkage of the winding denoted by its respective subscript, r_s is the stator phase resistance, and r'_r is the rotor phase resistance referred to the stator winding.

The flux linkage of stator phase a winding can be written as

$$\lambda_{as} = L_s i_{as} + L_M \left[i_{as} \cos \theta_r + i_{bs} \cos \left(\theta_r - \frac{2\pi}{3} \right) + i_{cs} \cos \left(\theta_r + \frac{2\pi}{3} \right) \right] \quad (3.4)$$

In the above equation L_s represents the total phase a stator inductance and L_M represents the maximum value of mutual inductance between the stator and rotor windings.

Similarly, the referred flux linkage of rotor phase a winding can be written as

$$\lambda'_{ar} = L'_r i'_{ar} + L_M \left[i'_{ar} \cos \theta_r + i'_{br} \cos \left(\theta_r - \frac{2\pi}{3} \right) + i'_{cr} \cos \left(\theta_r + \frac{2\pi}{3} \right) \right] \quad (3.5)$$

where L'_r represents the total phase rotor inductance referred to the stator winding and L_M again, represents the maximum value of mutual inductance between the stator and rotor windings. Similar equations can be written for phase b and c stator and rotor flux linkages.

To complete the induction machine model, the mechanical part of the system needs to be defined. We first do this by defining the electromagnetic torque that is developed within the induction machine in terms of the phase currents and inductances that are present in each of the windings. It can be shown that the electromagnetic torque developed in the machine can be expressed as [49]

$$\begin{aligned} T_e = - \left(\frac{P}{2} \right) L_M \left\{ \left[i_{as} \left(i'_{ar} - \frac{1}{2} i'_{br} - \frac{1}{2} i'_{cr} \right) + i_{bs} \left(i'_{br} - \frac{1}{2} i'_{ar} - \frac{1}{2} i'_{cr} \right) \right. \right. \\ \left. \left. + i_{cs} \left(i'_{cr} - \frac{1}{2} i'_{br} - \frac{1}{2} i'_{ar} \right) \right] \sin(\theta_r) \right. \\ \left. + \frac{\sqrt{3}}{2} [i_{as}(i'_{br} - i'_{cr}) + i_{bs}(i'_{cr} - i'_{ar}) + i_{cs}(i'_{ar} - i'_{br})] \cos(\theta_r) \right\} \end{aligned} \quad (3.6)$$

Where P is the number of poles in the doubly-fed induction machine. The torque and rotor mechanical speed can be related by

$$T_e - T_m - K_{fric} \omega_{rm} = J \frac{d\omega_{rm}}{dt} = J \frac{2}{P} \frac{d\omega_r}{dt} \quad (3.7)$$

where $\omega_{rm} = \frac{2}{P} \omega_r$, K_{fric} is the rotor friction coefficient and J is the combined polar moment of inertia of the rotor and the connected load and T_m is the mechanical torque applied to the shaft of the rotor.

It can be seen from equations (3.4) and (3.6) that a significant amount of coupling occurs between the phases due to the currents that flow in each of the three windings. This coupling complicates the analysis and simulation of the induction machine and can make it quite cumbersome.

3.1.2 *qd0* Model of Doubly-Fed Induction Machine

The equations presented in section 3.1.1 can be greatly simplified if they are transformed from the stationary *abc* reference frame to a two axis, *qd0* reference frame as illustrated in Figure 3.2. By projecting the *abc* phase quantities onto the two axis reference frame, the coupling that occurs in the *abc* phase model of the induction machine can be eliminated. It is assumed that the *q*-axis of this reference frame is 90° ahead of the *d*-axis in the direction of rotation. The *q*-axis is chosen to coincide with the phase *a* axis at time $t = 0$.

It is important to note here that in general, the *qd0* reference frame is one that is defined as rotating synchronously with the rotor circuit of a rotating machine. For the sake of this thesis, the *qd0* reference frame will be defined as a two axis reference frame that is rotating at an arbitrary speed which is not necessarily synchronous to the rotating circuit of an electric machine.

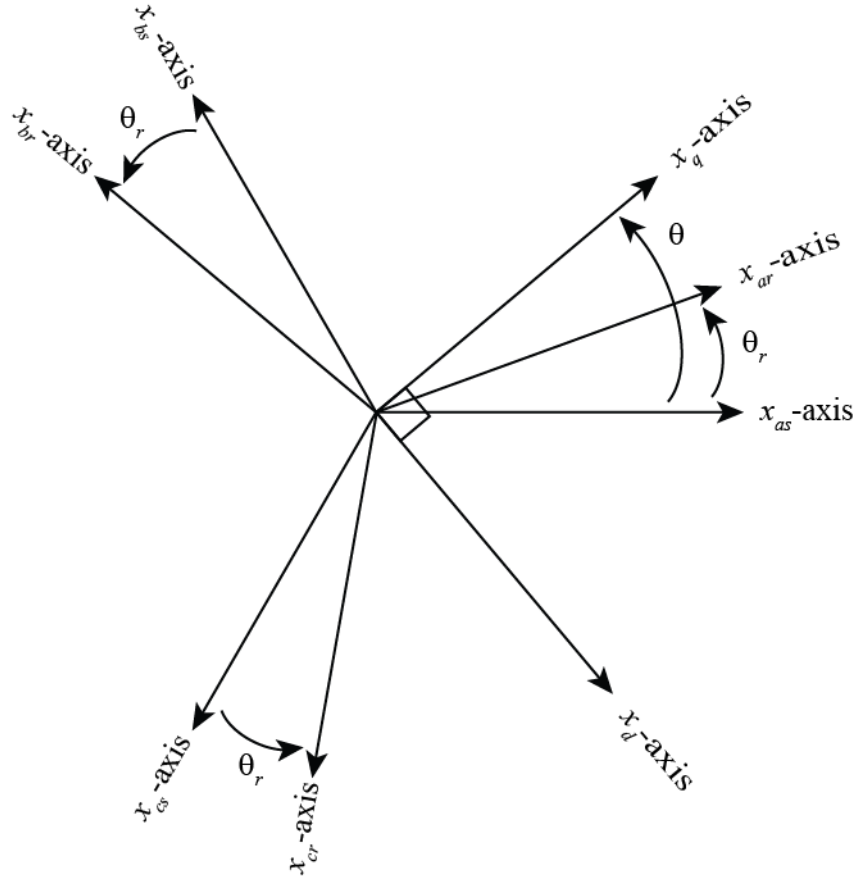


Figure 3.2 *qd0* magnetic axis

To make this transformation we use the commonly known Park's Transformation which utilizes a transformation matrix \mathbf{K} such that

$$\begin{aligned} x_{qd0} &= \mathbf{K} x_{abc} \\ x_{abc} &= \mathbf{K}^{-1} x_{qd0} \end{aligned} \tag{3.8}$$

Where $x_{abc} = [x_a \ x_b \ x_c]^T$, $x_{qd0} = [x_q \ x_d \ x_0]^T$ and x represents either voltage, current or flux linkage quantities for the stator or rotor windings.

The stator transformation matrix, \mathbf{K}_s and rotor transformation matrix, \mathbf{K}_r of a rotating reference frame are defined as follows.

$$\mathbf{K}_s = \frac{2}{3} \begin{bmatrix} \cos(\theta) & \cos\left(\theta - \frac{2\pi}{3}\right) & \cos\left(\theta + \frac{2\pi}{3}\right) \\ \sin(\theta) & \sin\left(\theta - \frac{2\pi}{3}\right) & \sin\left(\theta + \frac{2\pi}{3}\right) \\ 1/2 & 1/2 & 1/2 \end{bmatrix} \quad (3.9)$$

$$\mathbf{K}_r = \frac{2}{3} \begin{bmatrix} \cos(\theta - \theta_r) & \cos\left(\theta - \theta_r - \frac{2\pi}{3}\right) & \cos\left(\theta - \theta_r + \frac{2\pi}{3}\right) \\ \sin(\theta - \theta_r) & \sin\left(\theta - \theta_r - \frac{2\pi}{3}\right) & \sin\left(\theta - \theta_r + \frac{2\pi}{3}\right) \\ 1/2 & 1/2 & 1/2 \end{bmatrix} \quad (3.10)$$

It can be shown that

$$\mathbf{K}_s^{-1} = \begin{bmatrix} \cos(\theta) & \sin(\theta) & 1 \\ \cos\left(\theta - \frac{2\pi}{3}\right) & \sin\left(\theta - \frac{2\pi}{3}\right) & 1 \\ \cos\left(\theta + \frac{2\pi}{3}\right) & \sin\left(\theta + \frac{2\pi}{3}\right) & 1 \end{bmatrix} \quad (3.11)$$

In the above matrices, θ represents the angular displacement of the q -axis from its original position, θ_0 and is represented by the following equation.

$$\theta = \omega t + \theta_0 \quad (3.12)$$

Where ω is the angular velocity of the $qd0$ reference frame in rad/s.

The angle θ_r is the angular position of the rotor with respect to its original position θ_{r0} and is represented with the following equations.

$$\theta_r = \omega_r t + \theta_{r0} \quad (3.13)$$

Applying equations (3.9) and (3.10) directly to (3.2) and (3.3) respectively, and assuming the machine is operated in a balanced three phase manner, we get the voltage equations for the $qd0$ reference frame.

Stator qd0 voltage equations:

$$\begin{aligned}
v_{qs} &= r_s i_{qs} + \omega \lambda_{ds} + \frac{d}{dt} \lambda_{qs} \\
v_{ds} &= r_s i_{ds} - \omega \lambda_{qs} + \frac{d}{dt} \lambda_{ds} \\
v_{0s} &= r_s i_{0s} + \frac{d}{dt} \lambda_{0s}
\end{aligned} \tag{3.14}$$

Rotor qd0 voltage equations:

$$\begin{aligned}
v'_{qr} &= r'_r i'_{qr} + (\omega - \omega_r) \lambda'_{dr} + \frac{d}{dt} \lambda'_{qr} \\
v'_{dr} &= r'_r i'_{dr} - (\omega - \omega_r) \lambda'_{qr} + \frac{d}{dt} \lambda'_{dr} \\
v'_{0r} &= r'_r i'_{0r} + \frac{d}{dt} \lambda'_{0r}
\end{aligned} \tag{3.15}$$

In equations (3.14) and (3.15), λ_{qs} , λ_{ds} , λ_{0s} , λ'_{qr} , λ'_{dr} , and λ'_{0r} represent the stator and rotor flux linkages in the *qd0* reference frame and are represented by the equations below.

Stator qd0 flux linkages:

$$\begin{aligned}
\lambda_{qs} &= L_s i_{qs} + L_M (i_{qs} + i'_{qr}) \\
\lambda_{ds} &= L_s i_{ds} + L_M (i_{ds} + i'_{dr}) \\
\lambda_{0s} &= L_s i_{0s}
\end{aligned} \tag{3.16}$$

Rotor qd0 flux linkages:

$$\begin{aligned}
\lambda'_{qr} &= L'_r i'_{qr} + L_M (i_{qs} + i'_{qr}) \\
\lambda'_{dr} &= L'_r i'_{dr} + L_M (i_{ds} + i'_{dr}) \\
\lambda'_{0r} &= L'_r i'_{0r}
\end{aligned} \tag{3.17}$$

As you can see in equations (3.16) and (3.17), the large amount of coupling that was present between the phases in equations (3.4) and (3.5) is no longer present. This greatly simplifies the induction machine model and reduces the computational burden that is present in the abc phase model of the Induction Machine. Figure 3.3 depicts the equivalent $qd0$ circuit of a 3-phase symmetric induction machine in an arbitrary rotating reference frame.

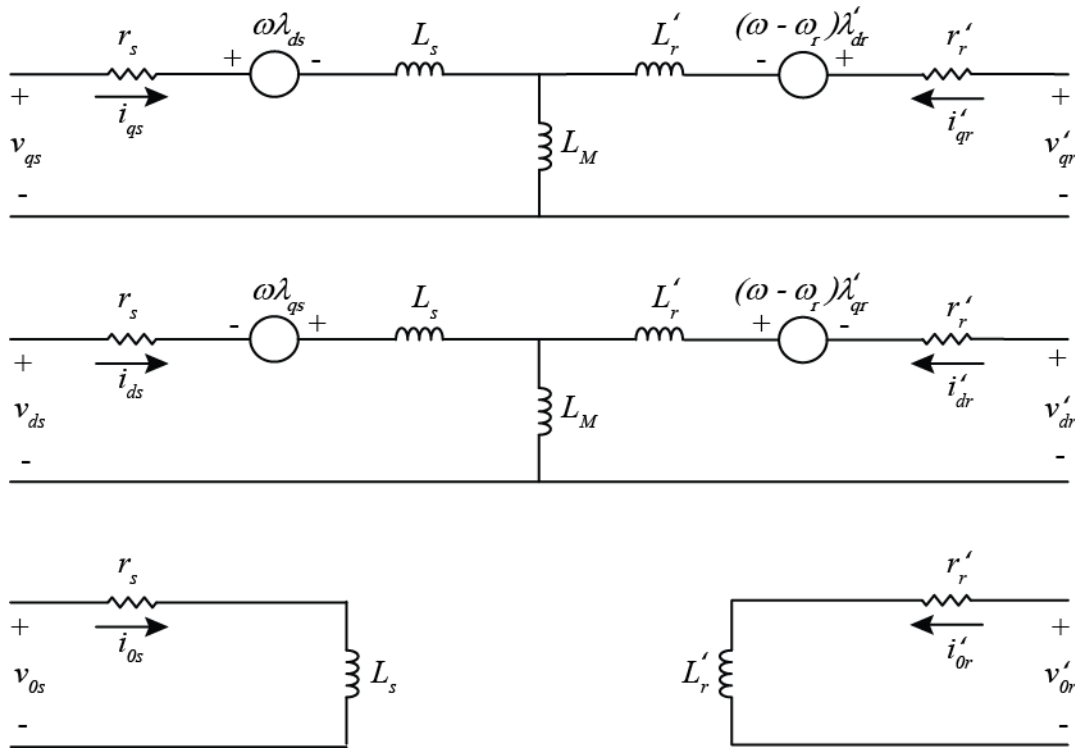


Figure 3.3 $qd0$ equivalent circuit of three phase induction machine

To complete the transformation and develop all of the equations needed to implement the model, we need to define electrical torque in terms of the $qd0$ reference frame quantities. It can be shown that the electromagnetic torque developed in the $qd0$ reference frame can be expressed as follows.

$$T_e = \left(\frac{3}{2}\right) \left(\frac{P}{2}\right) (\lambda_{ds} i_{qs} - \lambda_{qs} i_{ds}) \quad (3.18)$$

The electromagnetic torque developed by the motor drives the mechanical load attached to the shaft of the motor. If there is a mismatch between the electromagnetic torque developed and the load torque applied to the rotor shaft, the torque will accelerate the rotor according to the following equation.

$$T_e - T_m - K_{fric} \omega_{rm} = J \frac{d\omega_{rm}}{dt} = J \frac{2}{P} \frac{d\omega_r}{dt} \quad (3.19)$$

In equation (3.19), J is the combined polar moment of inertia of the rotor and the connected load and T_m is the mechanical torque applied to the shaft of the rotor.

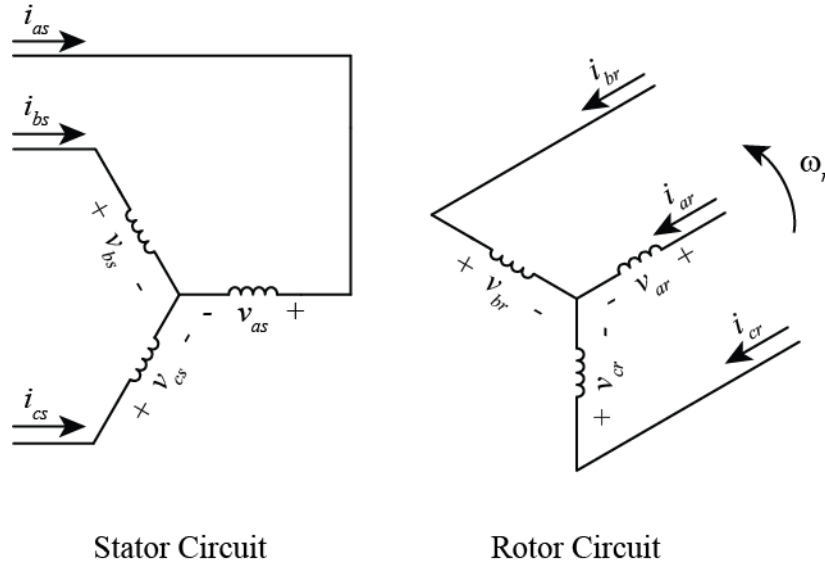


Figure 3.4 Y-connection of stator and rotor circuits of doubly-fed induction machine

In most cases, induction machines are wired in either a Y-connected configuration as illustrated in Figure 3.4 or a Δ -connected configuration. In either case, there is generally no access to the neutral point in the circuit. In such cases, there is no return path for zero-sequence currents to flow and as such these components are zero. Therefore the zero-sequence equations in equations (3.14) through (3.17) and the zero sequence circuit in Figure 3.3 can generally be neglected.

3.1.3 Complex Vector Model of Doubly-Fed Induction Machine

We are now in a position to be able to express the induction machine model in terms of complex space vector. We do this by respectively letting the q -axis and d -axis in Figure 3.2 correspond to the positive real and negative imaginary axis of the arbitrarily rotating complex reference frame. By doing this, we can express the stator circuit quantities as

$$\vec{f}_{qds} = f_{qs} - jf_{ds} = \frac{2}{3} \left[f_{as}e^{-j\theta} + f_{bs}e^{-j(\theta-\frac{2\pi}{3})} + f_{cs}e^{-j(\theta+\frac{2\pi}{3})} \right] \quad (3.20)$$

which can be expressed as

$$\begin{aligned} \vec{f}_{qds} &= \frac{2}{3} e^{-j\theta} [f_{as} + \alpha f_{bs} + \alpha^2 f_{cs}] \\ &= e^{-j\theta} \vec{f}_{abcs} \end{aligned} \quad (3.21)$$

Similarly, the rotor circuit quantities can be expressed in the arbitrarily rotating complex reference plane as

$$\begin{aligned} \vec{f}_{qdr} &= \frac{2}{3} e^{-j(\theta-\theta_r)} [f_{ar} + \alpha f_{br} + \alpha^2 f_{cr}] \\ &= e^{-j(\theta-\theta_r)} \vec{f}_{abcr} \end{aligned} \quad (3.22)$$

Using equations (3.20) through (3.22) the $qd0$ model equations in Section 3.1.2 can be combined to represent the induction machine quantities in terms of complex space vectors as follows. The qd voltage equations for the stator circuit can be combined into the complex space vector form

$$\vec{v}_{qds} = r_s \vec{i}_{qds} + \frac{d}{dt} \vec{\lambda}_{qds} + j\omega \vec{\lambda}_{qds}. \quad (3.23)$$

Similarly, for the rotor circuit qd voltage equations we get

$$\vec{v}'_{qdr} = r'_r \vec{i}'_{qdr} + \frac{d}{dt} \vec{\lambda}'_{qdr} + j(\omega - \omega_r) \vec{\lambda}'_{qdr} \quad (3.24)$$

where

$$\vec{\lambda}_{qds} = L_s \vec{i}_{qds} + L_M (\vec{i}_{qds} + \vec{i}'_{qdr}) \quad (3.25)$$

and

$$\vec{\lambda}'_{qdr} = L'_r \vec{i}'_{qdr} + L_M (\vec{i}_{qds} + \vec{i}'_{qdr}). \quad (3.26)$$

For completeness the zero sequence quantities can be included here but, as mentioned in the previous section they can generally be neglected due to the connection of the induction machine. The zero sequence components are exactly the same in the complex space vector representation as they are in the $qd0$ representation, equations (3.14) through (3.17) of the induction machine model. So for the zero sequence quantities we have

$$v_{0s} = r_s i_{0s} + \frac{d}{dt} \lambda_{0s} \quad (3.27)$$

and

$$v'_{0r} = r'_r i'_{0r} + \frac{d}{dt} \lambda'_{0r}. \quad (3.28)$$

where $\lambda_{0s} = L_s i_{0s}$ and $\lambda'_{0r} = L'_r i'_{0r}$ are the zero sequence flux linkages in the stator and rotor circuits, respectively. It is important to note here that the zero sequence quantities are not complex vectors but strictly real quantities. Figure 3.5 shows the equivalent circuit of the complex space vector representation of the doubly-fed induction machine including the zero sequence components of the model.

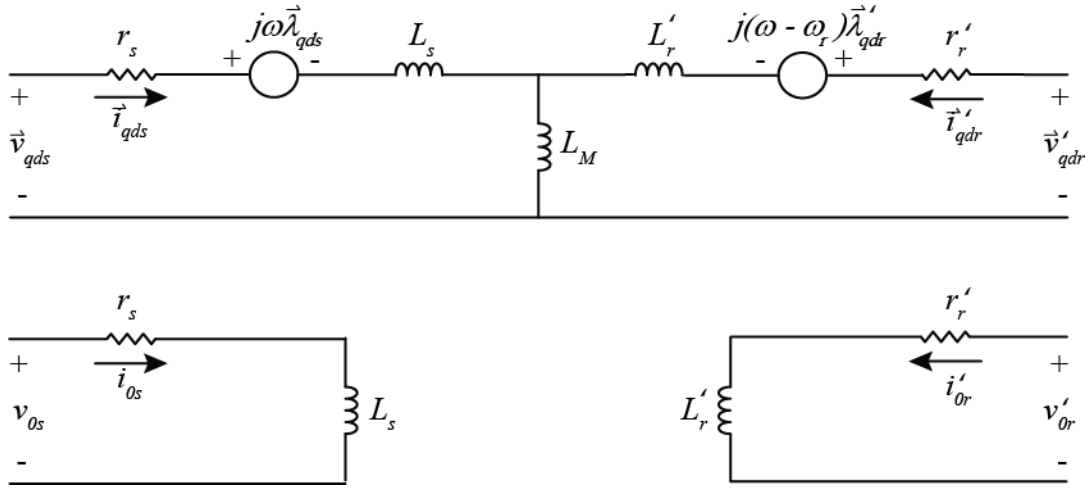


Figure 3.5 Complex Space Vector equivalent circuit of 3-phase induction machine

We now need to express the electrical torque developed in the machine in terms of the complex space vectors that have been defined. We know that the electrical torque is a real quantity so we need to manipulate the complex space vector quantities involved to give us the electrical torque in the same form as equation (3.18) which is defined in terms of the qd axis quantities. This can be done by multiplying the complex conjugate of the stator flux space vector with the stator current space vector;

$$\begin{aligned} \vec{\lambda}_{qds}^* \vec{i}_{qds} &= (\lambda_{qs} + j\lambda_{ds})(i_{qs} - ji_{ds}) \\ &= \lambda_{qs}i_{qs} + \lambda_{ds}i_{ds} + j(\lambda_{ds}i_{qs} - \lambda_{qs}i_{ds}) \end{aligned} \quad (3.29)$$

It can be seen that the imaginary part of equation (3.29) is of the form that we need to express the electrical torque developed in the machine. That is, we can express the electrical torque developed in the machine using the complex space vector quantities by taking only the imaginary part of equation (3.29) as follows.

$$T_e = \left(\frac{3}{2}\right) \left(\frac{P}{2}\right) \mathcal{Im}\{ \vec{\lambda}_{qds}^* \vec{i}_{qds} \} \quad (3.30)$$

It is important to note here that there are other ways to express the electromagnetic torque developed in the machine using different circuit quantities. Many of these are outline by Novotny [47]. The reason that the electromagnetic torque was chosen to be represented in terms of the stator circuit flux linkage and current is due to its independence of the magnetizing inductance L_M . The advantage of this will become more apparent in our discussion of induction machine saturation in Chapter 4.

The mechanical equation for the complex space vector model is identical to that of the previous models as the quantities involved are all real valued quantities and so again we can express the equation for the mechanical and electric torque coupling as

$$T_e - T_m - K_{fric} \omega_{rm} = J \frac{d\omega_{rm}}{dt} = J \frac{2}{P} \frac{d\omega_r}{dt}. \quad (3.31)$$

3.2 Dynamic Phasor Model of Doubly-Fed Induction Machine

We are now at a point where we can apply the concepts of dynamic phasors that were presented in Chapter 2 to the induction machine model. The dynamic phasor model of the

doubly-fed induction machine can be developed by applying equation (2.25) to the complex space vector quantities presented in Section 3.1.3. It is again noted here that there are only positive and negative sequence components present and the zero sequence quantities are equal to zero. Applying equation (2.25) to the stator voltage equation (3.23) we get the stator circuit quantities expressed in terms of dynamic phasors.

$$\begin{aligned}
\underline{V}_{ps}e^{j\omega_s t} + \underline{V}_{ns}^*e^{-j\omega_s t} \\
= r_s(\underline{I}_{ps}e^{j\omega_s t} + \underline{I}_{ns}^*e^{-j\omega_s t}) + \frac{d}{dt}(\underline{\Lambda}_{ps}e^{j\omega_s t} + \underline{\Lambda}_{ns}^*e^{-j\omega_s t}) \\
+ j\omega(\underline{\Lambda}_{ps}e^{j\omega_s t} + \underline{\Lambda}_{ns}^*e^{-j\omega_s t})
\end{aligned} \tag{3.32}$$

If the differentiation in equation (3.32) is carried out and like terms are separated, we get the dynamic phasor equations for the stator voltage of the induction machine dynamic phasor model.

$$\begin{aligned}
\underline{V}_{ps} &= r_s\underline{I}_{ps} + \frac{d}{dt}\underline{\Lambda}_{ps} + j(\omega + \omega_s)\underline{\Lambda}_{ps} \\
\underline{V}_{ns}^* &= r_s\underline{I}_{ns}^* + \frac{d}{dt}\underline{\Lambda}_{ns}^* + j(\omega - \omega_s)\underline{\Lambda}_{ns}^*
\end{aligned} \tag{3.33}$$

where

$$\begin{aligned}
\underline{\Lambda}_{ps} &= L_s\underline{I}_{ps} + L_M(\underline{I}_{ps} + \underline{I}_{pr}) \\
\underline{\Lambda}_{ns}^* &= L_s\underline{I}_{ns}^* + L_M(\underline{I}_{ns}^* + \underline{I}_{nr}^*)
\end{aligned} \tag{3.34}$$

For the rotor circuit we have to consider the second harmonic of the rotor speed due to the torque ripple that is introduced into the machine during unbalanced operating conditions. The second harmonic torque ripple that is introduced into the system can be easily verified by doing a simple observation during simulation of the time domain models. For example,

Figure 3.6 illustrates the simulation of a typical 500 hp induction machine under a single phase unbalanced fault condition. It can be observed that under these circumstances a second harmonic ripple is introduced into the electromagnetic torque produced in the machine which in turn causes the rotor speed to have a small second harmonic torque ripple as well.

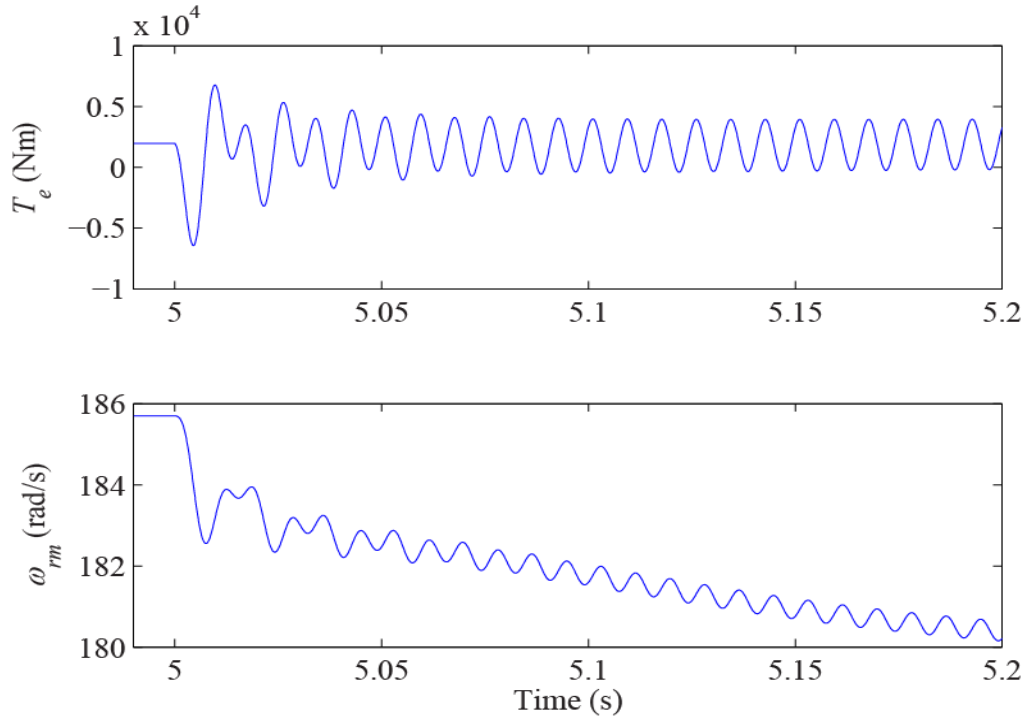


Figure 3.6 Torque and speed ripple during unbalanced machine operation

The torque ripple caused by unbalanced operating conditions is taken into account by considering both the dc component of the rotor speed and its second harmonic dynamic phasor, which are expressed as $\underline{\Omega}_{r,0}$ and $\underline{\Omega}_{r,2}$ respectively. It is important to note here that in this case $\underline{\Omega}_{r,0}$ is real valued but for the sake of consistency it is expressed as a dynamic phasor. Applying equation (2.25) to the rotor voltage space vector equation (3.24) and taking into account the second harmonic dynamic phasor of the rotor speed we get

$$\begin{aligned}
& \underline{V}_{pr} e^{j\omega_s t} + \underline{V}_{nr}^* e^{-j\omega_s t} \\
&= r_r' (\underline{I}_{pr} e^{j\omega_s t} + \underline{I}_{nr}^* e^{-j\omega_s t}) + \frac{d}{dt} (\underline{\Lambda}_{pr} e^{j\omega_s t} + \underline{\Lambda}_{nr}^* e^{-j\omega_s t}) \\
&+ j(\omega - \underline{\Omega}_{r,0} - \underline{\Omega}_{r,2} e^{j2\omega_s t} - \underline{\Omega}_{r,2}^* e^{-j2\omega_s t}) (\underline{\Lambda}_{pr} e^{j\omega_s t} \\
&+ \underline{\Lambda}_{nr}^* e^{-j\omega_s t})
\end{aligned} \tag{3.35}$$

Which, after expanding and separating like terms we can get the dynamic phasor equations of the rotor circuit voltage.

$$\begin{aligned}
\underline{V}_{pr} &= r_r' \underline{I}_{pr} + \frac{d}{dt} \underline{\Lambda}_{pr} + j(\omega + \omega_s - \underline{\Omega}_{r,0}) \underline{\Lambda}_{pr} - j2\underline{\Omega}_{r,2} \underline{\Lambda}_{nr}^* \\
\underline{V}_{nr}^* &= r_r' \underline{I}_{nr}^* + \frac{d}{dt} \underline{\Lambda}_{nr}^* + j(\omega - \omega_s - \underline{\Omega}_{r,0}) \underline{\Lambda}_{nr}^* - j2\underline{\Omega}_{r,2}^* \underline{\Lambda}_{pr}
\end{aligned} \tag{3.36}$$

where

$$\begin{aligned}
\underline{\Lambda}_{pr} &= L_r' \underline{I}_{pr} + L_M (\underline{I}_{ps} + \underline{I}_{pr}) \\
\underline{\Lambda}_{nr}^* &= L_r' \underline{I}_{nr}^* + L_M (\underline{I}_{ns}^* + \underline{I}_{nr}^*)
\end{aligned} \tag{3.37}$$

Note here that the prime symbol has been removed from the dynamic phasor rotor quantities to avoid clutter in the equations. However, they still represent rotor quantities that have been referred to the stator side circuit.

Figure 3.7 shows the dynamic phasor equivalent circuit of the 3-phase doubly-fed induction machine. Notice here that the zero sequence components of the induction machine have been neglected for reasons outlined in the previous sections of this chapter.

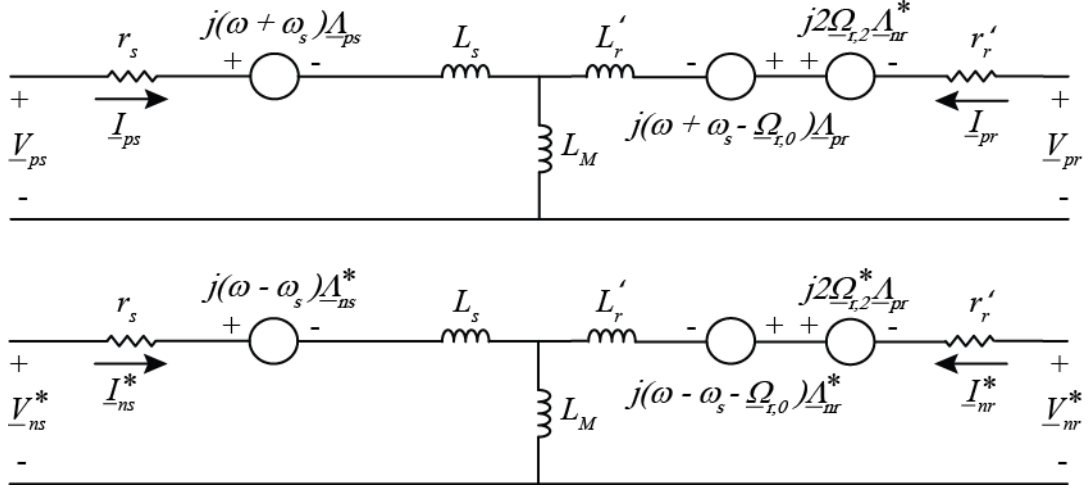


Figure 3.7 Dynamic phasor equivalent circuit of 3-phase induction machine

For the electromagnetic torque developed in the machine we have to also consider the second harmonic dynamic phasor as explained above. If we now apply equation (2.25) to the complex space vector equation (3.30) and take into account the second harmonic dynamic phasor to account for torque ripple we get the following equation for the electromagnetic torque developed in the machine in terms of dynamic phasors.

$$\begin{aligned}
 \underline{T}_{e,0} + \underline{T}_{e,2}e^{j2\omega_s t} + \underline{T}_{e,2}^*e^{-j2\omega_s t} \\
 = \left(\frac{3P}{4}\right) \mathcal{Im}\{(\underline{A}_{ps}^*e^{-j\omega_s t} + \underline{A}_{ns}e^{j\omega_s t})(\underline{I}_{ps}e^{j\omega_s t} + \underline{I}_{ns}^*e^{-j\omega_s t})\}
 \end{aligned} \tag{3.38}$$

Expanding out the equation (3.38) and collecting like terms we get dynamic phasor equations for the dc and second harmonic components of the electromagnetic torque developed in the machine.

$$\begin{aligned}
\underline{T}_{e,0} &= \left(\frac{3P}{4}\right) \mathcal{I}m\{\underline{\Lambda}_{ps}^* \underline{I}_{ps} + \underline{\Lambda}_{ns} \underline{I}_{ns}^*\} \\
\underline{T}_{e,2} &= \frac{3P}{j8} (\underline{\Lambda}_{ns} \underline{I}_{ps} - \underline{\Lambda}_{ps} \underline{I}_{ns})
\end{aligned} \tag{3.39}$$

To couple the electrical quantities to the mechanical quantities we can express the mechanical equation for the doubly-fed induction machine in terms of dynamic phasors as follows.

$$\begin{aligned}
J \frac{d}{dt} (\underline{\Omega}_{rm,0} + \underline{\Omega}_{rm,2} e^{j2\omega_s t}) \\
= (\underline{T}_{e,0} + \underline{T}_{e,2} e^{j2\omega_s t}) - T_m - K_{fric} (\underline{\Omega}_{rm,0} + \underline{\Omega}_{rm,2} e^{j2\omega_s t})
\end{aligned} \tag{3.40}$$

Which can be expanded and separated into like terms and finally we get the dynamic phasor equations for the dc and second harmonic components of the mechanical rotor speed as follows.

$$\begin{aligned}
J \frac{d}{dt} \underline{\Omega}_{rm,0} &= \left(\frac{3P}{4}\right) \mathcal{I}m\{\underline{\Lambda}_{ps}^* \underline{I}_{ps} + \underline{\Lambda}_{ns} \underline{I}_{ns}^*\} - T_m - K_{fric} \underline{\Omega}_{rm,0} \\
J \frac{d}{dt} \underline{\Omega}_{rm,2} &= \frac{3P}{j8} (\underline{\Lambda}_{ns} \underline{I}_{ps} - \underline{\Lambda}_{ps} \underline{I}_{ns}) - (K_{fric} + j2J\omega_s) \underline{\Omega}_{rm,2}
\end{aligned} \tag{3.41}$$

As in the previous induction machine models the rotor mechanical speed and the rotor electrical speed are related by the number of electromagnetic poles in the machine.

$$\begin{aligned}
\underline{\Omega}_{r,0} &= \frac{P}{2} \underline{\Omega}_{rm,0} \\
\underline{\Omega}_{r,2} &= \frac{P}{2} \underline{\Omega}_{rm,2}
\end{aligned} \tag{3.42}$$

We now have all of the dynamic phasor equations needed in order to implement the model and verify that it is representative of the induction machine dynamic behavior.

3.3 Model Verification

A series of tests are carried out in this section to verify that the dynamic phasor model is representative of the time domain electromagnetic transient model with considerable accuracy. The studies are carried out to represent different operating conditions and transient events to illustrate the behavior of the doubly-fed induction machine. These studies are carried out on a typical 500 hp induction machine with the machine parameters listed in Appendix A.

The studies that are carried out cover a range of operating circumstances that might typically be faced by an induction machine. These studies include; machine start-up from standstill; a change in mechanical torque; balanced voltage dips; and unbalanced voltage dips. These operating studies are carried out in the following sub-sections.

For comparison, the dynamic phasor model of the induction machine is compared to the $dq0$ induction machine model to verify its accuracy. This is done by simulating both models using a very small time step to show that the dynamic phasor model results converge to the well know $dq0$ model results. The time-step used throughout the model verification studies in the following sub-sections is $\Delta t = 50 \mu s$. Also, a stationary reference frame, $\omega = 0$, is used in both the $dq0$ induction machine model and the dynamic phasor induction machine model.

3.3.1 Free Acceleration of Induction Machine

The model verification begins at time $t=0$ s when a rated voltage of 2300 V_{L-L} is applied to the motor which is allowed to accelerate freely from standstill. The resulting waveforms for the stator phase a current i_a , electromagnetic torque T_e and the mechanical rotor speed ω_{rm} are illustrated below in Figure 3.8, Figure 3.9 and Figure 3.10 respectively. These figures contain the time domain $dq0$ model quantities (EMT), the magnitude of the dynamic phasor quantities (DP) as well as the time domain result obtained using the dynamic phasor quantities (DP-EMT).

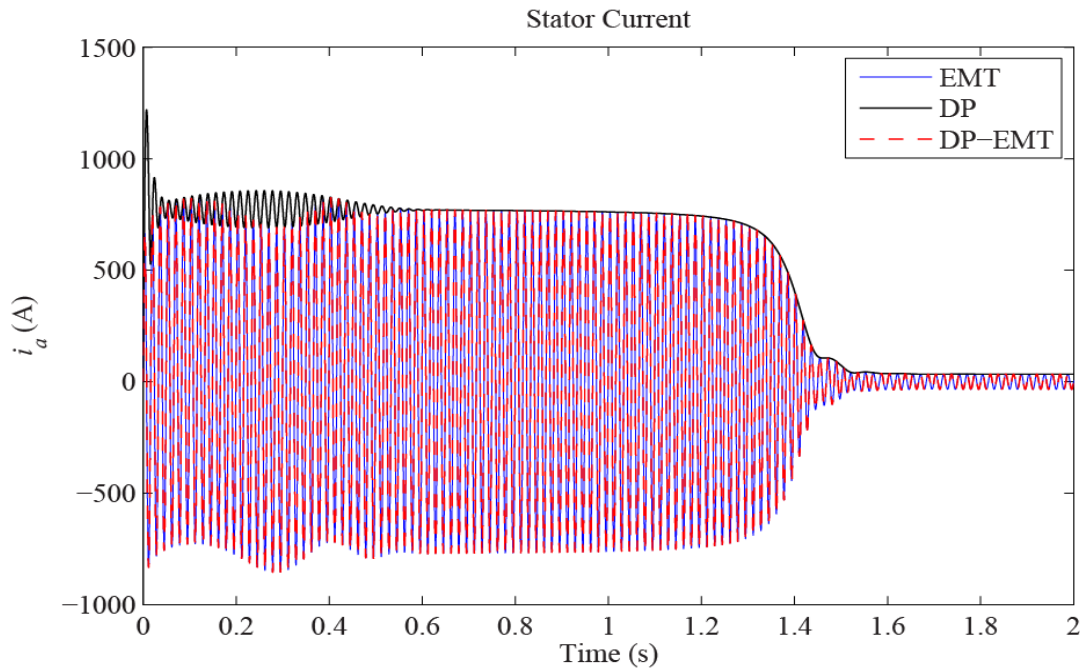


Figure 3.8 Stator current during free acceleration ($\Delta t=50\mu s$)

In Figure 3.8 it is observed the time domain result obtained using the dynamic phasor quantities matches very accurately the results obtained using the time domain $dq0$ induction machine model. Also, the magnitude of the dynamic phasor quantity illustrates that it acts as

an envelope for the time domain waveform. This can be advantageous in model simulations where current magnitudes are being studied and the actual details of the time domain waveforms are not the main focus of the study. For example, when one wants to determine the starting current magnitude of the induction machine, the dynamic phasor model can provide such information without having to determine all of the information of the time domain waveform.

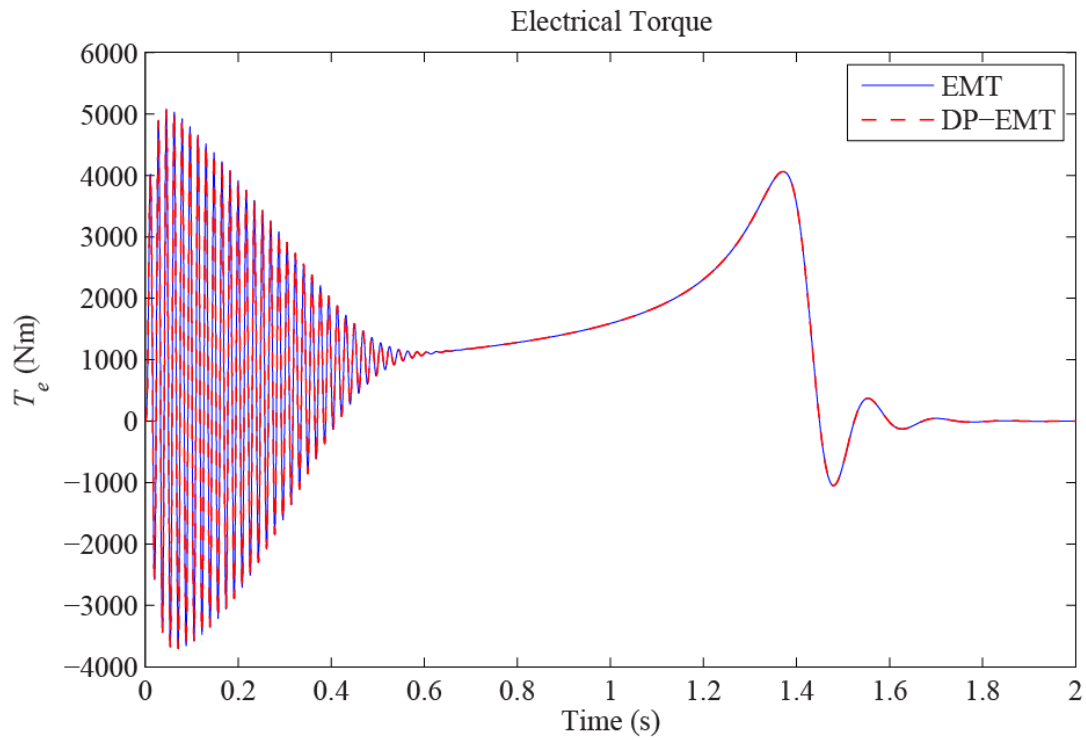


Figure 3.9 Electrical torque during free acceleration ($\Delta t=50\mu s$)

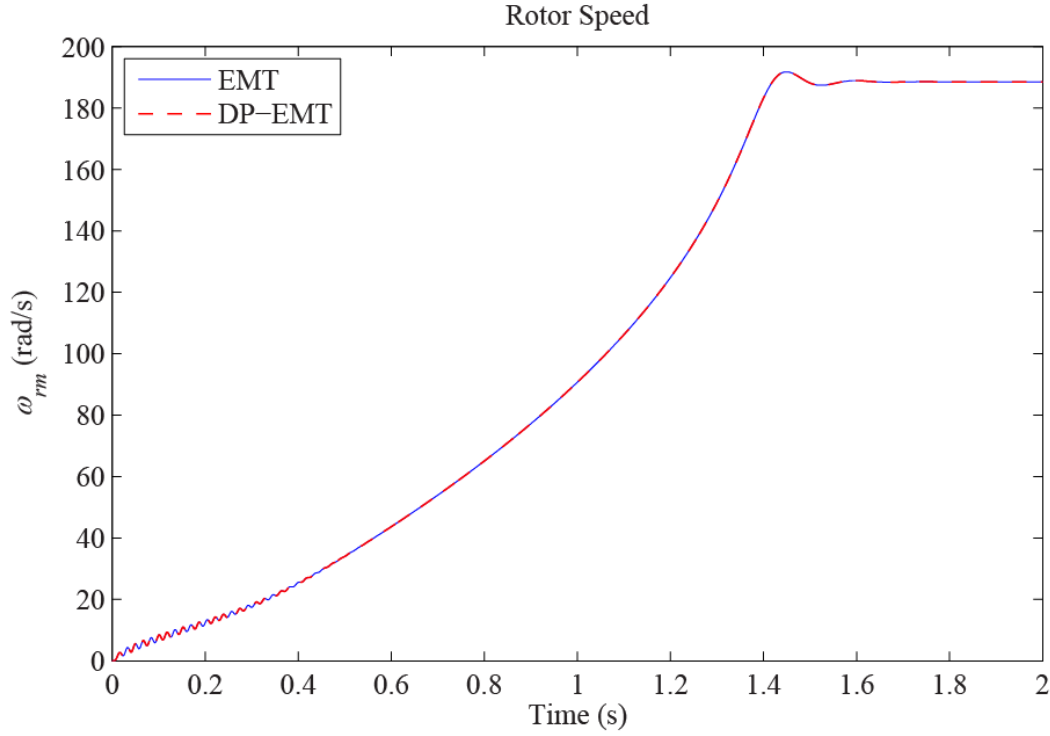


Figure 3.10 Rotor speed during free acceleration ($\Delta t=50\mu s$)

For the electromagnetic torque and the rotor mechanical speed in Figure 3.9 and Figure 3.10 respectively, the dynamic phasor quantity is identical to the time domain result obtained by the dynamic phasor quantity. This is because under balanced operating conditions only the dc component of the electromagnetic torque and rotor speed is present and as mentioned previously, the dc components of these quantities are strictly real and contain no imaginary component. It is also observed that these quantities match with considerable accuracy the results obtained using the $dq0$ induction machine model.

3.3.2 Mechanical Torque Change

At time $t=2.5s$ a rated motoring torque of 1980 Nm is applied to the motor and then at $t=3s$ the torque is reversed to a rated load torque. The same quantities that were plotted in the

previous study are again plotted here in Figure 3.11, Figure 3.12 and Figure 3.13 depicting the dynamic phasor magnitudes and both of the time domain results obtained using the dynamic phasor quantities and the $dq0$ induction machine model. It is observed that again the time domain result obtained using the dynamic phasor quantities represents very well the results obtained using the $dq0$ induction machine model and that the magnitudes of the dynamic phasor quantity in Figure 3.11 acts as an envelope to the time domain waveform.

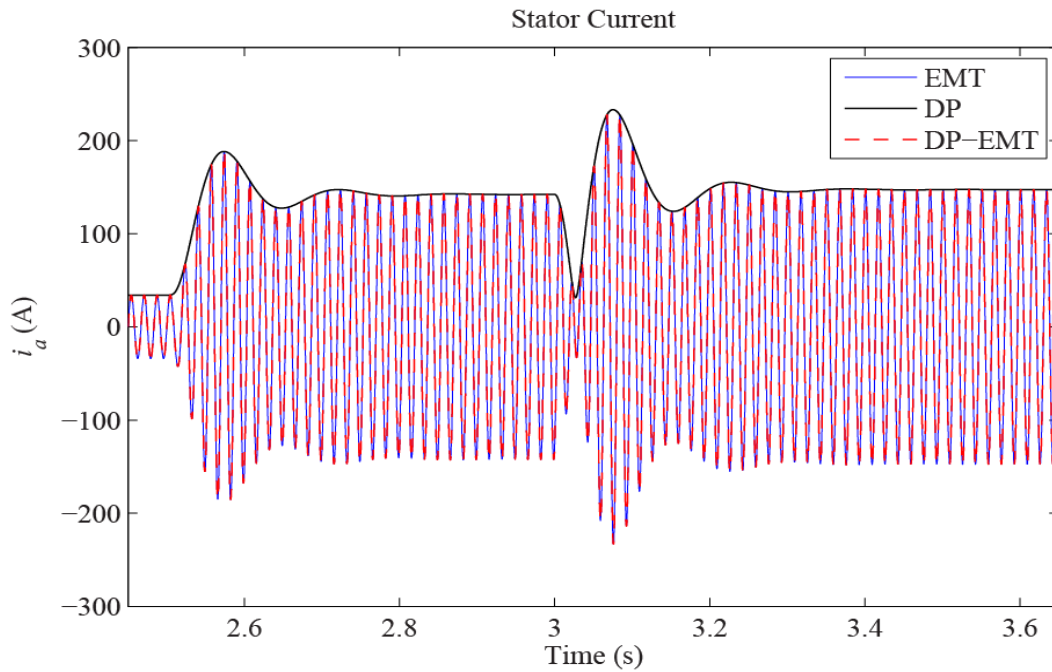


Figure 3.11 Stator current during mechanical torque change ($\Delta t=50\mu s$)

Again, the electromagnetic torque developed in the machine and the rotor mechanical speed contain only the dc component of the dynamic phasor as the machine is operating under balanced conditions where no second harmonic torque component is developed. The time domain result is also accurately represented as illustrated in Figure 3.12 and Figure 3.13 for both the torque and rotor speed respectively.

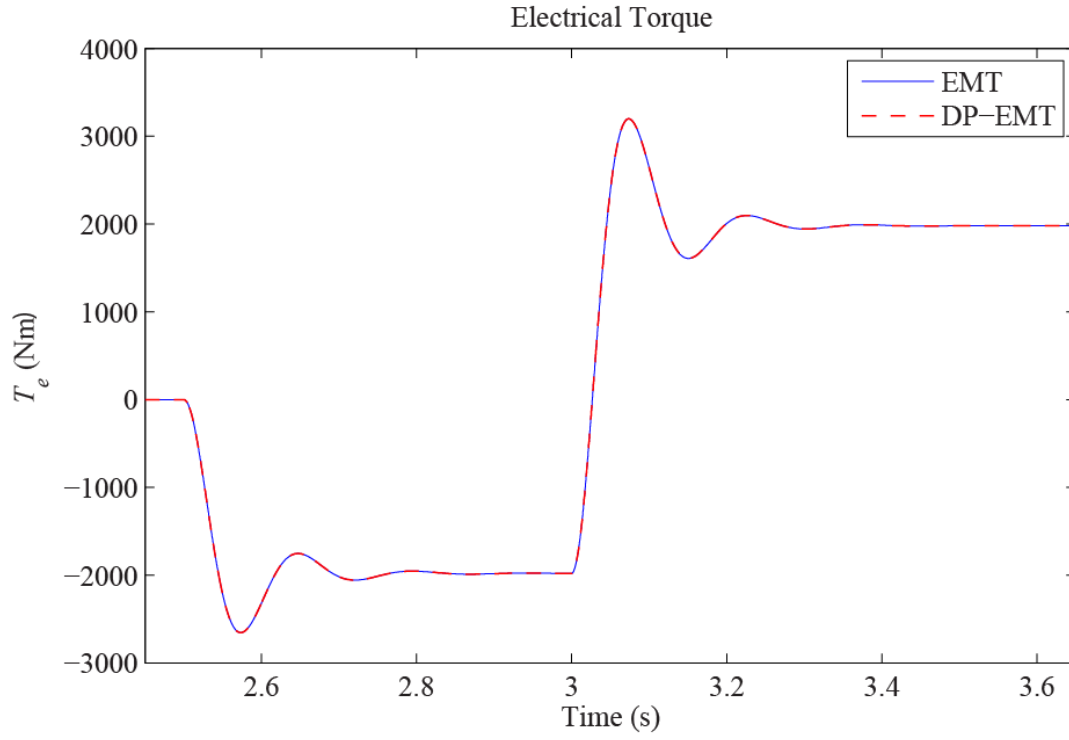


Figure 3.12 Electrical torque during mechanical torque change ($\Delta t=50\mu s$)

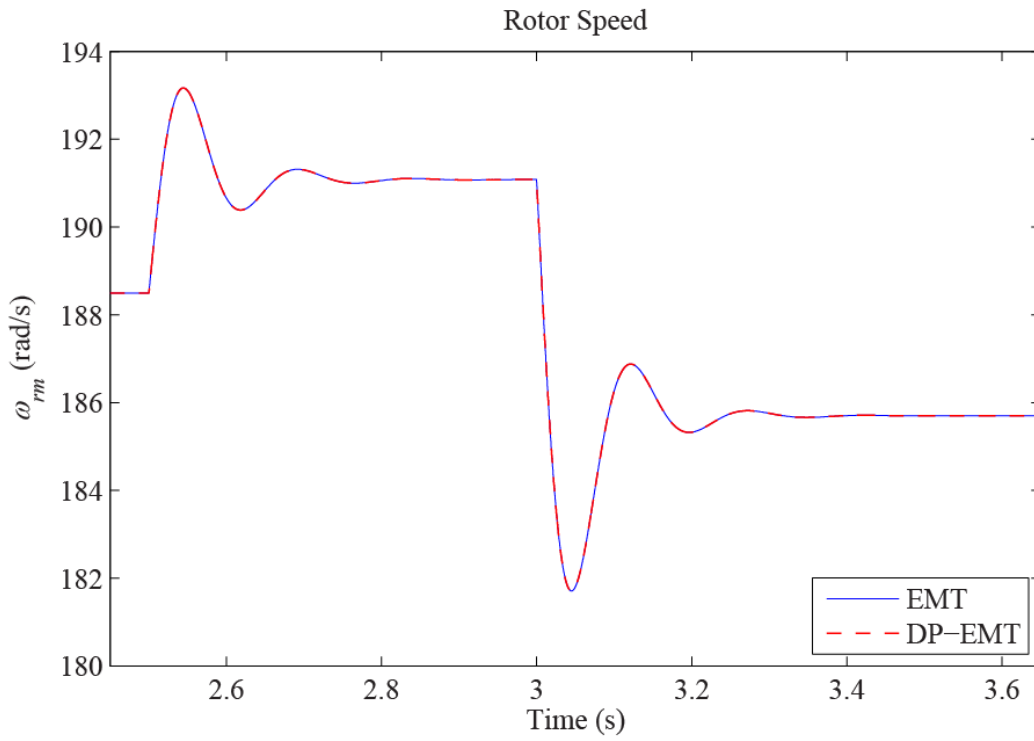


Figure 3.13 Rotor speed during mechanical torque change ($\Delta t=50\mu s$)

3.3.3 Balanced 3-phase Voltage Dip

At time $t=4\text{s}$ of the simulation a balanced 30% voltage dip is applied to the terminals of the machine for 6 cycles and then cleared. The resulting phase a current, electromagnetic torque and rotor mechanical speed quantities are plotted below in Figure 3.14, Figure 3.15 and Figure 3.16, respectively. Again, it is observed that the dynamic phasor model results match the $dq0$ model results with considerable accuracy and the magnitude of the dynamic phasor current quantity provides an accurate representation of the envelope of the time domain current waveform.

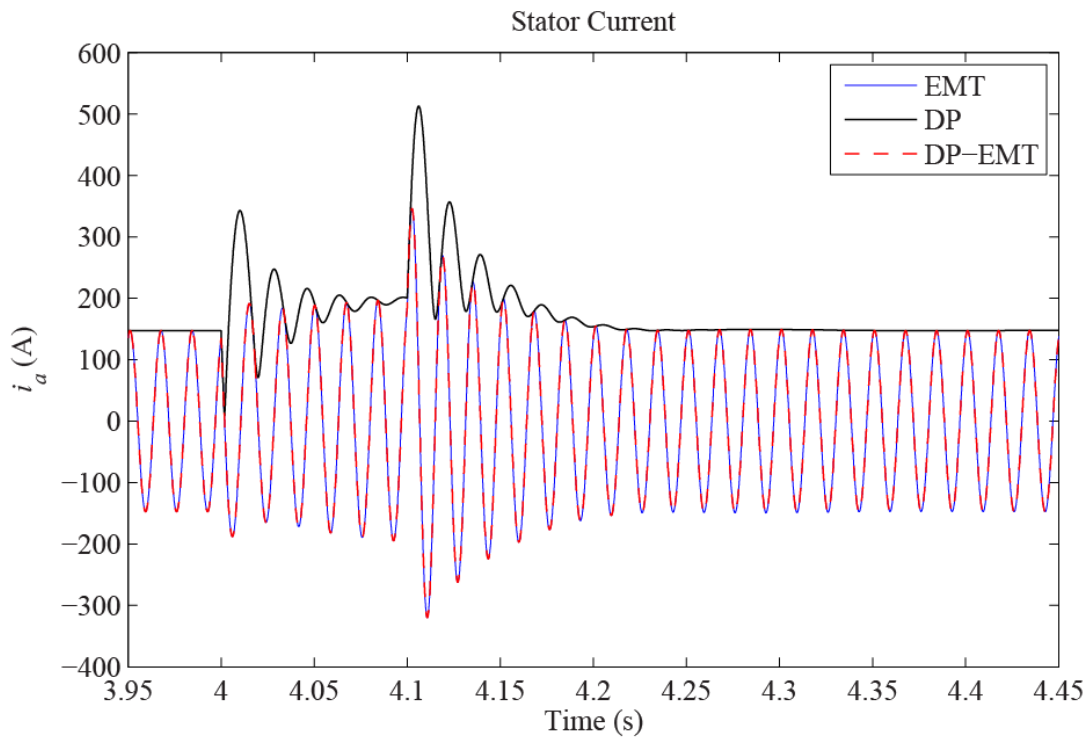


Figure 3.14 Stator current during balanced 3-phase voltage dip ($\Delta t=50\mu\text{s}$)

Under balanced operation again, the electromagnetic torque developed in the machine as well as the rotor mechanical speed contain only the dc component as mentioned previously.

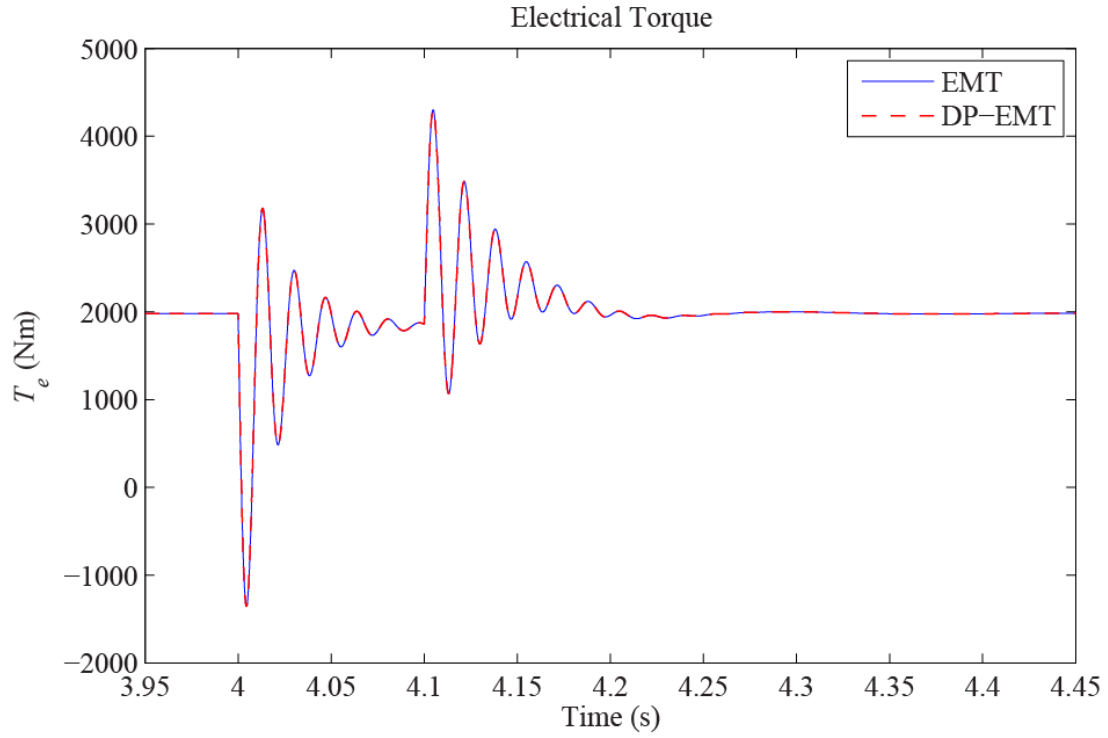


Figure 3.15 Electrical torque during balanced 3-phase voltage dip ($\Delta t=50\mu s$)

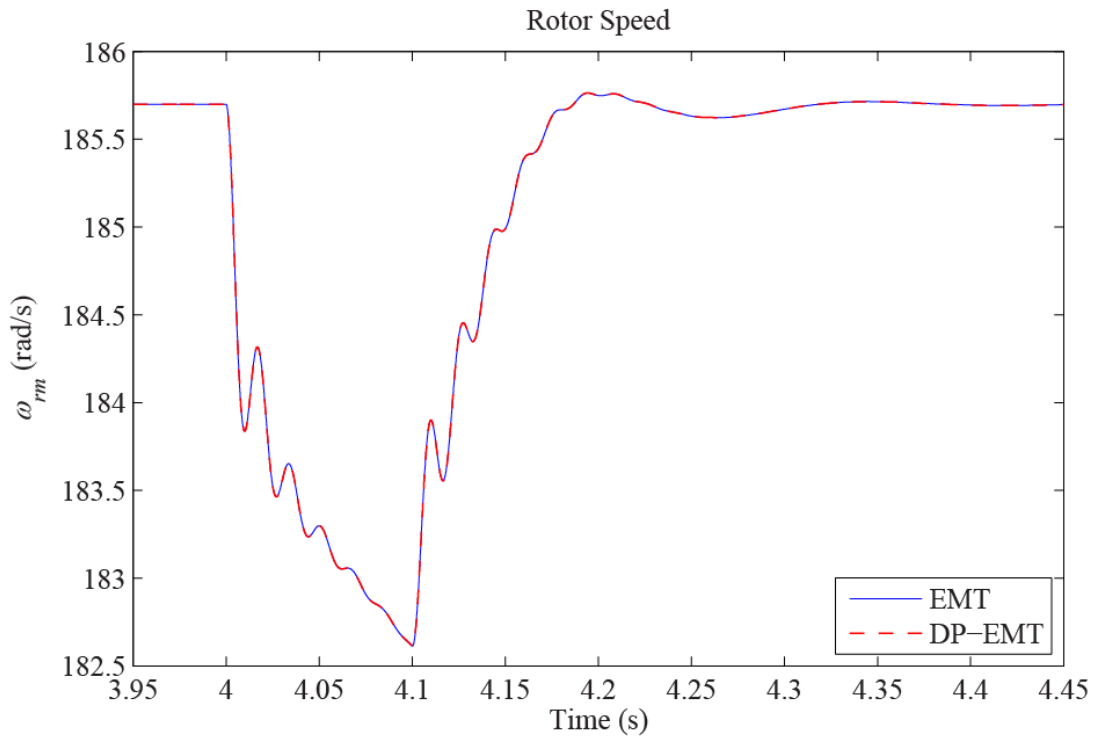


Figure 3.16 Rotor speed during balanced 3-phase voltage dip ($\Delta t=50\mu s$)

3.3.4 Unbalanced Single Line-to-Ground Fault

At time $t=5\text{s}$ an unbalanced single phase-to-ground fault is applied to the terminals of the machine and cleared after 6 cycles. In the case of an unbalanced fault we have both positive and negative sequence quantities in the machine. With the dynamic phasor model the positive and negative sequence dynamic phasors are treated separately and can therefore be studied separately. For example, Figure 3.17 and Figure 3.18 show the real and imaginary parts of the positive and negative sequence stator current dynamic phasors respectively.

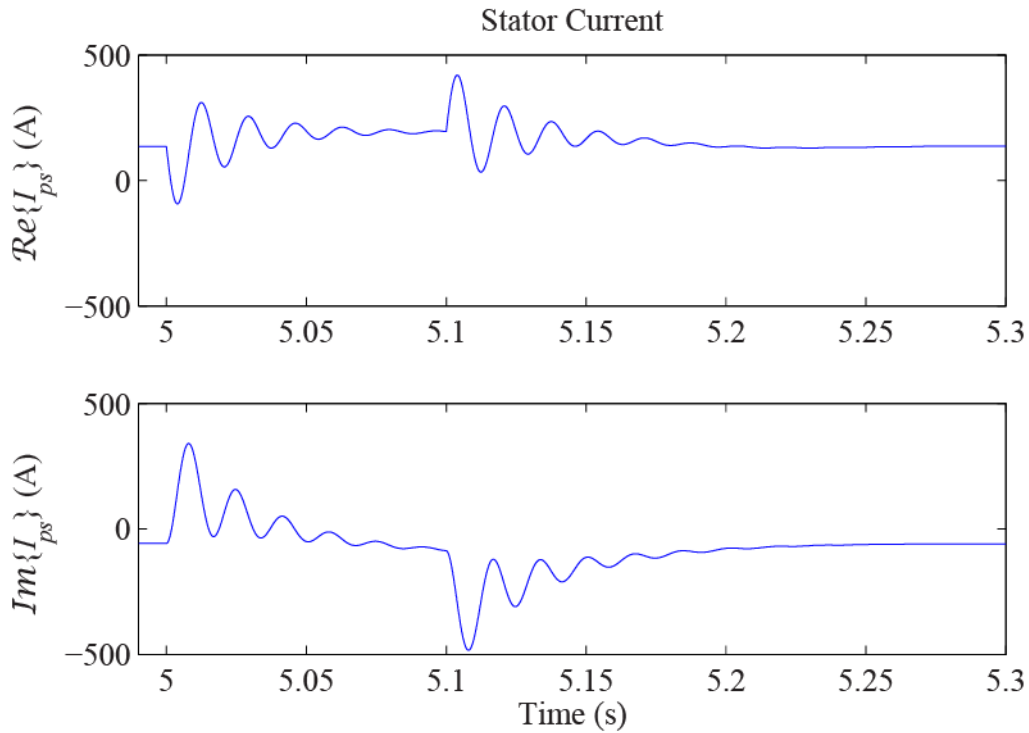


Figure 3.17 Real and imaginary parts of positive sequence stator current dynamic phasor

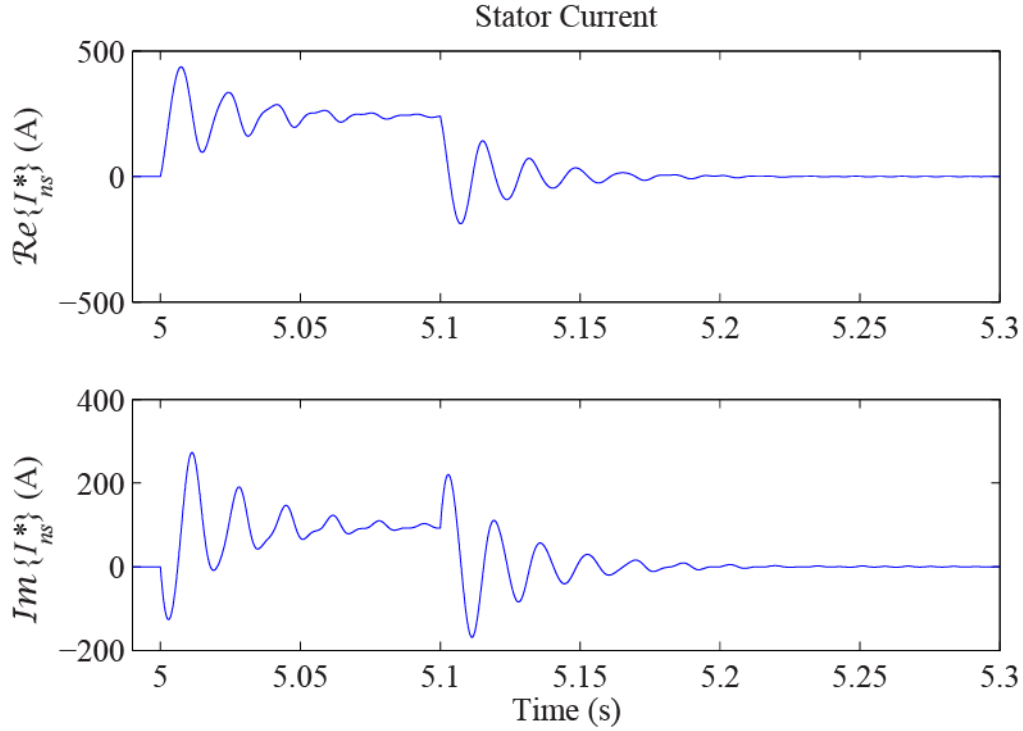


Figure 3.18 Real and imaginary parts of negative sequence stator current dynamic phasor

Using equations (2.21) and (2.25) the dynamic phasors can be combined to form the time domain result for the stator current as illustrated below in Figure 3.19. This figure also illustrates the comparison between the $qd0$ model results (EMT), the time domain results obtained from the dynamic phasor model (DP-EMT) and the magnitude of the current envelope using the dynamic phasor model (DP).

When an unbalanced fault is introduced to the system it brings with it a slight error that propagates through the model as well. This error is difficult to notice in Figure 3.19 but becomes more apparent in the plot of the mechanical rotor speed in Figure 3.25. It is believed that this error is introduced to the model not by the introduction of the negative sequence current dynamic phasor but from the lack of higher frequency components that are not taken

into account during the transient period of the simulation as mentioned by Stankovic [31] and explained in greater detail by Sanders [45]. The introduction of these higher harmonics during switching transients and other events would increase the accuracy of the dynamic phasor model however the complexity of the model would greatly increase as well. Further investigation is required however, as the errors do not occur in any of the balanced operating conditions and seem to be introduced into the model only when unbalanced operating conditions are introduced to the model. The source of the errors was not definitively located in the model and requires further investigation at the time that this thesis was written.

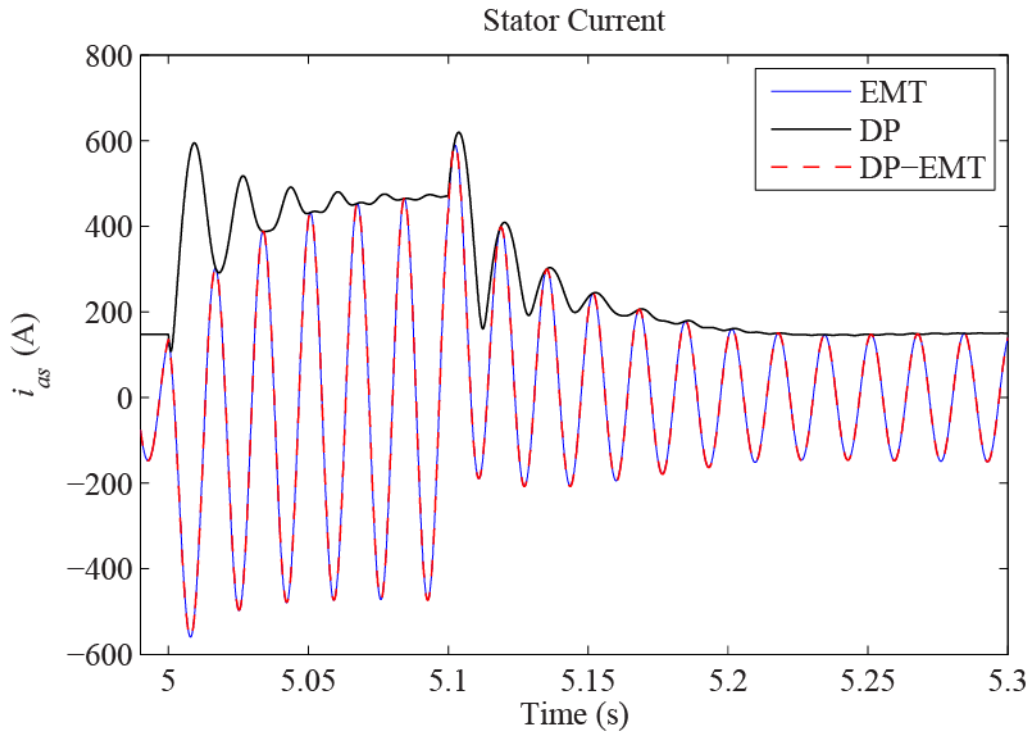


Figure 3.19 Stator current during unbalanced fault ($\Delta t=50\mu s$)

As in the case of current dynamic phasors, the electromagnetic torque produced in the model as well as the rotor mechanical speed are analyzed as separate harmonic dynamic phasors.

The difference in these cases is that these quantities in this particular model contain only the dc component and 2nd harmonic dynamic phasors as mentioned in the previous section.

Figure 3.20 and Figure 3.21 respectively show the dc component and the real and imaginary components of the 2nd harmonic electromagnetic torque dynamic phasor developed in the machine model. These quantities can be recombined using the dynamic phasor equation (2.5) with $K = \{0,2\}$. Note here that electromagnetic torque is a real valued quantity so we have $\underline{T}_{e,-2} = \underline{T}_{e,2}^*$ so we can obtain the time domain result as $T_e = \underline{T}_{e,0} + 2\text{Re}\{\underline{T}_{e,2}e^{j2\omega_s t}\}$. The time domain result for the electromagnetic torque is shown in Figure 3.22 along with the result obtained using the $dq0$ model result for comparison.

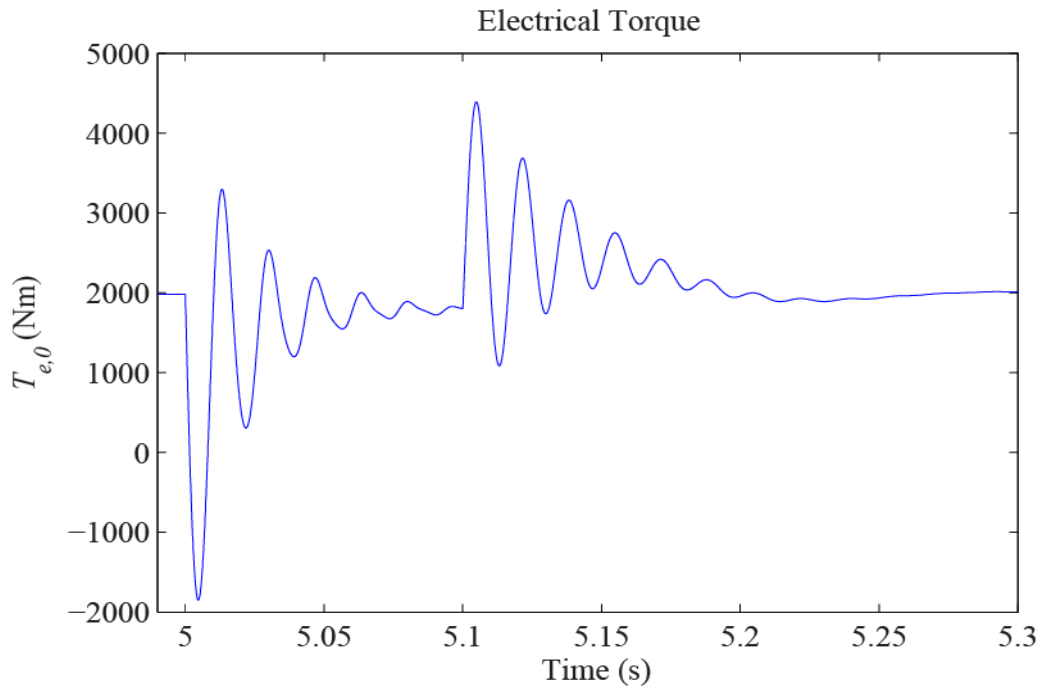


Figure 3.20 DC component of electrical torque dynamic phasor

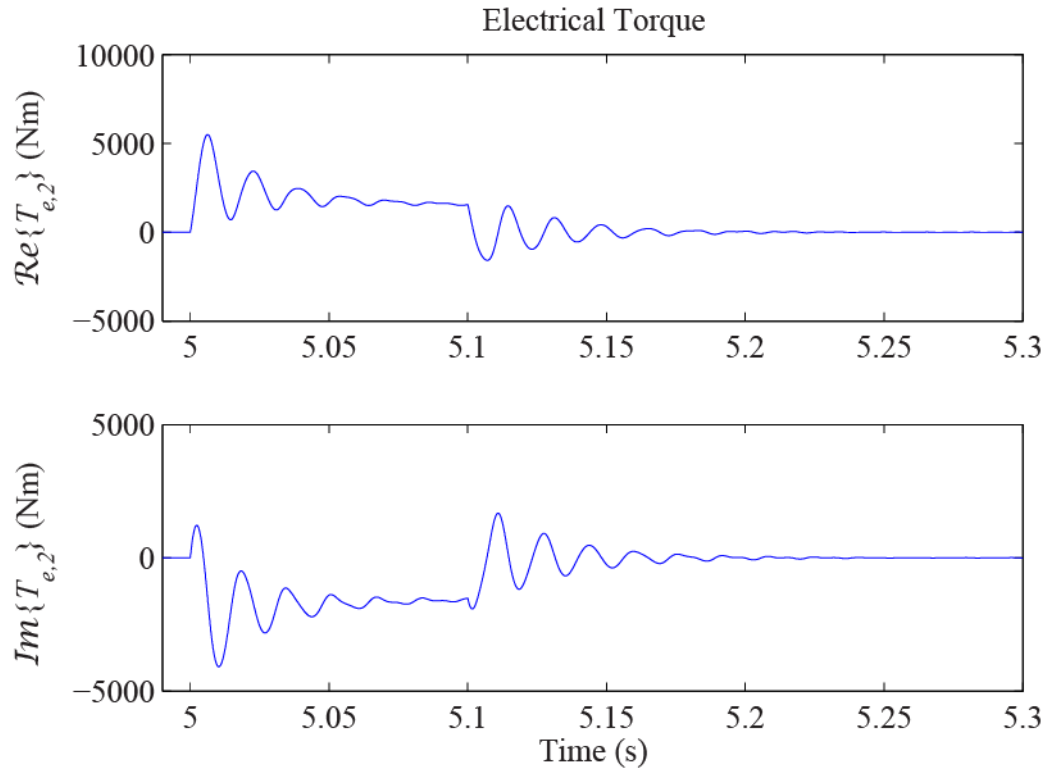


Figure 3.21 2nd harmonic component of electrical torque dynamic phasor

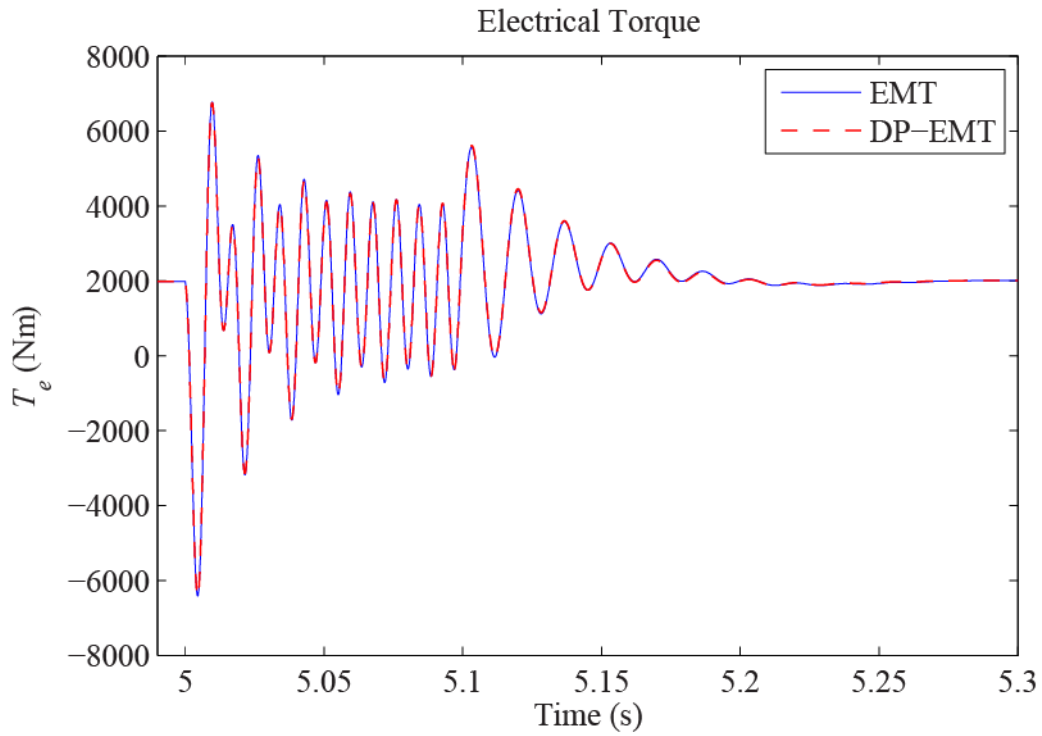


Figure 3.22 Electrical torque during unbalanced fault ($\Delta t=50\mu s$)

Similarly, the rotor speed is illustrated as its separate dynamic phasor components (dc, and 2nd harmonic) in Figure 3.23 and Figure 3.24, respectively. Also, as in the case of the electromagnetic torque, the mechanical rotor speed dynamic phasors can be combined to obtain the real valued time domain result using equation (2.5) with $K = \{0,2\}$. Doing this we get the time domain result for the mechanical rotor speed as $\omega_{rm} = \underline{\Omega}_{e,0} + 2\text{Re}\{\underline{\Omega}_{e,2}e^{j2\omega_st}\}$. The time domain result for the mechanical rotor speed is illustrated below in Figure 3.25 along with the results obtained using the $dq0$ model for comparison.

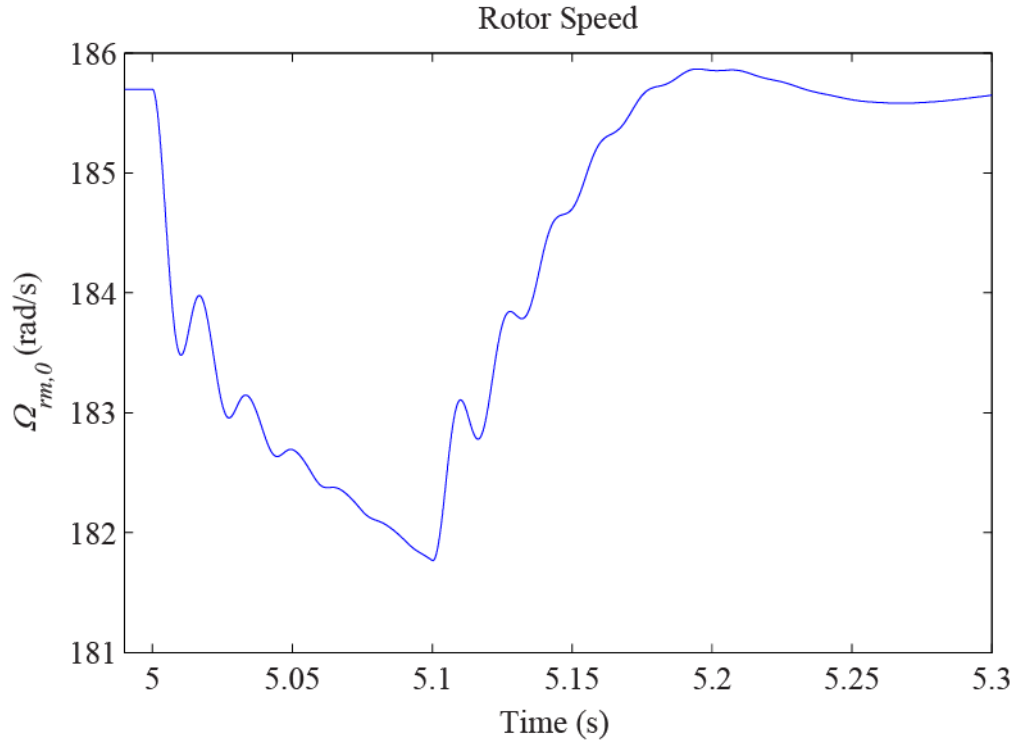


Figure 3.23 DC component of rotor speed dynamic phasor

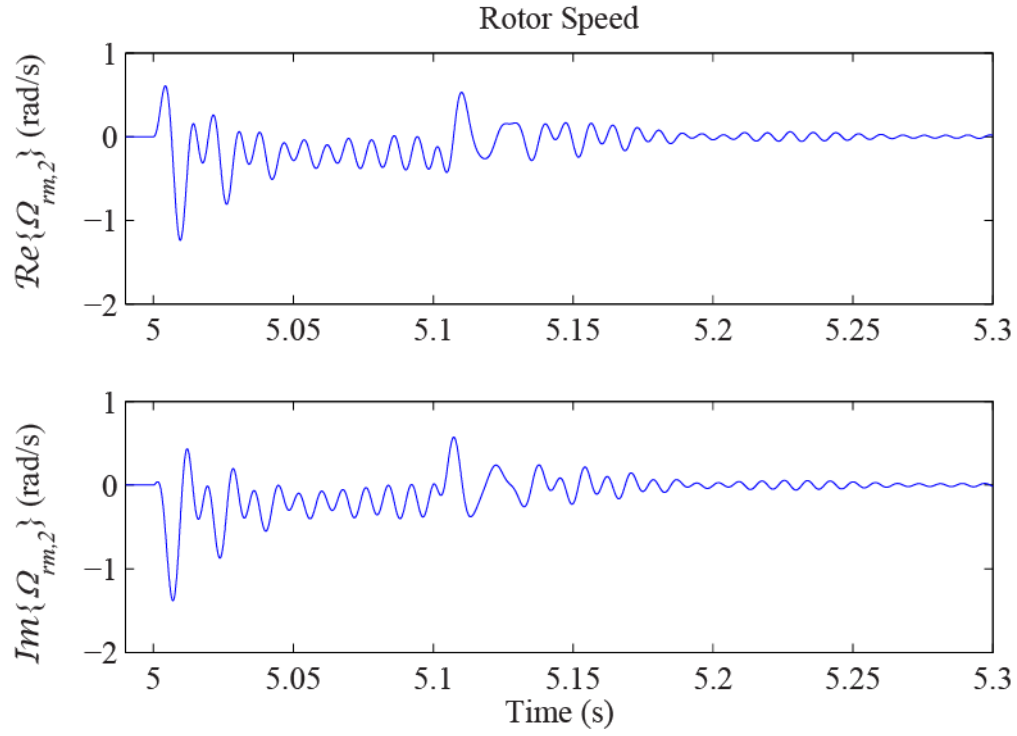


Figure 3.24 2nd harmonic component of rotor speed dynamic phasor

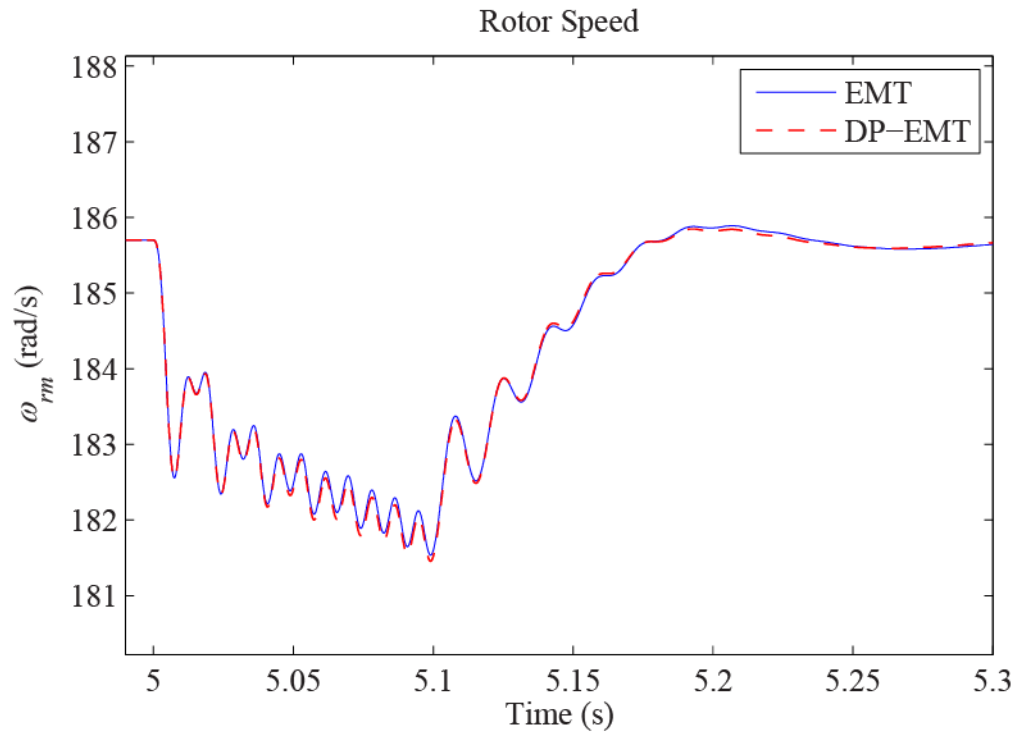


Figure 3.25 Rotor speed during unbalanced fault ($\Delta t=50\mu s$)

As mentioned previously, there is a slight error that is introduced in the results of the dynamic phasor model during unbalanced operating conditions. These errors introduced into the model were studied and the results are presented here in Table 3.1 which illustrates the maximum errors introduced into the model quantities both in absolute values and in percent error from the results obtained using the $dq0$ induction machine model. The maximum errors that are introduced into the model are quite small and are within $\pm 1.9\%$ and are well within range to validate the dynamic phasor model during unbalanced operating conditions.

Table 3.1 Maximum error introduced by dynamic phasor model

Variable	Maximum Absolute Error	Maximum Percent Error (%)
i_{as}	7.5162 (A)	1.8924
T_e	64.5221 (Nm)	1.4021
ω_{rm}	0.0987 (rad/s)	0.0541

Chapter 4: Modeling of Saturation in Induction Machines

4.1 Time Domain Modeling of Induction Machine Saturation

The induction machine models that were presented in Chapter 3 were based on the assumption that the main magnetizing flux linkage produced in the machine changed linearly with respect to the magnetizing branch current. In reality, the magnetizing flux does not follow such a linear relationship to the magnetizing current but instead starts to deviate from the linear relationship as the magnetizing current increases due to the effects of magnetic saturation in the induction machine [32-43]. Thus, there are some inaccuracies that occur in the models based on the linear magnetizing relationship. Saturation effects also occur in the leakage inductances present in each of the windings but are much more difficult to model so the analysis here will focus on saturation effects of the main magnetizing flux path. In order to produce a more accurate model the effects of saturation should be taken into account.

In induction machine modeling, saturation is often applied to the magnetizing flux as it takes into account the cross-saturation effects between the q - and d -axis of the machine [36, 49]. One method of modeling main flux linkage saturation is to apply a flux correction term to the magnetizing flux quantity known as magnetizing flux correction [49, 50]. Figure 4.1 illustrates the concept of the flux correction method. It depicts a typical saturation curve which is defined in terms of the magnitude of the magnetizing flux versus the magnitude of the magnetizing current. Along with the saturation curve there is also the linear relationship depicted along with the flux correction term $\Delta(\lambda_m)$.

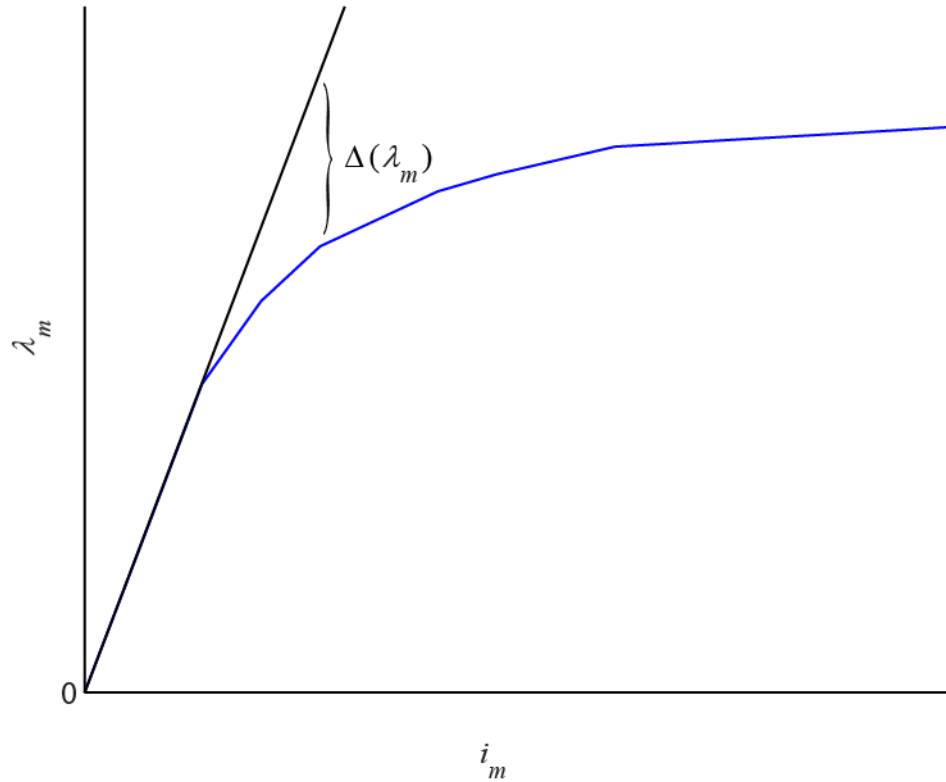


Figure 4.1 Typical magnetization curve of an induction machine

In the linear model the magnetizing flux is related to the magnetizing current by the magnetizing inductance $\lambda_m = L_m i_m$. We can correct this term to take into account the effects of saturation by subtracting the flux correction term from the linear model as follows.

$$\lambda_m = L_m i_m - \Delta(\lambda_m) \quad (4.1)$$

Solving the above equation for $\Delta(\lambda_m)$ we get

$$\Delta(\lambda_m) = L_m i_m - \lambda_m \quad (4.2)$$

We now need to express $\Delta(\lambda_m)$ in terms of qd quantities in order to implement it into the time domain $qd0$ induction machine model. Referring to Figure 4.2 and assuming again that

we are dealing with a symmetric induction machine we can express the magnetizing flux in the qd reference frame as follows.

$$\lambda_m = \sqrt{\lambda_{mq}^2 + \lambda_{md}^2} \quad (4.3)$$

And the qd quantities of $\Delta(\lambda_m)$ as

$$\begin{aligned} \Delta(\lambda_m)_q &= \frac{\lambda_{mq}}{\lambda_m} \Delta(\lambda_m) \\ \Delta(\lambda_m)_d &= \frac{\lambda_{md}}{\lambda_m} \Delta(\lambda_m) \end{aligned} \quad (4.4)$$

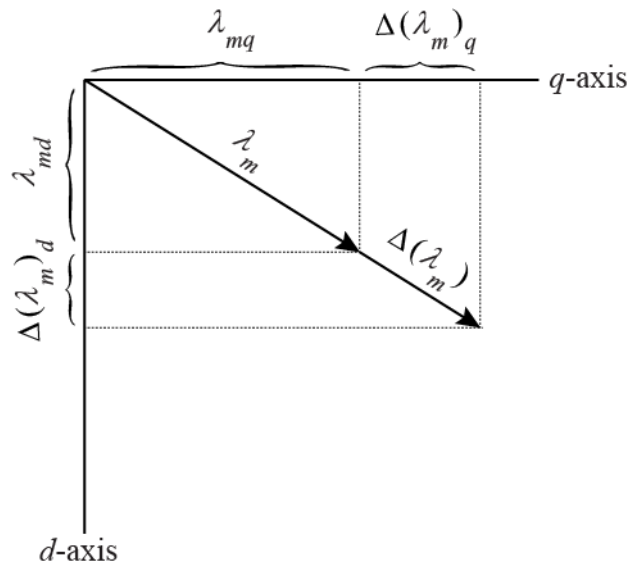


Figure 4.2 qd decomposition of flux correction term

Now, to include the effects of saturation in the induction machine model we can simply subtract the qd quantities of $\Delta(\lambda_m)$ from the linear values of the qd quantities of λ_m as follows.

$$\begin{aligned}
\lambda_{mq} &= L_m(i_{qs} + i'_{qr}) - \Delta(\lambda_m)_q \\
&= L_m \left(\frac{\lambda_{qs}}{L_s} - \frac{\lambda_{mq}}{L_s} + \frac{\lambda'_{qr}}{L'_r} - \frac{\lambda_{mq}}{L'_r} \right) - \Delta(\lambda_m)_q \\
&= L_{aq} \left(\frac{\lambda_{qs}}{L_s} + \frac{\lambda'_{qr}}{L'_r} \right) - \frac{L_{aq}}{L_m} \Delta(\lambda_m)_q
\end{aligned} \tag{4.5}$$

and

$$\begin{aligned}
\lambda_{md} &= L_m(i_{ds} + i'_{dr}) - \Delta(\lambda_m)_d \\
&= L_m \left(\frac{\lambda_{ds}}{L_s} - \frac{\lambda_{md}}{L_s} + \frac{\lambda'_{dr}}{L'_r} - \frac{\lambda_{md}}{L'_r} \right) - \Delta(\lambda_m)_d \\
&= L_{ad} \left(\frac{\lambda_{ds}}{L_s} + \frac{\lambda'_{dr}}{L'_r} \right) - \frac{L_{ad}}{L_m} \Delta(\lambda_m)_d
\end{aligned} \tag{4.6}$$

In equations (4.5) and (4.6) the terms L_{aq} and L_{ad} are equivalent inductance terms that are expressed as follows.

$$L_{aq} = L_{ad} = \left(\frac{1}{L_m} + \frac{1}{L_s} + \frac{1}{L'_r} \right)^{-1} \tag{4.7}$$

Equations (4.5) through (4.7) can now be used to implement the effects of magnetic saturation of the induction machine into the induction machine model.

4.2 Dynamic Phasors Model of Induction Machine Saturation

We can extend the concept of the flux correction method to dynamic phasors by considering that we can represent a complex space vector as a sum of dynamic phasors rotating at different harmonics as explained previously in Section 2.2.2. So, in the case of the induction

machine dynamic phasor model we can represent the magnetizing flux as the sum of the two positive and negative sequence magnetizing flux components. That is we have

$$\vec{\lambda}_m = \underline{\Lambda}_{mp} e^{j\omega_s \tau} + \underline{\Lambda}_{mn}^* e^{-j\omega_s \tau} \quad (4.8)$$

We can also express the flux correction term in terms of its dynamic phasors as well which gives us

$$\Delta(\lambda_m) = \Delta(\Lambda_{mp}) e^{j\omega_s \tau} + \Delta(\Lambda_{mn}^*) e^{-j\omega_s \tau} \quad (4.9)$$

Note here that the vector arrow and dynamic phasor under-bar have been dropped to avoid clutter in equation (4.9) and the rest of the equations in this section.

In a similar fashion as in section 4.1, we can express the corrected magnetizing flux vector in terms of its positive and negative sequence dynamic phasors.

$$\begin{aligned} \Lambda_{mp} &= L_m \underline{I}_{mp} - \Delta(\Lambda_{mp}) \\ \Lambda_{mn}^* &= L_m \underline{I}_{mn}^* - \Delta(\Lambda_{mn}^*) \end{aligned} \quad (4.10)$$

So we get

$$\begin{aligned} \Delta(\Lambda_{mp}) &= L_m \underline{I}_{mp} - \underline{\Lambda}_{mp} \\ \Delta(\Lambda_{mn}^*) &= L_m \underline{I}_{mn}^* - \underline{\Lambda}_{mn}^* \end{aligned} \quad (4.11)$$

A problem that we run into here is the fact that saturation data is generally given in terms of the magnitudes of the magnetizing flux vector versus the magnitude of the magnetizing branch current as mention earlier. So we have to determine the total dynamic phasor magnitude as $|\vec{\lambda}_m|$. This causes the model to lose some of its advantage as we have to

recombine the positive and negative dynamic phasors to determine the magnitude of the magnetizing flux vector.

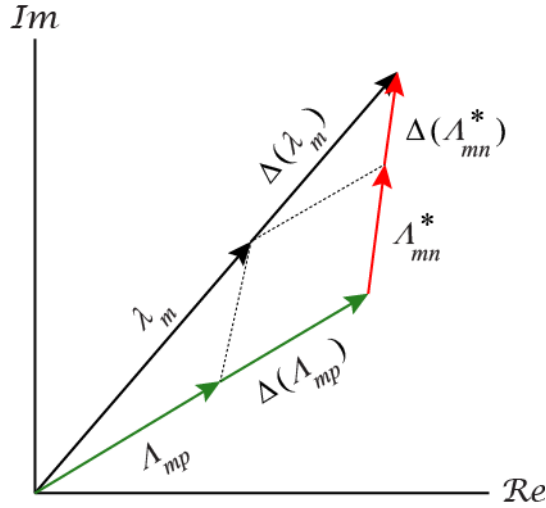


Figure 4.3 Saturation of main magnetizing flux linkage in terms of dynamic phasors

Once we have done this however we can determine the correction values for the positive and negative sequence magnetizing flux dynamic phasors in a similar manner as before. Figure 4.3 illustrates how we can break the rotating magnetizing flux vector down into its positive and negative sequence dynamic phasors and use them to graphically determine what the correction terms should be to include the effects of saturation in the dynamic phasor model of the induction machine. Doing this we get

$$\begin{aligned}\Delta(\lambda_{mp}) &= \frac{\lambda_{mp}}{\lambda_m} \Delta(\lambda_m) \\ \Delta(\lambda_{mn}^*) &= \frac{\lambda_{mn}^*}{\lambda_m} \Delta(\lambda_m)\end{aligned}\tag{4.12}$$

Once we have determined the correction terms we can implement them in the model by simply subtracting the correction terms from the linear model. So the positive and negative sequence dynamic phasors of the magnetizing flux can be expressed as

$$\begin{aligned}\Lambda_{mp} &= L_{eq} \left(\frac{\Lambda_{ps}}{L_s} + \frac{\Lambda_{pr}}{L'_r} \right) - \Delta(\Lambda_{mp}) \\ \Lambda_{mn}^* &= L_{eq} \left(\frac{\Lambda_{ns}^*}{L_s} + \frac{\Lambda_{nr}^*}{L'_r} \right) - \Delta(\Lambda_{mn}^*)\end{aligned}\tag{4.13}$$

Where

$$L_{eq} = \left(\frac{1}{L_m} + \frac{1}{L_s} + \frac{1}{L'_r} \right)^{-1}\tag{4.14}$$

We now have all the pieces necessary to implement the effects of saturation into the dynamic phasor model.

4.3 Saturation Model Verification

A few studies are carried out in this section to verify that the modeling technique used to model the effects of magnetizing flux saturation in the dynamic phasor model are representative of the saturated *qd0* induction machine model. We start by using the same machine parameters for a 500 hp induction machine contained in Appendix A. We then implement the saturation models outlined in sections 4.1 and 4.2 using the saturation data listed in Appendix B using a look-up table in Matlab/Simulink with the interpolation-extrapolation look-up method enabled for data occurring between the data points listed in Table B.1.

To illustrate the effects of saturation in the induction machine the model is started from standstill at 70% of its rated voltage and is allowed to reach steady state. At steady state, the machine is operating in the linear region of the magnetization curve. At time $t = 3.5\text{s}$, the machine voltage is raised to its full rated voltage of $2300\text{ V}_{\text{L-L}}$ which brings the machine into the saturation region of operation. The machine is then allowed to reach steady state in the saturation region. Figure 4.4 and Figure 4.5 illustrate the transition of the machine model from the linear region of operation to the saturation region of operation for the stator phase a current and the magnetizing flux respectively. Figure 4.4 and Figure 4.5 also provide a comparison between the unsaturated model quantities (EMT), the $qd0$ time domain saturated quantities (EMT Sat), the dynamic phasor saturated quantities (DP Sat) and the time domain results of the saturated dynamic phasor model (DP-EMT Sat).

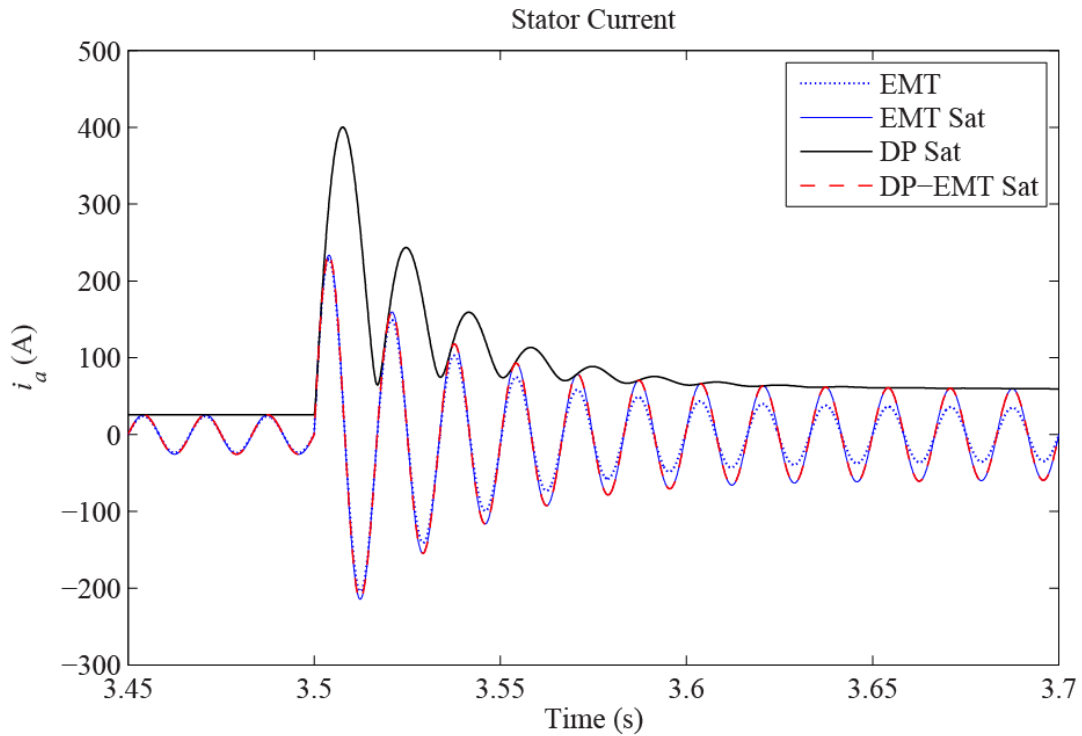


Figure 4.4 Stator current in saturation region

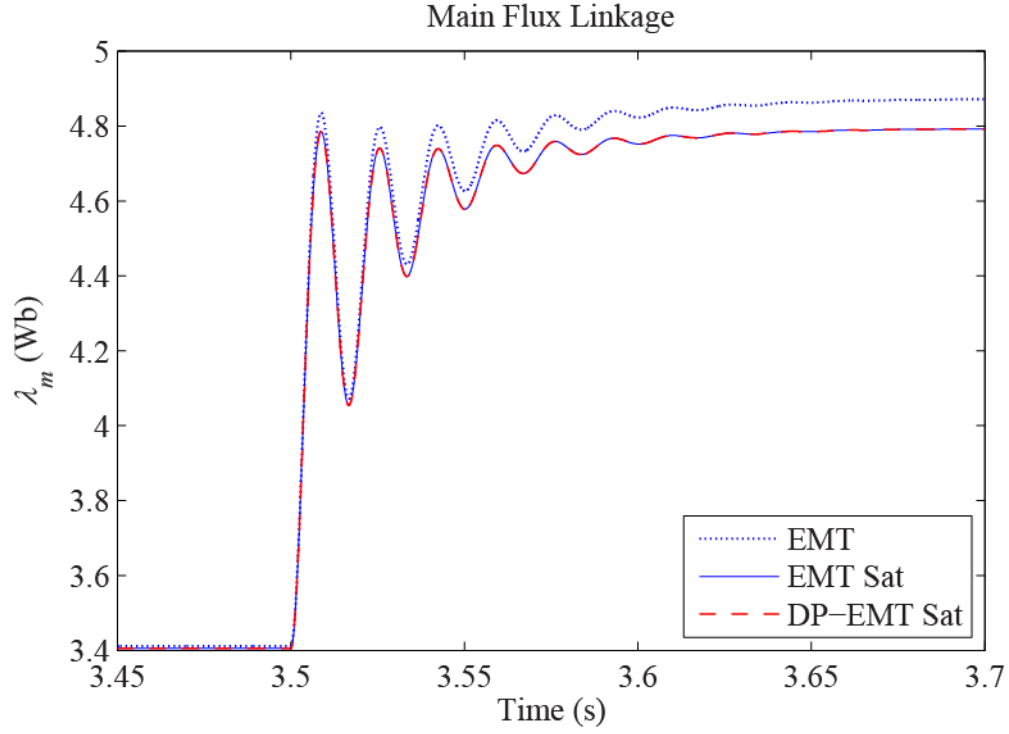


Figure 4.5 Magnetizing flux linkage in saturation region

We can see from Figure 4.6 and Figure 4.7, which are zoomed in sections of Figure 4.4 and Figure 4.5 respectively, that the dynamic phasor model is quite accurate when compared to the time domain $qd0$ induction machine model during balanced operation. There is very little error between the time domain $qd0$ model results and the time domain results obtained using the dynamic phasor model. Also the magnitude of the dynamic phasor provides an accurate envelope curve to the time domain results obtained using both models.

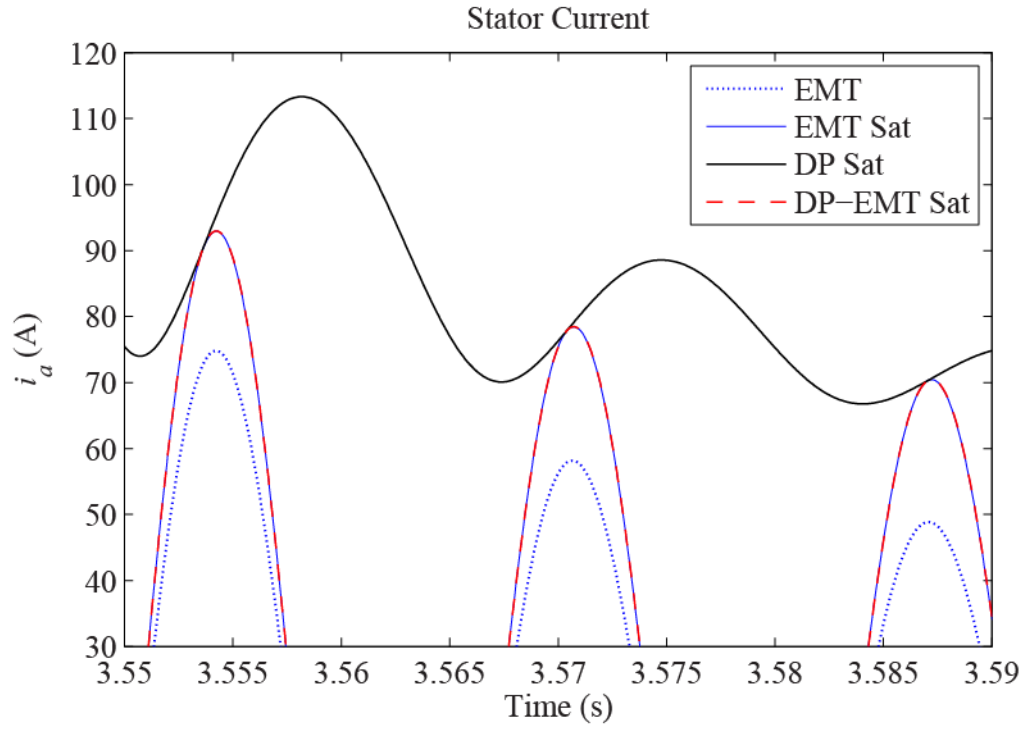


Figure 4.6 Zoomed view of stator current in saturation region

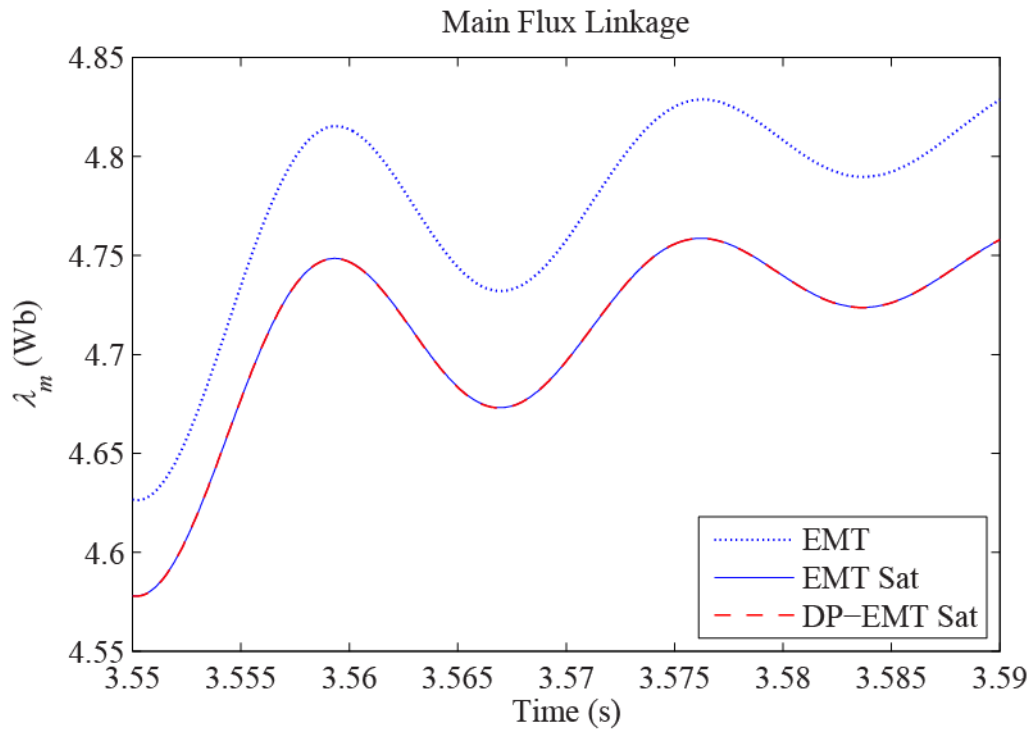


Figure 4.7 Zoomed view of magnetizing flux linkage in saturation region

The next study demonstrates the validity of the saturated dynamic phasor model during unbalanced machine operation. At time $t = 4$ s, an unbalanced single phase to ground fault is applied to the terminals of the machine for six cycles, at which time the fault is cleared and the machine is allowed to reach steady state in normal balanced operating conditions. Figure 4.8 and Figure 4.9 illustrate the operation of the machine models in the saturation region during unbalanced supply conditions. They also provide a comparison between the unsaturated model quantities (EMT), the $qd0$ time domain saturated quantities (EMT Sat), the dynamic phasor saturated quantities (DP Sat) and the time domain results of the saturated dynamic phasor model (DP-EMT Sat).

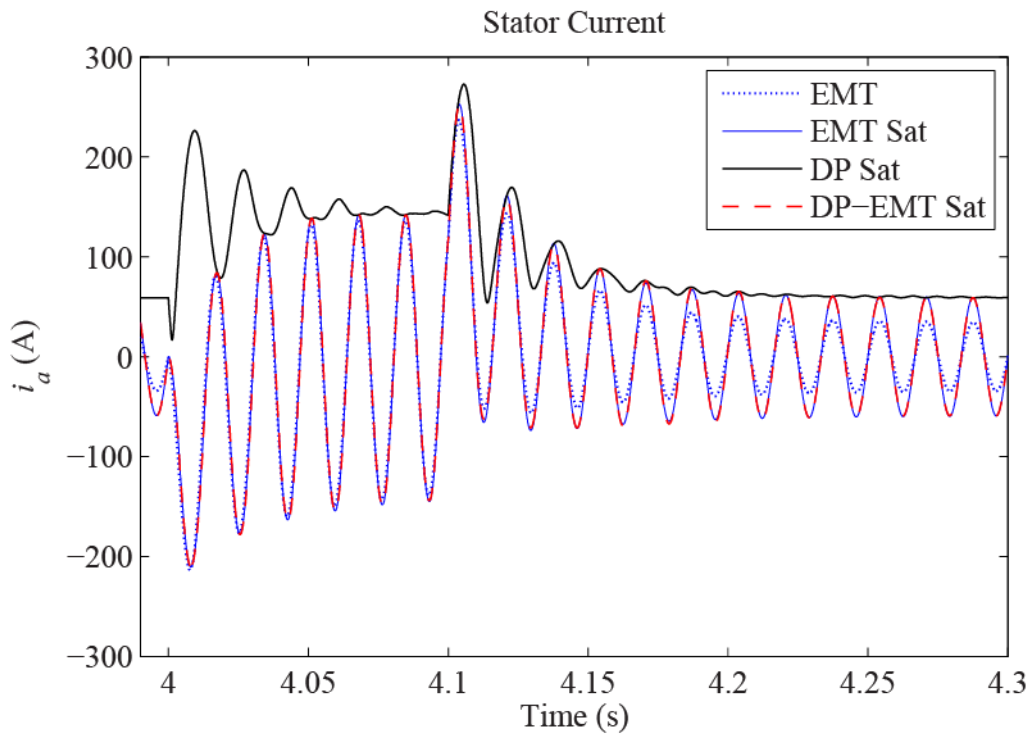


Figure 4.8 Stator current in saturation region during unbalanced fault

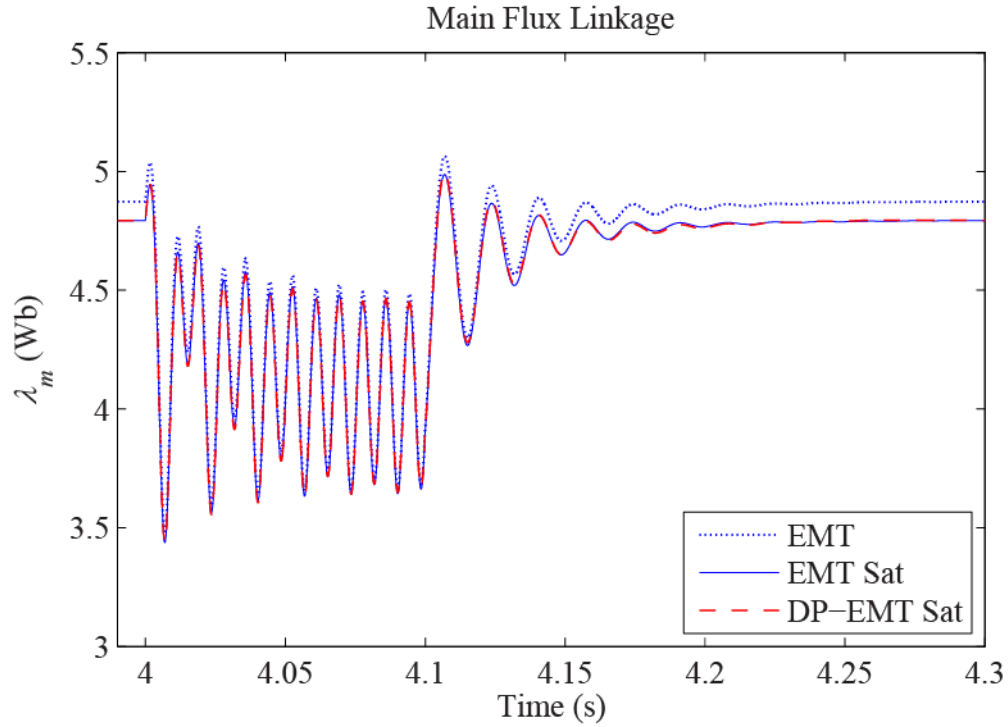


Figure 4.9 Magnetizing flux linkage in saturation region during unbalanced fault

We can again zoom in to the curves, Figure 4.10 and Figure 4.11, to illustrate that again the results obtained using the dynamic phasor model closely match those obtained using the $qd0$ induction machine model with little error. The error that is introduced during unbalanced machine operation is shown below in Table 4.1. From this we can see that the dynamic phasor model is again fairly representative of the $qd0$ induction machine model.

Table 4.1 Maximum error introduced by saturated dynamic phasor model

Variable	Maximum Absolute Error	Maximum Percent Error (%)
i_{as}	3.7327 (A)	2.1459
λ_m	0.0136(Wb)	0.3162

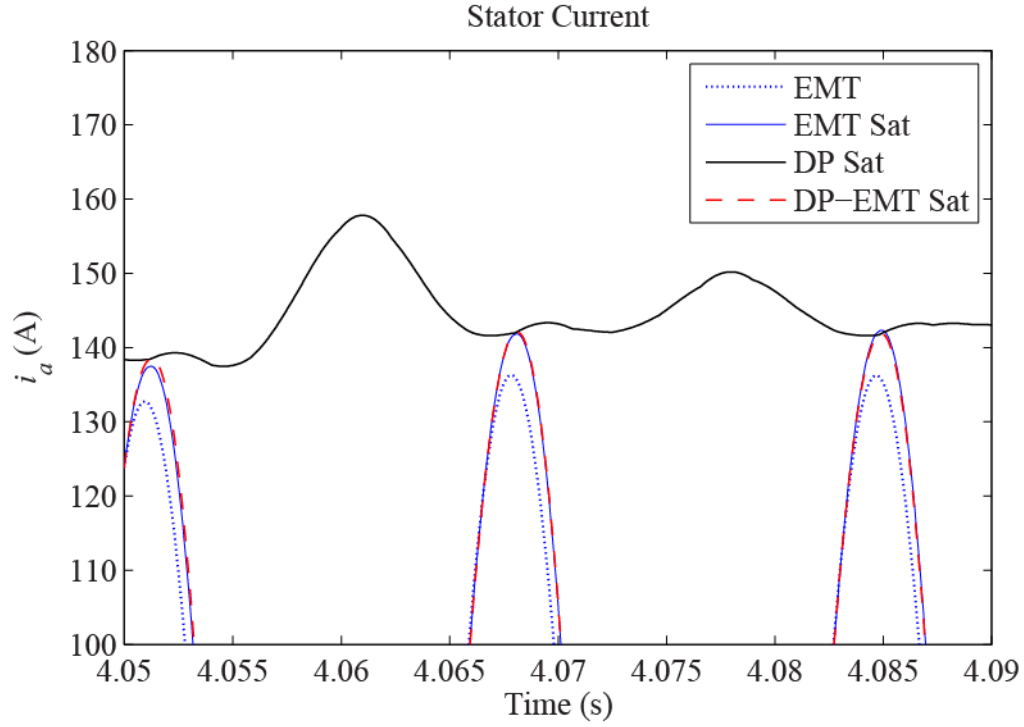


Figure 4.10 Zoomed view of stator current in saturation region during unbalanced fault

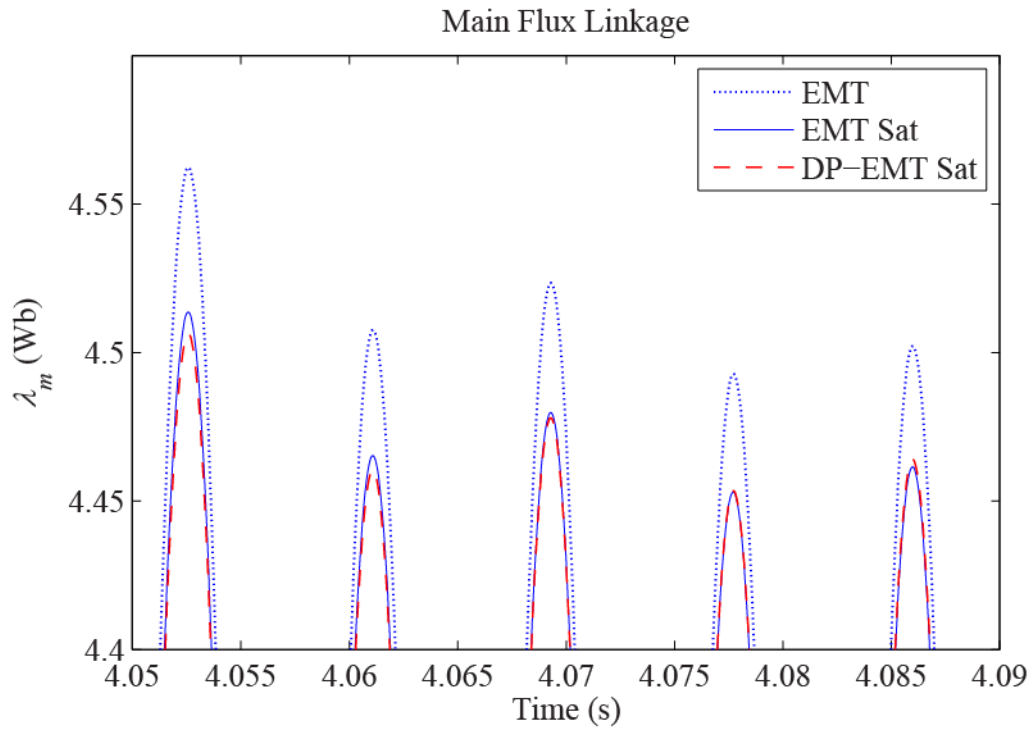


Figure 4.11 Zoomed view of magnetizing flux in saturation region during unbalanced fault

The studies performed in this section have validated the saturated dynamic phasor model and shown that it is quite representative of the well know $qd0$ induction machine model with little error. We are now in a position to be able to study the performance of the dynamic phasor model in terms of the time step that can be used in the model simulation while still producing reasonable results. The next chapter looks at the dynamic phasor model performance by conducting various studies using different time steps and analyzing the results obtained from the model.

Chapter 5: Induction Machine Dynamic Phasor Model Performance

5.1 Fixed Time-Step Model Performance

To test the performance of the dynamic phasor induction machine model we perform simulations using the same test cases that were used in Chapter 4 using different time steps. The simulations are performed in Matlab/Simulink using the ode4 (Runge-Kutta) fixed time-step solver [51] which utilizes a fourth order Runge-Kutta formula to calculate the model states at each time-step. Three different time-steps were used in this study to show the accuracy of the model using small to large time steps which are; a small time-step of $\Delta t=1.0\text{ms}$, a medium time-step of $\Delta t=2.0\text{ms}$ and a large time-step of $\Delta t=3.5\text{ms}$. The machine parameters in Appendix A are utilized again here for the following studies.

First, the machine is started from standstill by applying a rated voltage of 23 kV to the input of the machine and allowed to freely accelerate to steady state. At time $t = 2.5\text{s}$ a rated generating torque of 1980 Nm is applied to the model input and then reversed to a rated load torque of 1980 Nm at time $t = 3\text{s}$. Once the machine has again reached a steady-state a balanced 3-phase to ground fault is applied to the input terminals of the model at time $t = 4\text{s}$ and then cleared after 6 electrical cycles. Then finally, a single phase to ground fault is applied to the terminals of the machine at time $t = 5\text{s}$ which is again cleared after 6 electrical cycles. Figure 5.1 through Figure 5.4 show the stator current results for the previous test cases respectively. They contain the stator current envelope results obtained using both the conventional $qd0$ and the dynamic phasor model at different time-steps along with the time

domain stator current results obtained using the conventional $qd0$ model with a very small time-step of $50\text{ }\mu\text{s}$; which is assumed to be the accurate solution for these test cases.

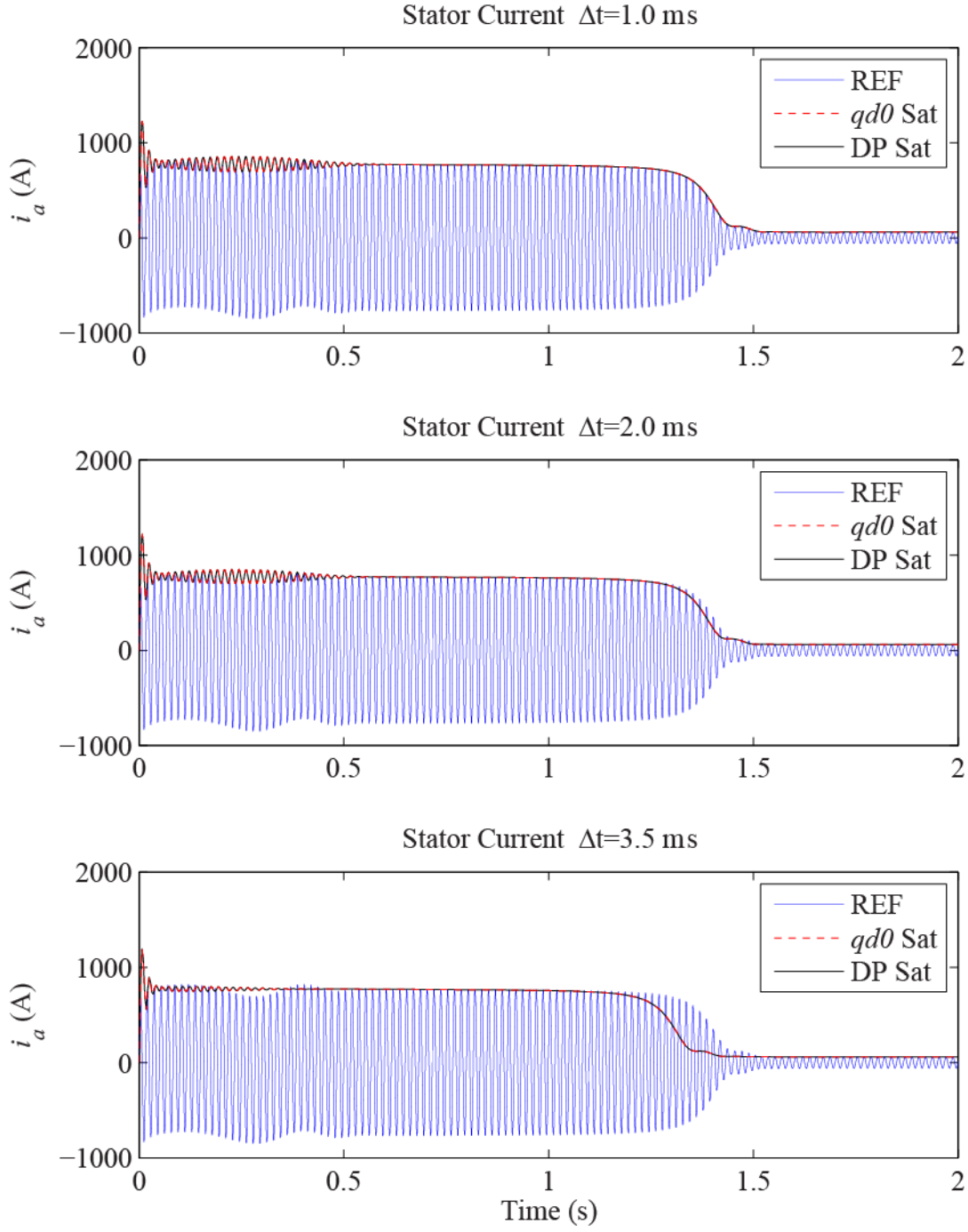


Figure 5.1 Stator current during start-up for fixed Δt studies

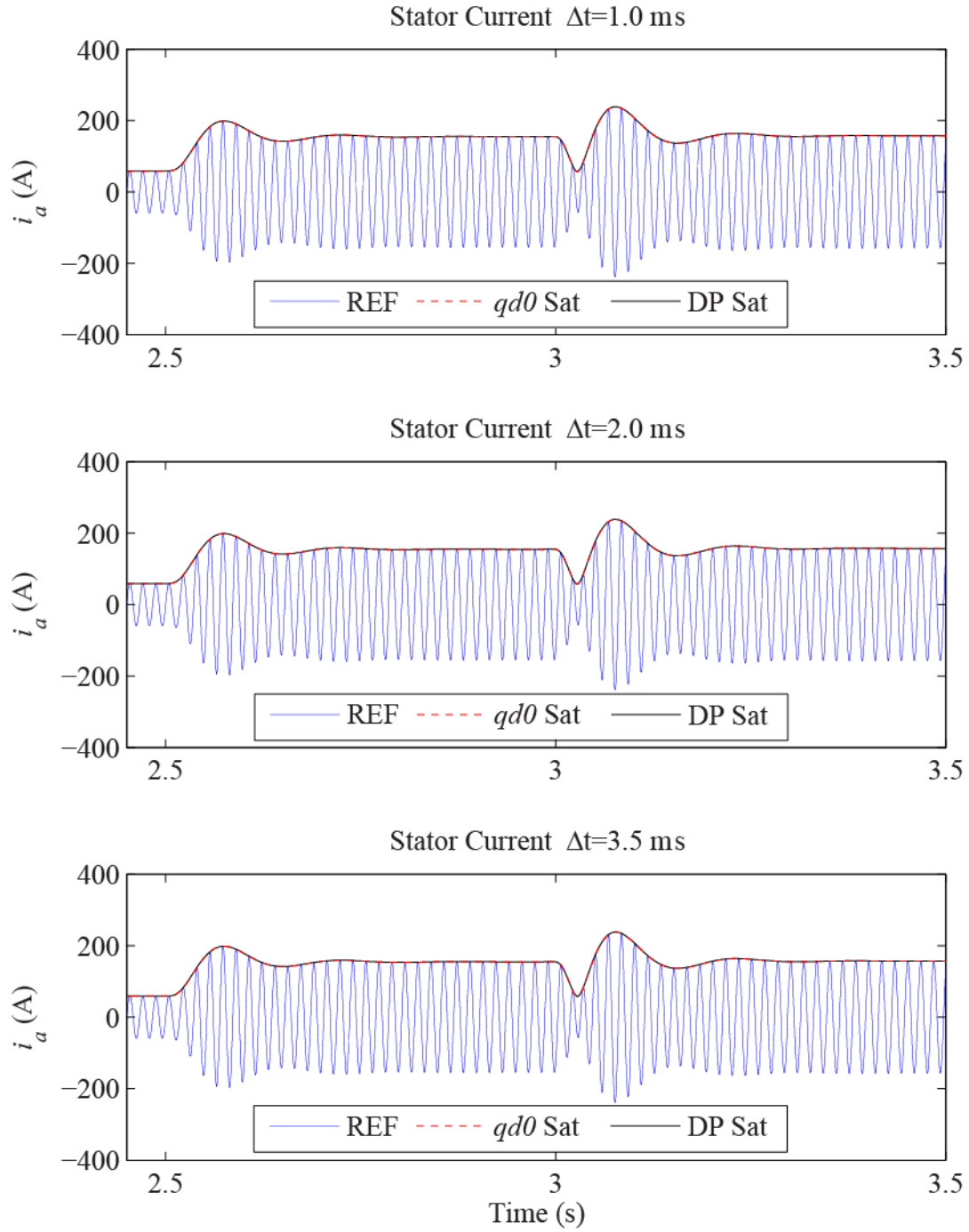


Figure 5.2 Stator current during load torque change for fixed Δt studies

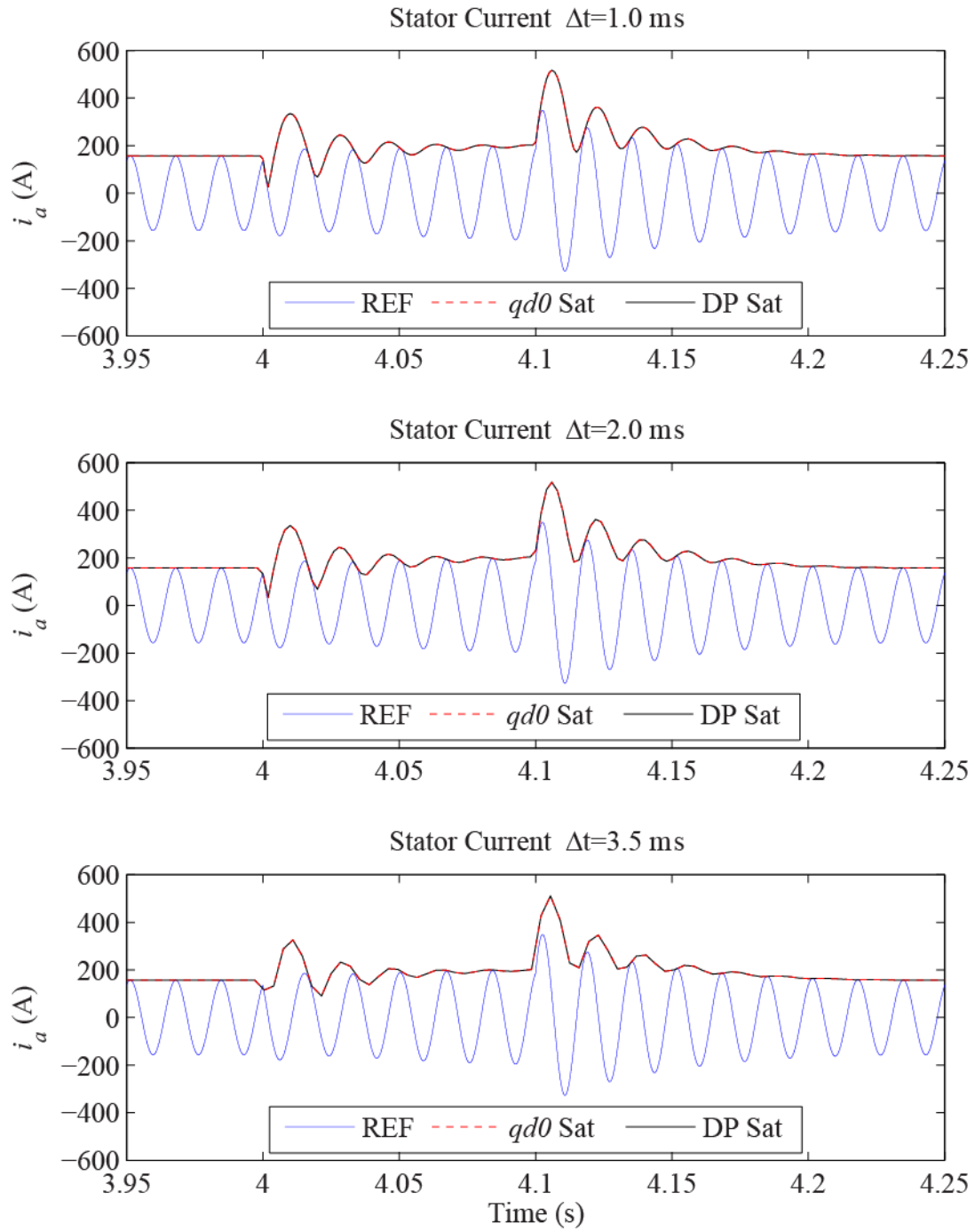


Figure 5.3 Stator current during balanced 3-phase fault for fixed Δt studies

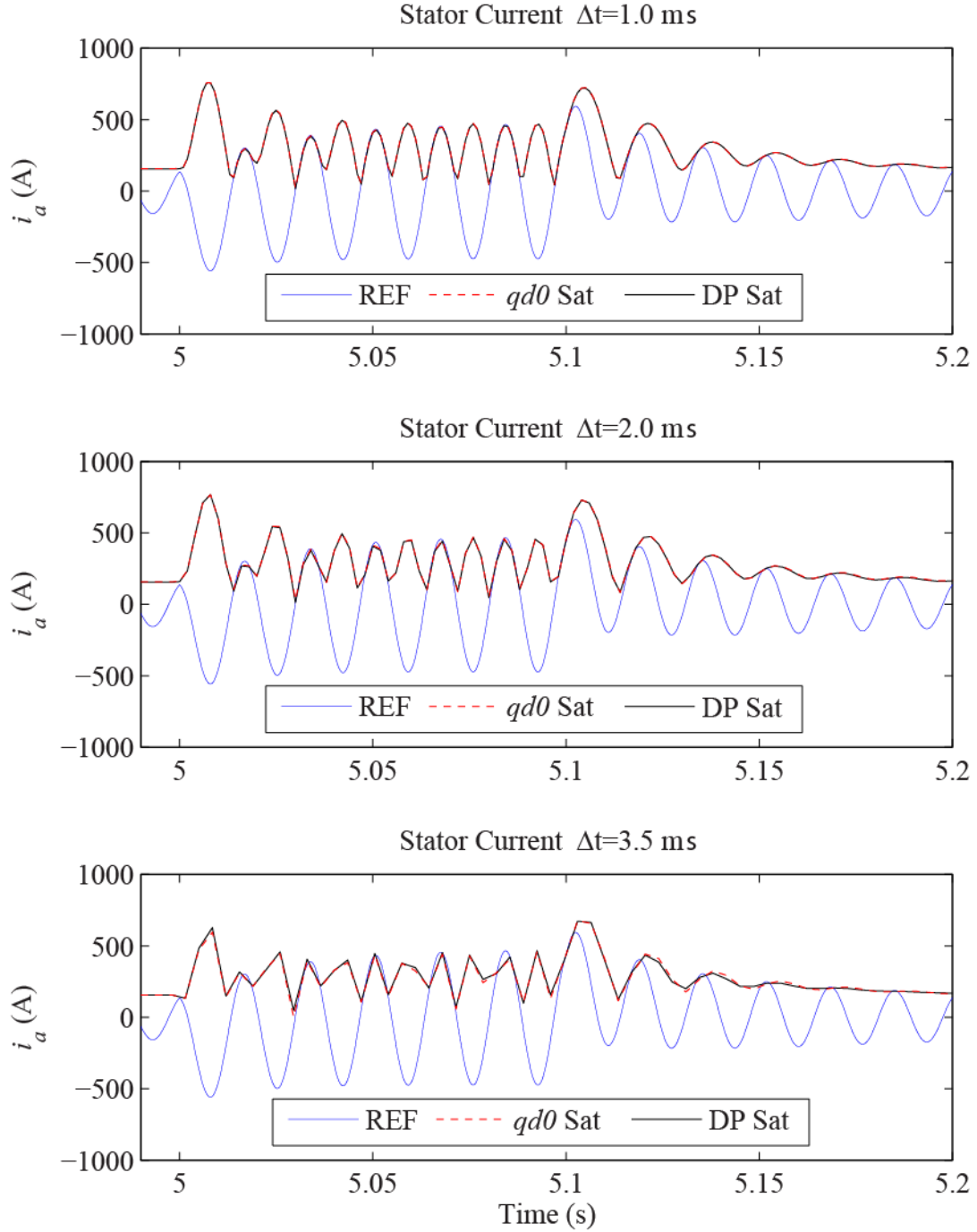


Figure 5.4 Stator current during unbalanced fault for fixed Δt studies

It can be seen from Figure 5.1 through Figure 5.4 that the results obtained using the dynamic phasor induction machine model are virtually identical to those obtained using the

convention $qd0$ model; even at a large time-step of 3.5 ms. Looking at Figure 5.4 however, we can see that the results obtained using the dynamic phasor induction machine model begin to deviate slightly from the results obtained using the convention $qd0$ induction machine model during unbalanced operation. The discrepancy becomes more pronounced at higher time-steps, but still the results are quite similar to each other.

As before, the current results for the dynamic phasor induction machine model are obtained by combining the positive and negative sequence dynamic phasors which are shown below in Figure 5.5 and Figure 5.6, respectively. It can be seen from these two figures that the large time-step results are still fairly representative of the more accurate results obtained at smaller time-steps for both the positive and negative dynamic phasor stator current quantities.

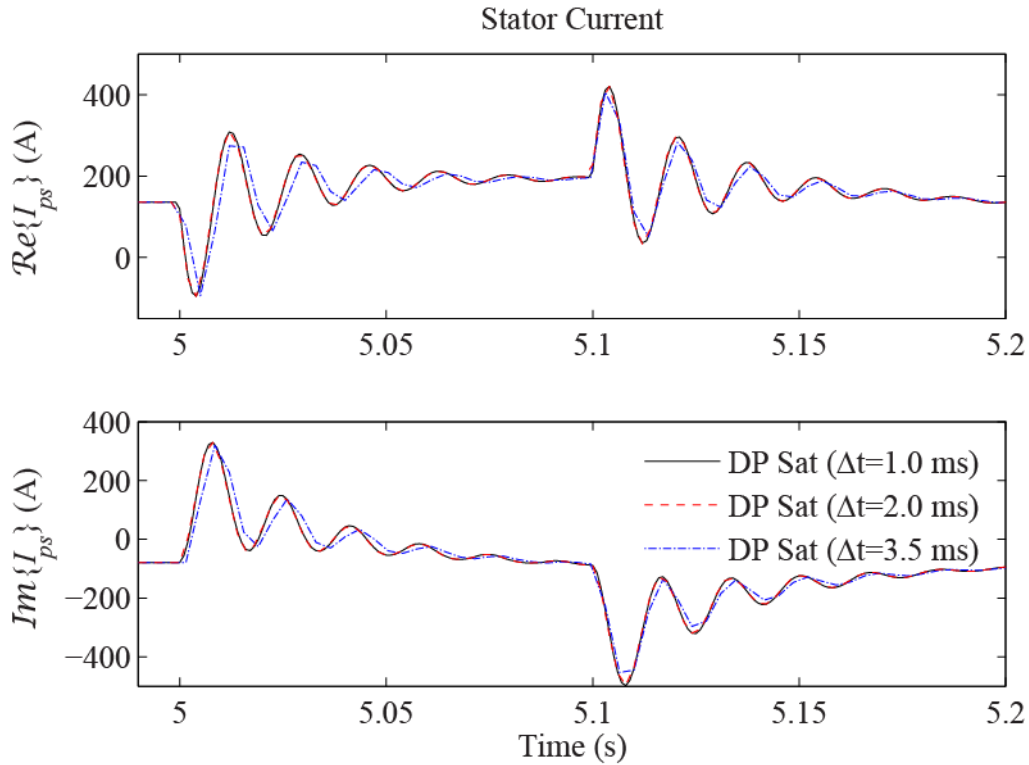


Figure 5.5 Positive sequence stator current dynamic phasor using different Δt

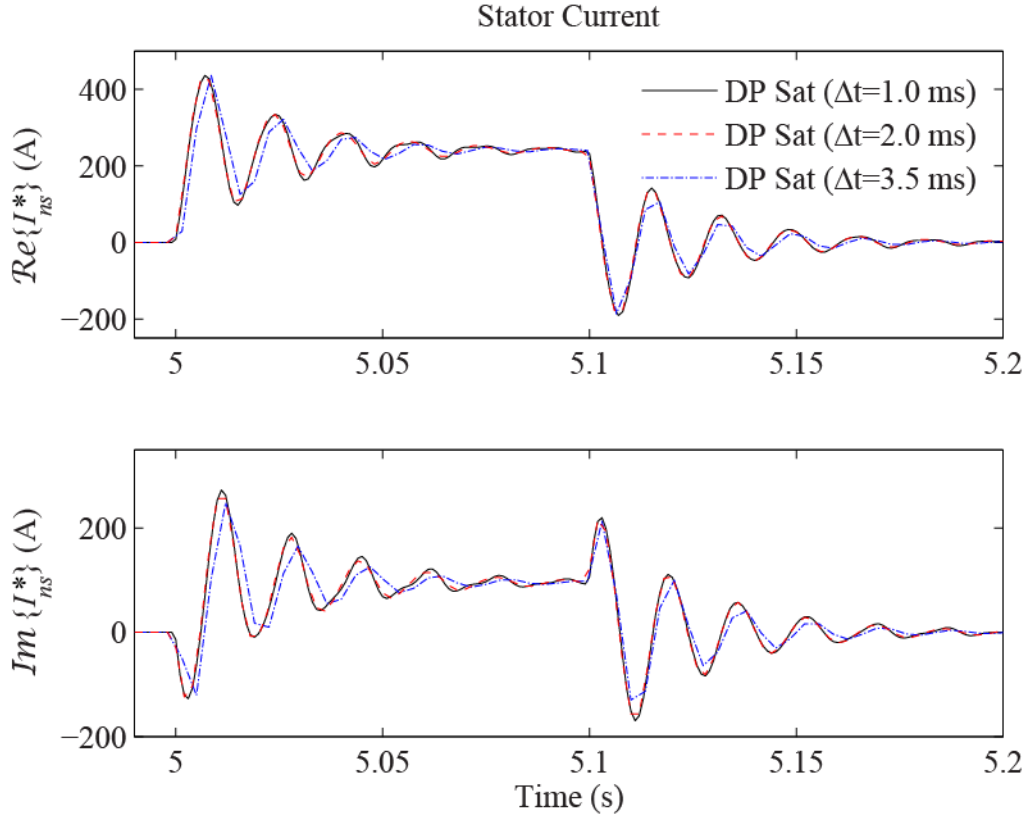


Figure 5.6 Negative sequence stator current dynamic phasor using different Δt

Similar results can be obtained for the electrical torque developed in the machine. Figure 5.7 illustrates the results for the electrical torque obtained using the dynamic phasor model at different time-steps. It can be seen from this figure that the results obtained using the larger time-step do deviate from the more accurate result. This is to be expected as the transient of the electrical torque contains both the dc component and the much quicker 2nd harmonic component which is changing at a rate of twice the system frequency, so when the dynamic phasor results are combined to form the results shown in Figure 5.7 the waveform becomes more distorted due to the error that is introduced at the higher time-steps. If we look at only the dynamic phasors themselves however, we can see from Figure 5.8 and Figure 5.9 that the results at larger time-steps are still quite consistent with those at the smaller time-step.

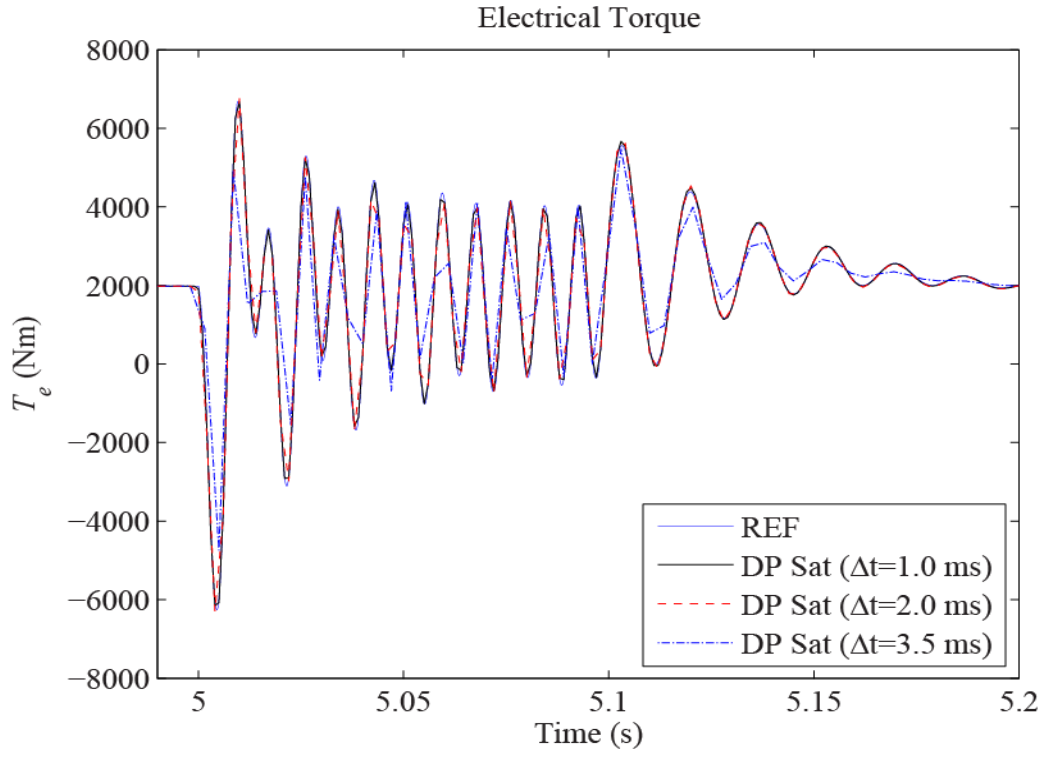


Figure 5.7 Electrical torque using different Δt

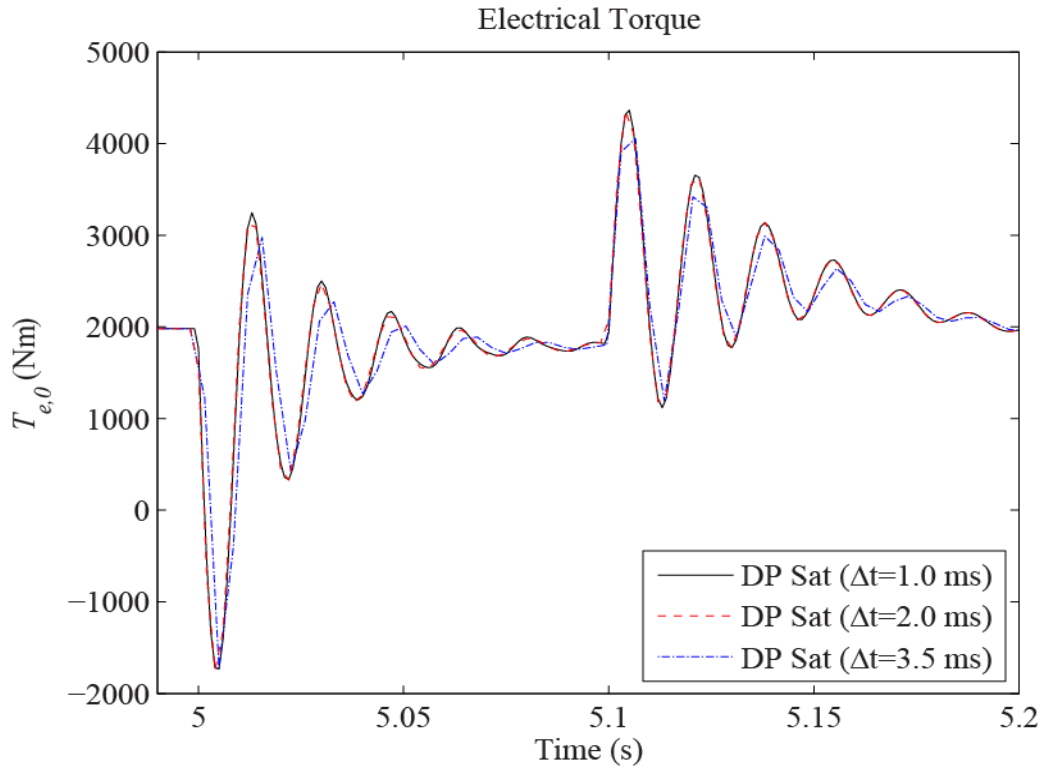


Figure 5.8 DC component of electrical torque dynamic phasor using different Δt

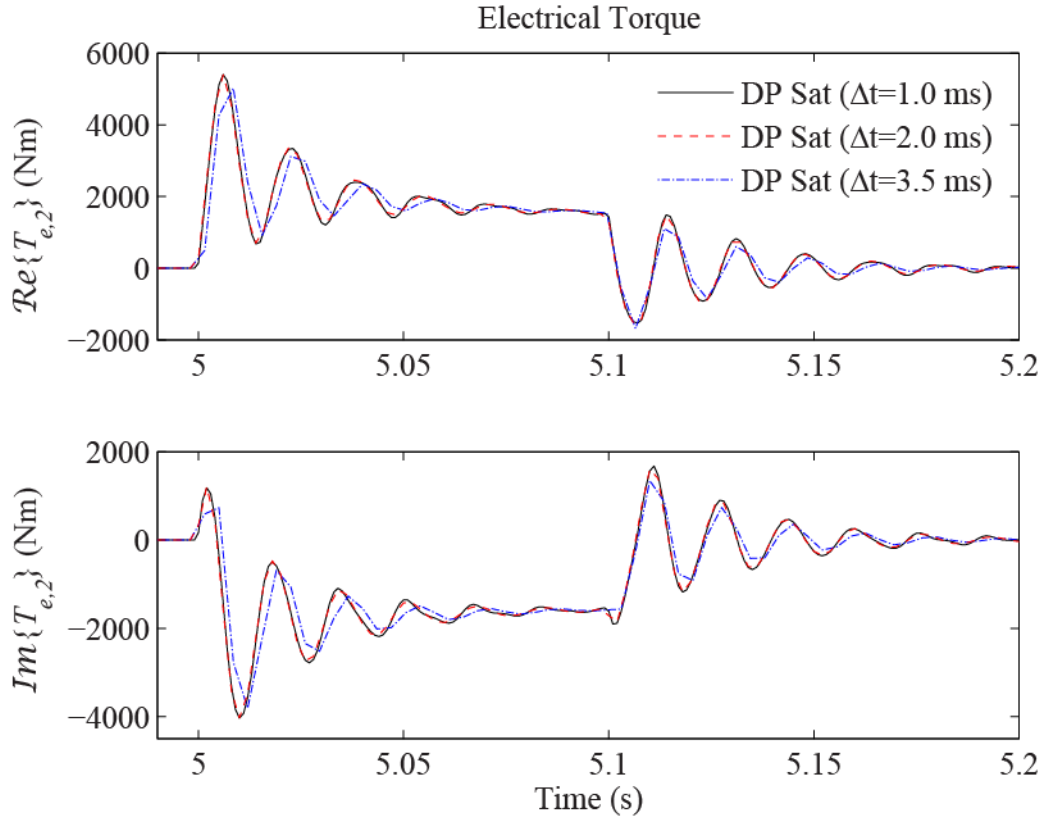


Figure 5.9 2nd harmonic component of electrical torque dynamic phasor using different Δt

Looking at the mechanical rotor speed in Figure 5.10 we can again see that the overall time domain result starts to deviate from the reference result at higher time-steps. This is again due to the 2nd harmonic component in the rotor mechanical speed similar to the electromagnetic torque which is a component that changes at twice the system frequency.

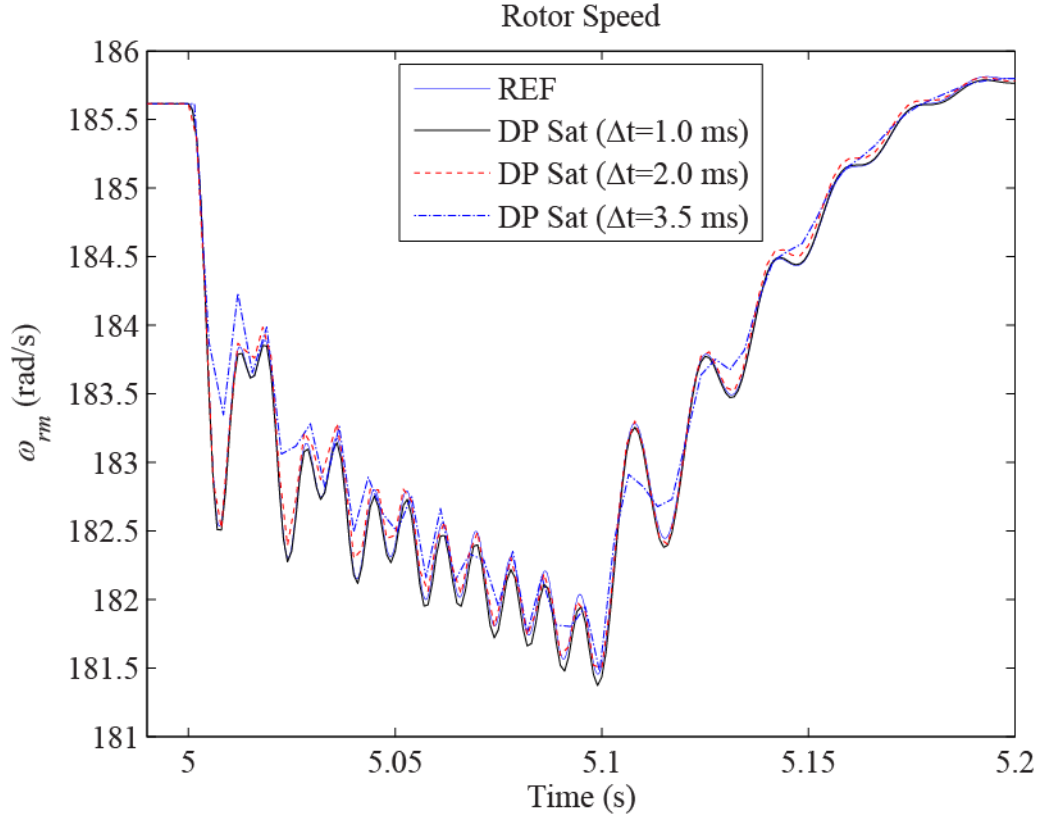


Figure 5.10 Rotor speed using different Δt

If we look at the dc component and the 2nd harmonic dynamic phasor separately as shown in Figure 5.11 and Figure 5.12 we can again see that the dc component at larger time-steps is still quite representative of the results at the small time-step. However, looking at the 2nd harmonic positive and negative sequence dynamic phasors we can see that the transient in the waveform reaches a steady value much more quickly at larger time-steps than it does at the small time-step, this is the major contributing factor in the error present in the overall time-domain result in Figure 5.10.

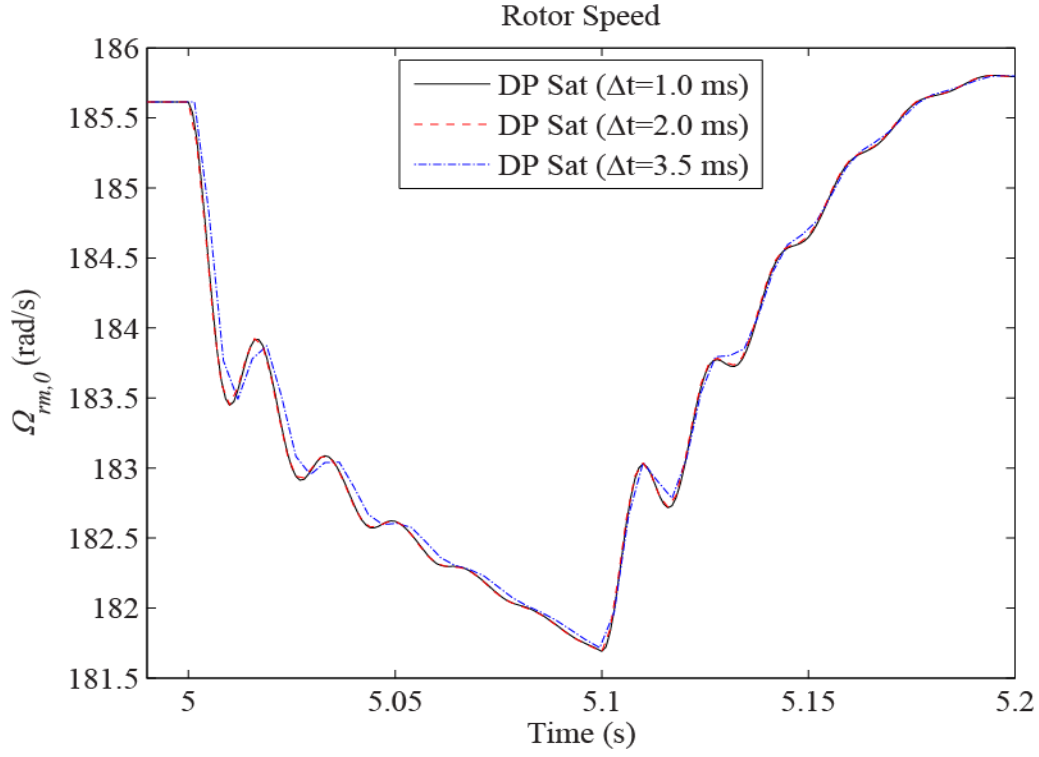


Figure 5.11 DC component of rotor speed dynamic phasor using different Δt

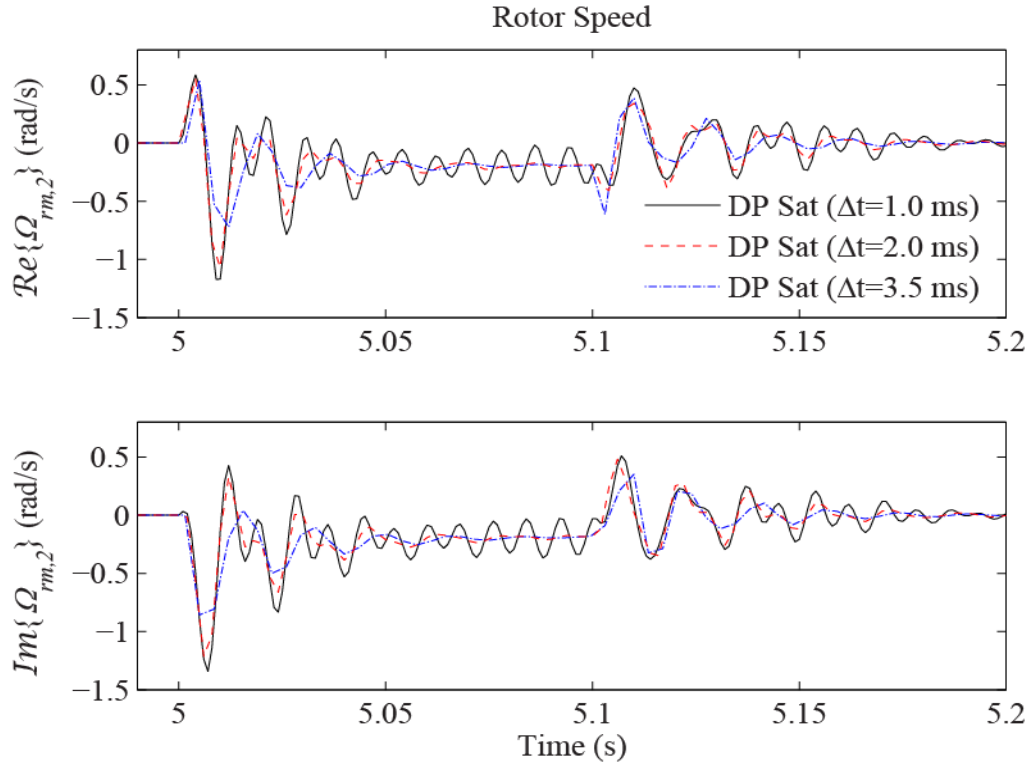


Figure 5.12 2nd harmonic component of rotor speed dynamic phasor using different Δt

We can see from the above test cases that the dynamic phasor induction machine model provides a fairly accurate and comparable model to the conventional $qd0$ induction machine model and can be used to simulate the induction machine during fast transients that occur during balanced and unbalanced faults as well as slow mechanical transients that occur during load changes. For example, Figure 5.13 shows the stator current results from the dynamic phasor model and we can see that during the slow transients of a load change we can see that the dynamic phasor model can accurately reproduce the current envelope even at the very large time-step of 7.5 ms.

Table 5.1 shows the CPU times for the simulation up to the 5 second point of the test case. We can see from this table that the dynamic phasor model is quite comparable to the conventional $qd0$ induction machine model with slightly faster CPU times for the simulation. It should be noted here that the CPU times presented for the dynamic phasor model reflect simulation during balanced machine operation only, meaning that there are no negative sequence phasors present. This reduces the total number of equations present in the dynamic phasor induction machine model to equal the number of equations in the qd induction machine model. With negative sequence dynamic phasors present the number of equations is doubled in the dynamic phasor model as presented in Section 3.2 of this thesis and the CPU times presented in Table 5.1 would be greater.

Table 5.1 CPU times for test case simulation

Time-step	Simulation Time	$qd0$ (saturated)	Dynamic Phasor (saturated)
$\Delta t = 0.5$ ms	5	0.5898 s	0.4636 s
$\Delta t = 1.0$ ms	5	0.3620 s	0.2798 s
$\Delta t = 5.0$ ms	5	0.1778 s	0.1584 s
$\Delta t = 7.5$ ms	5	0.1650 s	0.1490 s

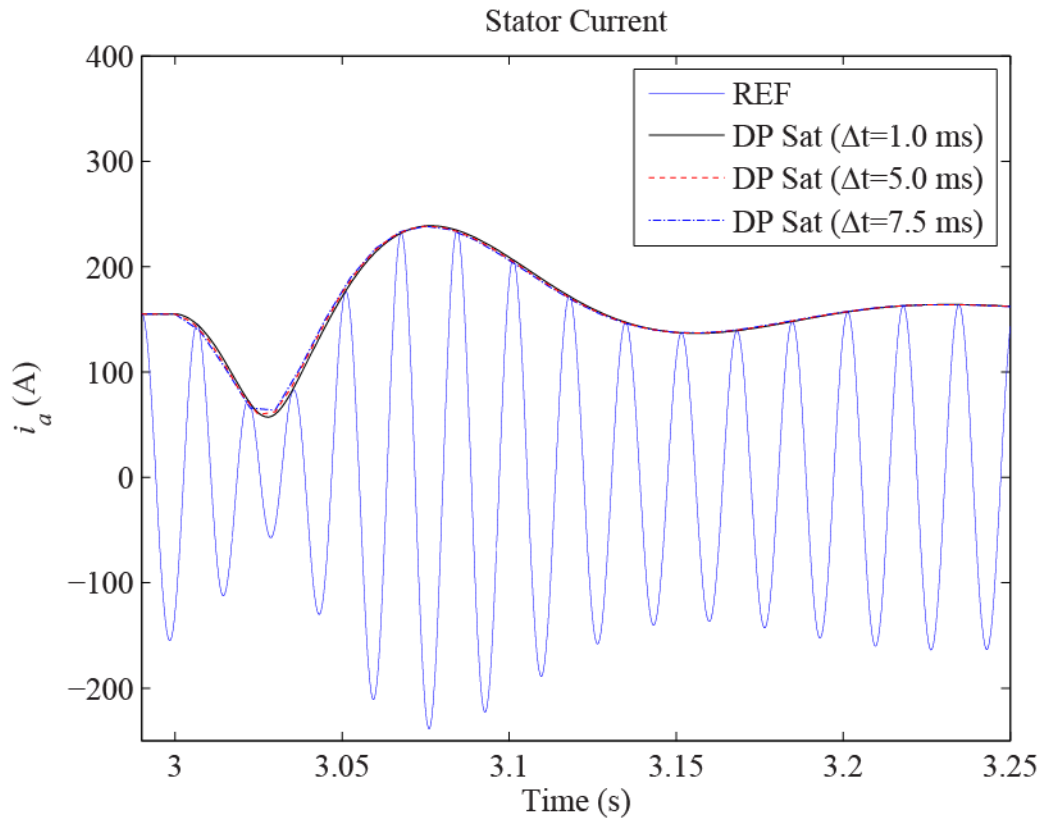


Figure 5.13 Load change results using dynamic phasor model

5.2 Variable Time-Step Model Performance

Due to the nature of dynamic phasor quantities; how their transient behaviour changes much slower with time and they reach a constant value at steady state, a real advantage in simulation can be achieved if variable time-step algorithms are used during simulation. To illustrate this, the dynamic phasor induction machine model is simulated in Matlab/Simulink using the ode45 (Dormand-Prince) variable time-step solver [51] which computes the models state at the next time-step using an explicit Runge-Kutta (4,5) formula, the Dormand-Prince pair for numerical integration. The maximum time-step parameter is set to 10 ms while the relative and absolute tolerances are set to 0.1 ms.

The 500 hp induction machine parameters are used to simulate a 5 second simulation in which the model is started from standstill and allowed to freely accelerate to steady state at which time ($t=2.5s$) a mechanical rated load torque is applied to the model. At time $t=3s$ the load torque is reversed to a generating torque and the model is again allowed to reach steady state. Then at time $t=4s$ a balanced 3-phase to ground fault is applied to the supply voltage which is then cleared after 6 electrical cycles. This 5 second simulation is performed using the saturated dynamic phasor model as well as the saturated time domain $qd0$ model and the model performance results are compared. A reference result is obtained using the conventional $qd0$ time domain model with a very small fixed time-step of 50 μs ; which is assumed to be the accurate result for comparison. Figure 5.14 through Figure 5.19 below show the results obtained for both the stator phase a current and the time-step used by the variable time-step solver for both the dynamic phasor induction machine model and convention $qd0$ induction machine model along with the reference solution for comparison.

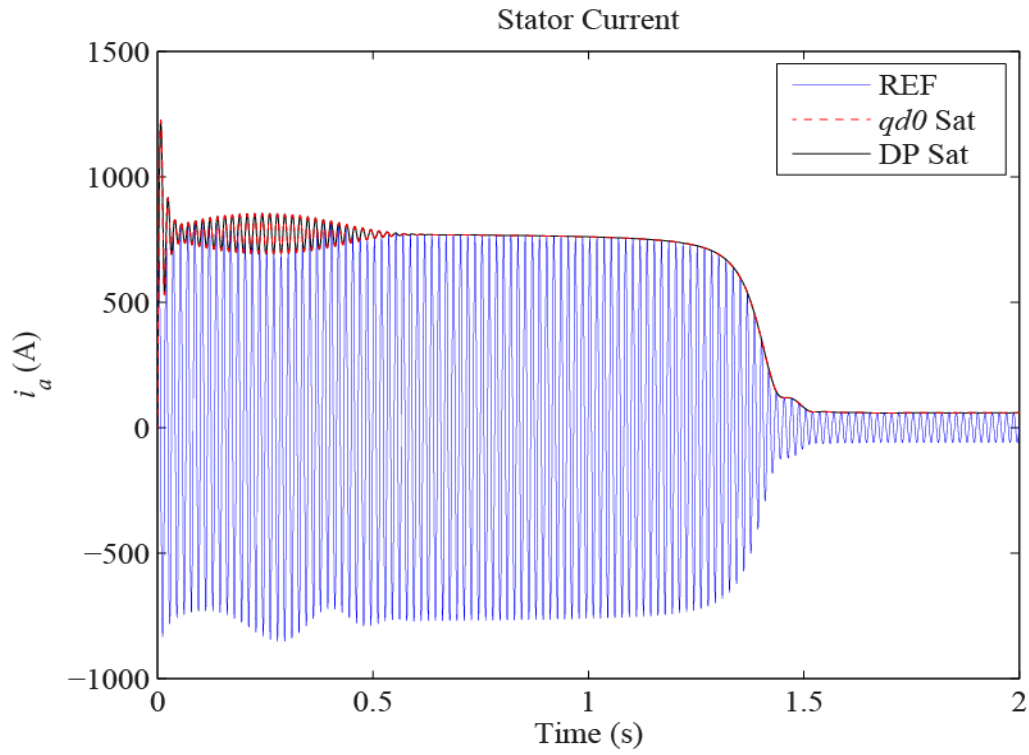


Figure 5.14 Stator current during free acceleration using variable Δt solver

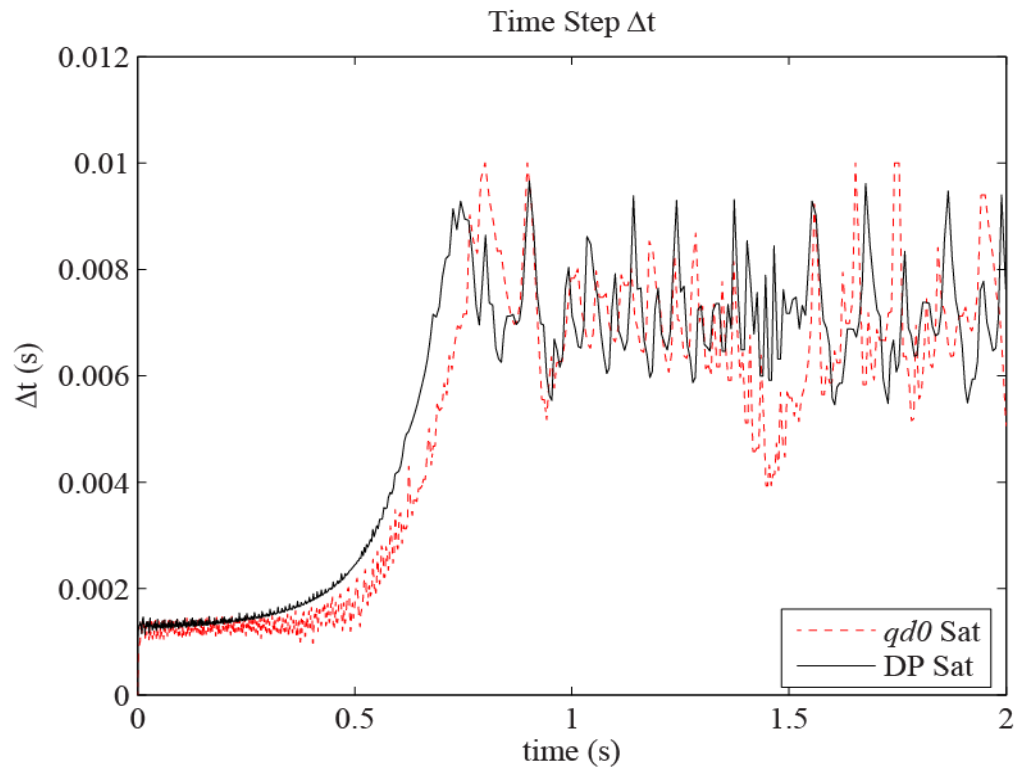


Figure 5.15 Time-step results during free acceleration using variable Δt solver

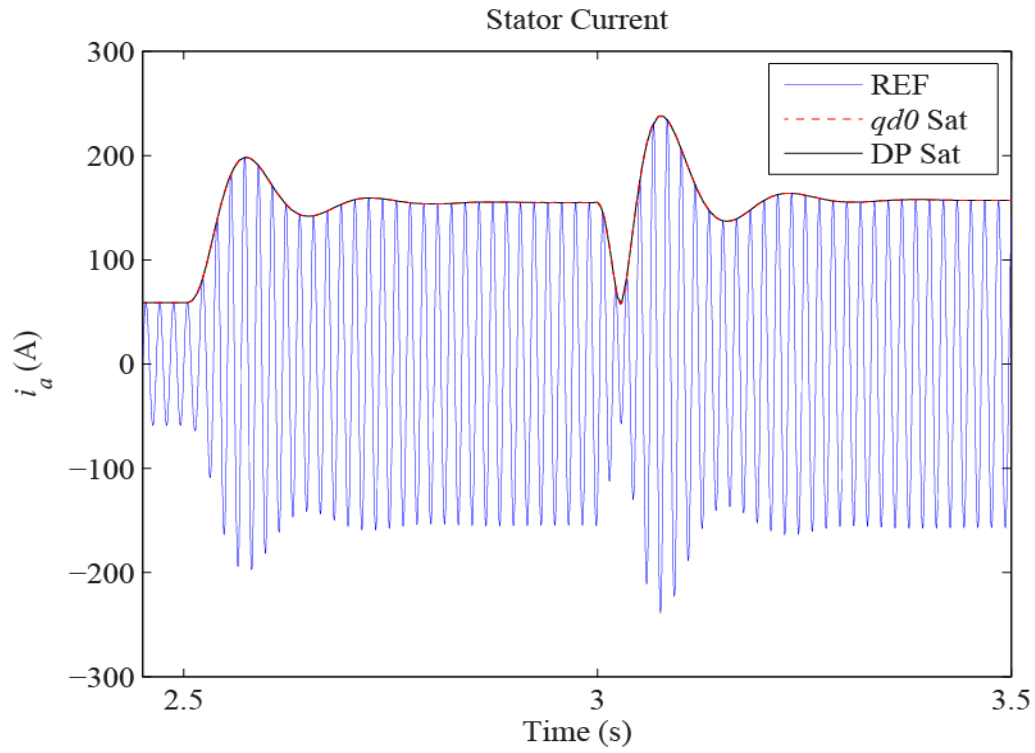


Figure 5.16 Stator current during load torque change using variable Δt solver

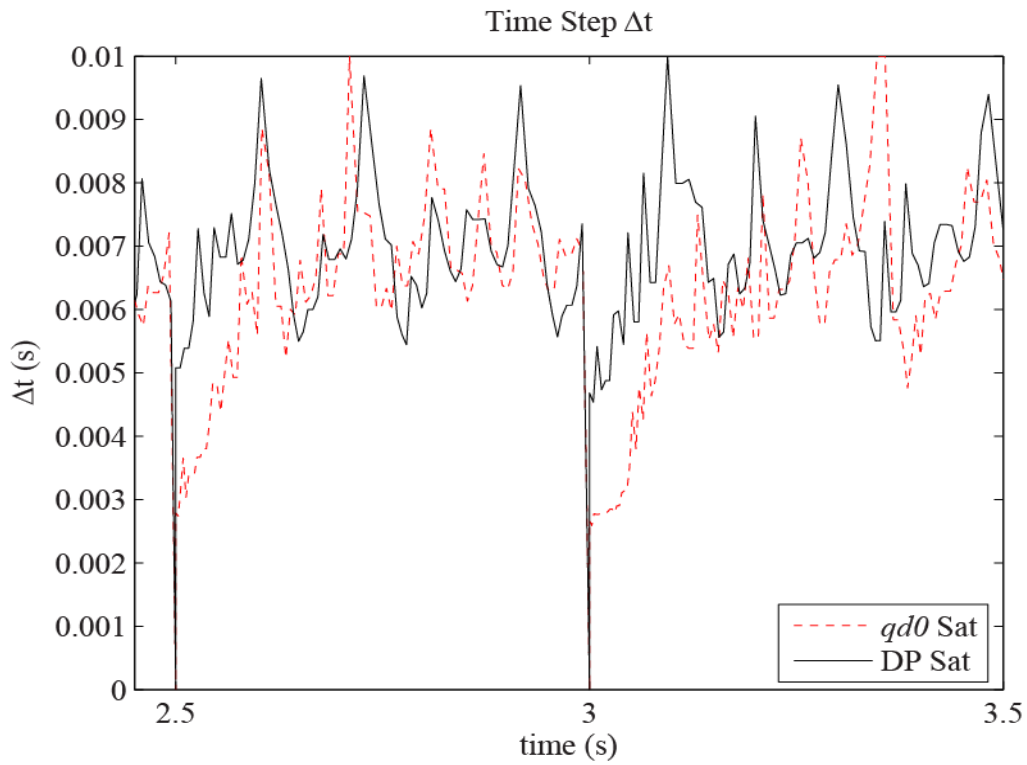


Figure 5.17 Time-step results during load torque change using variable Δt solver

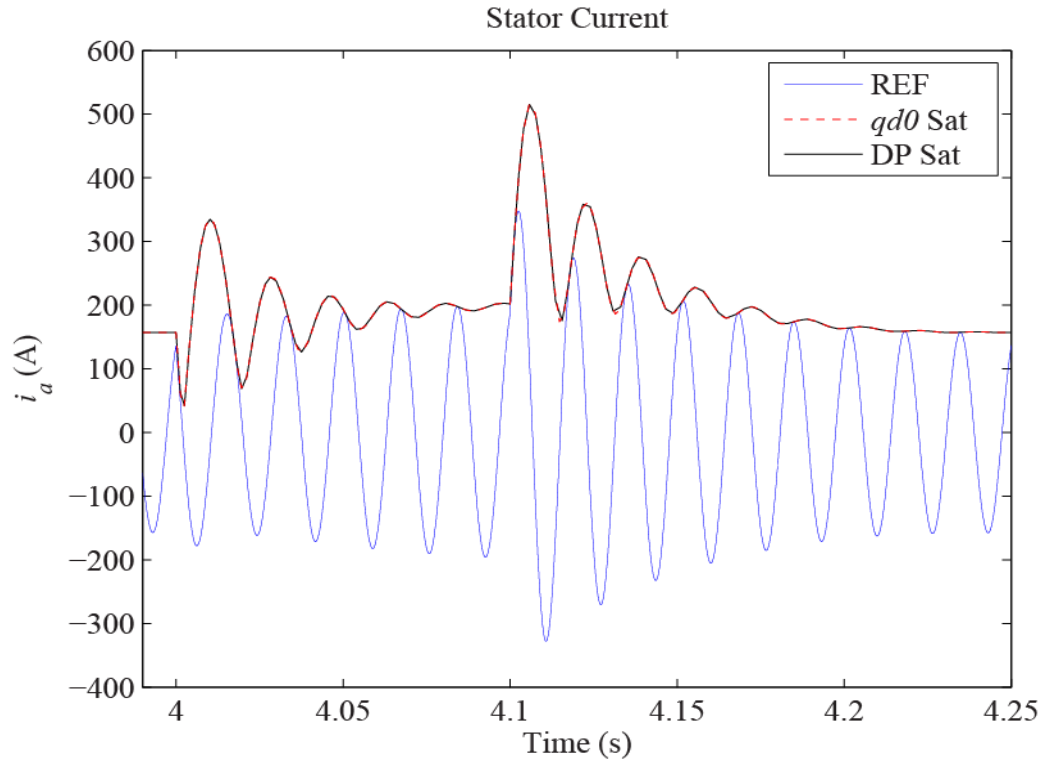


Figure 5.18 Stator current during balanced fault using variable Δt solver

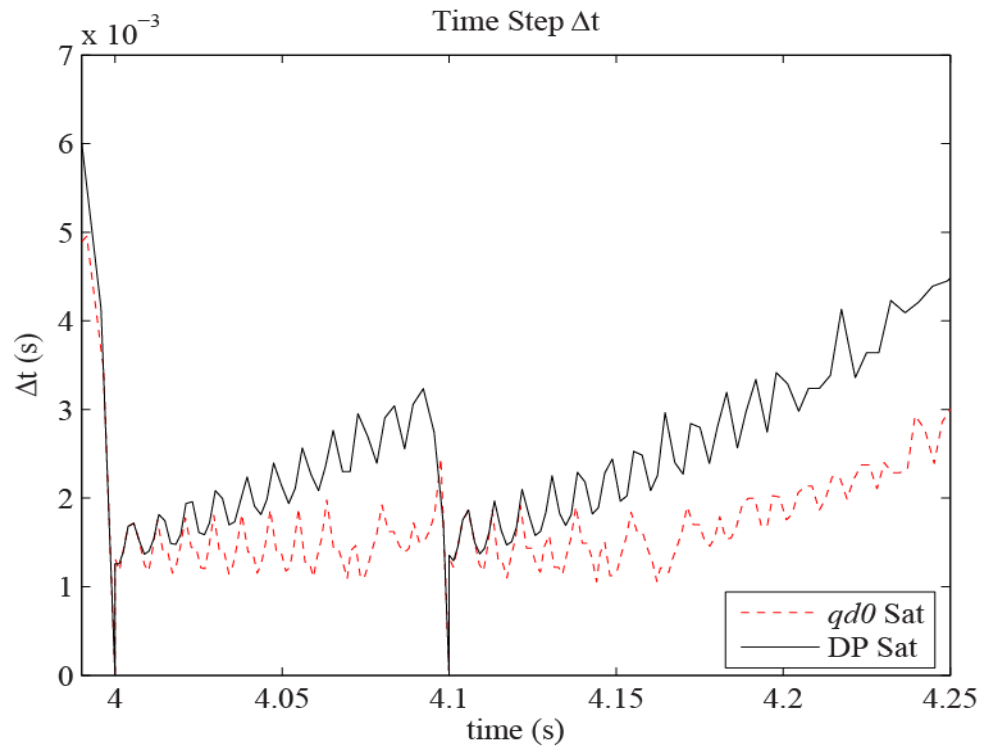


Figure 5.19 Time-step results during balanced fault using variable Δt solver

Table 5.2 summarizes the CPU times and the average time-step needed for the dynamic phasor and the *qd0* model simulations. It can be seen that the dynamic phasor induction machine model is approximately 13% faster than the conventional *qd0* induction machine model to achieve comparable accuracy using the variable step solver in Matlab/Simulink. It is also observed that the average time-step used during the 5 s simulation time for the dynamic phasor induction machine model is approximately 16% larger than that of the conventional *qd0* induction machine model. This is not a huge improvement in overall simulation efficiency but illustrates that some advantages can be gained when using the dynamic phasor model for simulation.

The advantages of the dynamic phasor model over the conventional *qd0* model are most evident during the faster transient sections of the simulation. For example, if we look at the time-step results of the simulation in Figure 5.15, Figure 5.17 and Figure 5.19 we can see that the time-step used by the dynamic phasor model is consistently greater than that used by the conventional *qd0* model during the periods where the waveform is changing rapidly. Only when the waveforms have reached somewhat of a steady-state and the transient have slowed are the time-steps used by each comparable. This demonstrates that the dynamic phasor model does improve the efficiency of the simulation during transient periods but is fairly comparable to the conventional *qd0* model in efficiency during steady-state simulation.

Table 5.2 Model performance using variable time-step solver

Model	Simulation Time (s)	CPU Time (s)	Average Δt (ms)
<i>qd0</i> (saturated)	5	0.1760	3.9463
Dynamic Phasor (saturated)	5	0.1539	4.5914

Chapter 6: Conclusion

6.1 Summary of Contributions

The aim of this thesis was to extend the simulation functionality of the dynamic phasor model of doubly-fed induction machines by incorporating the effects of saturation of main flux linkage into the model. This was accomplished by extending the time-domain flux correction method into frequency domain dynamic phasor quantities and implementing them in the model using saturation data for a 500 hp induction machine and a look up table in Matlab/Simulink. The main contributions provided by this thesis are listed below.

- I. The theory and some key properties of dynamic phasors and frequency domain analysis are outlined and explained.
- II. Several conventional time-domain induction machine models are outlined and explained. The time-domain models being the 3-phase *abc* induction machine model, the two-axis *qd0* model and the complex space vector induction machine model.
- III. The dynamic phasor model of doubly-fed induction machines is derived from the complex space vector induction machine model and then verified by comparing it to the conventional *qd0* induction machine model.
- IV. An effective method for modeling the effects of saturation in the main flux linkage in terms of dynamic phasors is proposed; based on the flux correction method commonly used in time domain models of induction machines. The saturation model is also verified by comparing it to the convention time-domain flux correction method.

- V. The dynamic phasor induction machine model performance is then studied for both fixed time-step and variable time-step solution algorithms and found to be quite comparable and slightly better in performance than the convention $qd0$ time-domain induction machine model. The dynamic phasor model was found to be quite accurate and efficient for simulation of slow transient situations of mechanical load changes as well as fast transient situations such as machine start-up and balanced and unbalanced faults that occur in the system.

6.2 Future Research

The purpose of this thesis was to provide an initial starting point for research into modeling the effects of saturation in induction machines using the concept of dynamic phasors. There are many paths that can be investigated to further the research into dynamic phasor modeling of induction machines as well as modeling the effects of saturation using the dynamic phasor concept. The following list is definitely not exhaustive but provides a few topics that could be a good direction for further investigation and research in the area of AC machine modeling and saturation modeling using the dynamic phasor concept.

- I. In modeling of the main flux linkage saturation in an induction machine it was assumed that the rotor is round and that the air-gap between stator and rotor is uniform. By making this assumption it is reasonably assumed that the saturation in the machine affects the q - and d -axis components in the same manner, making it fairly straightforward to model. For machines that do not have a uniform air-gap such as salient pole synchronous machine this assumption cannot be made as the saturation

will affect the q - and d -axis differently [52]. There are many papers on the modeling of saturation in salient pole machines and this would provide a good area of research to extend the dynamic phasor saturation model to include the effects of saturation in salient pole machines.

- II. In this thesis, the method of flux correction is used to calculate the effects of saturation in the main magnetizing flux. This method requires first the calculation of the unsaturated main flux and then corrects it based on the saturation characteristics of the machine as outlined in Chapter 4. This formulation is implicit and introduces an algebraic loop which must be solved iteratively at every time-step and therefore adds computation costs to the simulation. By formulating the calculation of the effects of saturation in an explicit manner this algebraic loop can be avoided and make the model much more stable and efficient. One such method of explicit calculation of main flux linkage saturation is presented in [53]. This paper derives a simple algebraically exact formulation of main flux saturation for the general purpose qd induction machine model by introducing intermediate variables which provide an explicit relationship for the calculation of the main flux linkage. A similar process could be used to implement an explicit relationship for the calculation of main flux linkage saturation using the dynamic phasor concept. By doing this it would be possible to further extend the robustness and utility of the dynamic phasor induction machine model.

- III. In modeling of saturation of induction machines the effects of leakage flux saturation is generally ignored but can play an important part in the operation of induction machines, especially during transient operation [41]. The effects of leakage flux saturation are often ignored due to the fact that their saturation characteristics are very hard to determine experimentally and that data is often not available. Research in the area of leakage flux modeling using the concepts of dynamic phasors could be another rich area of research.
- IV. The dynamic phasor induction machine model that was presented in this thesis is based on the transformation of abc phase domain quantities to the stationary qd reference frame as it provides a much simpler starting point to base the dynamic phasor model off of. Despite the advantages of the reference frame transformation, when simulating the transformed qd induction machine model with an external an interface between the model and the external system is required as in many cases the external system is modeled in abc phase domain quantities. This interfacing can prove difficult and costly in many cases as a transformation back to abc phase domain quantities is required. Other difficulties can arise as well depending on which type of simulation tool you are using.

One method suggested for providing a direct interfacing induction machine model to external networks in simulation is the use of voltage-behind-reactance (VBR) induction machine model [54-57]. The VBR induction machine model presented in these papers has the stator of the induction machine modeled in abc direct-phase

coordinates as three-phase dependant *emf* sources behind an *RL* circuit, while the rotor is expressed in the *qd* coordinate reference frame. Modeling the machine in this manner provides a direct interface between the induction machine model and the external network. The VBR models could be extended to the dynamic phasor concept and would provide a good direction for research in extending the applications of dynamic phasors.

- V. Extending from further research IV, implementing the effects of magnetic saturation in the VBR models using the concept of dynamic phasors would be a good topic of research. Wang *et al.* [58] have presented a time domain model for the VBR induction machine which includes the effects of magnetic saturation. Modeling of magnetic saturation in the main magnetizing flux path is achieved using a piece-wise linear approach which is suitable for EMTP type simulations, and by applying saturation to the main magnetizing flux path the effects of cross saturation are taken into account. The method presented here could be extended with the dynamic phasor concept and could provide a much more versatile and accurate dynamic phasor induction machine model.

References

- [1] P. Kundur, J. Paserba, V. Ajjarapu, G. Andersson, A. Bose, C. Canizares, N. Hatziargyriou, D. Hill, A. Stankovic, C. Taylor, T. Van Cutsem and V. Vittal, "Definition and classification of power system stability IEEE/CIGRE joint task force on stability terms and definitions," *Power Systems, IEEE Transactions on*, vol. 19, pp. 1387-1401, 2004.
- [2] J. Yardley and G. Harris, "2nd Day of Power Failures Cripples Wide Swath of India," *New York Times*, July 31, 2012.
- [3] H. W. Dommel, *Electro-Magnetic Transients Program (EMTP) Theory Book*. Vancouver, BC: MicroTran Power System Analysis Corporation, 1996.
- [4] H. W. Dommel, "Digital Computer Solution of Electromagnetic Transients in Single- and Multiphase Networks," *Power Apparatus and Systems, IEEE Transactions on*, vol. PAS-88, pp. 388-399, 1969.
- [5] Manitoba HVDC Research Centre, *PSCAD User's Guide*. Winnipeg, Manitoba: Manitoba HVDC Research Centre, 2010.
- [6] Manitoba HVDC Research Centre Inc., *EMTDC User's Guide*. Winnipeg, Manitoba: Manitoba HVDC Research Centre Inc., 2005.
- [7] Canada/America EMTP Users Group, *ATP Rule Book*. Canada/America EMTP Users Group, 1998.
- [8] Microtran Power System Analysis Corporation, *MicroTran Reference Manual: Transient Analysis Program for Power and Power Electronic Circuits*. Vancouver, BC: Microtran Power System Analysis Corporation, 2002.

- [9] G. K. Morison, B. Gao and P. Kundur, "Voltage stability analysis using static and dynamic approaches," *Power Systems, IEEE Transactions on*, vol. 8, pp. 1159-1171, 1993.
- [10] B. Gao, G. K. Morison and P. Kundur, "Towards the development of a systematic approach for voltage stability assessment of large-scale power systems," *Power Systems, IEEE Transactions on*, vol. 11, pp. 1314-1324, 1996.
- [11] P. Löf, D. J. Hill, S. Arnborg and G. Andersson, "On the analysis of long-term voltage stability," *International Journal of Electrical Power & Energy Systems*, vol. 15, pp. 229-237, 8, 1993.
- [12] M. Stubbe, A. Bihain, J. Deuse and J. C. Baader, "STAG-a new unified software program for the study of the dynamic behaviour of electrical power systems," *Power Systems, IEEE Transactions on*, vol. 4, pp. 129-138, 1989.
- [13] V. Venkatasubramanian, "Tools for dynamic analysis of the general large power system using time-varying phasors," *International Journal of Electrical Power & Energy Systems*, vol. 16, pp. 365-376, 12, 1994.
- [14] V. Venkatasubramanian, H. Schattler and J. Zaborszky, "A time-delay differential-algebraic phasor formulation of the large power system dynamics," in *Circuits and Systems, 1994. ISCAS '94., 1994 IEEE International Symposium on*, 1994, pp. 49-52 vol.6.
- [15] V. Venkatasubramanian, H. Schattler and J. Zaborszky, "Fast time-varying phasor analysis in the balanced three-phase large electric power system," *Automatic Control, IEEE Transactions on*, vol. 40, pp. 1975-1982, 1995.

- [16] S. R. Sanders, J. M. Noworolski, X. Z. Liu and G. C. Verghese, "Generalized averaging method for power conversion circuits," in *Power Electronics Specialists Conference, 1990. PESC '90 Record., 21st Annual IEEE*, 1990, pp. 333-340.
- [17] H. Zhu, Z. Cai, H. Liu, Q. Qi and Y. Ni, "Hybrid-model transient stability simulation using dynamic phasors based HVDC system model," *Electr. Power Syst. Res.*, vol. 76, pp. 582-591, 4, 2006.
- [18] Wei Yao, Jinyu Wen, Shijie Cheng and Haibo He, "Modeling and simulation of VSC-HVDC with dynamic phasors," in *Electric Utility Deregulation and Restructuring and Power Technologies, 2008. DRPT 2008. Third International Conference on*, 2008, pp. 1416-1421.
- [19] Wang Gang, Li Zhikeng, Li Haifeng, Li Xiaolin and Fu Chuang, "Modeling of the HVDC convertor using dynamic phasor under asymmetric faults in the AC system," in *Sustainable Power Generation and Supply, 2009. SUPERGEN '09. International Conference on*, 2009, pp. 1-5.
- [20] E. Zhijun, D. Z. Fang, K. W. Chan and S. Q. Yuan, "Hybrid simulation of power systems with SVC dynamic phasor model," *International Journal of Electrical Power & Energy Systems*, vol. 31, pp. 175-180, 6, 2009.
- [21] P. C. Stefanov and A. M. Stankovic, "Modeling of UPFC operation under unbalanced conditions with dynamic phasors," *Power Systems, IEEE Transactions on*, vol. 17, pp. 395-403, 2002.
- [22] S. Henschel, "Analysis of Electromagnetic and Electromechanical Power System Transients with Dynamic Phasors," *Ph. D. Dissertation*, vol. University of British Columbia, Vancouver, BC, Canada, February, 1999.

- [23] P. Zhang, "Shifted Frequency Analysis for EMTF Simulation of Power System Dynamics," *Ph. D. Dissertation*, vol. University of British Columbia, Vancouver, BC, Canada, March, 2009.
- [24] A. M. Stankovic and T. Aydin, "Analysis of asymmetrical faults in power systems using dynamic phasors," *Power Systems, IEEE Transactions on*, vol. 15, pp. 1062-1068, 2000.
- [25] J. A. de la O Serna, "Dynamic phasor estimates for power system oscillations and transient detection," in *Power Engineering Society General Meeting, 2006. IEEE*, 2006, pp. 7 pp.
- [26] J. A. d. de la Serna, "Dynamic Phasor Estimates for Power System Oscillations," *Instrumentation and Measurement, IEEE Transactions on*, vol. 56, pp. 1648-1657, 2007.
- [27] A. T. Muoz and J. A. de la O Serna, "Shanks' Method for Dynamic Phasor Estimation," *Instrumentation and Measurement, IEEE Transactions on*, vol. 57, pp. 813-819, 2008.
- [28] M. A. Platas-Garza and J. A. de la O Serna, "Dynamic Phasor and Frequency Estimates Through Maximally Flat Differentiators," *Instrumentation and Measurement, IEEE Transactions on*, vol. 59, pp. 1803-1811, 2010.
- [29] Peng Zhang, J. R. Marti and H. W. Dommel, "Induction Machine Modeling Based on Shifted Frequency Analysis," *Power Systems, IEEE Transactions on*, vol. 24, pp. 157-164, 2009.
- [30] T. Demiray, "Simulation of Power System Dynamic Phasor Models," *Ph. D. Dissertation*, vol. Swiss Federal Institute of Technology, 2008.

- [31] A. M. Stankovic, S. Sanders and T. Aydin, "Dynamic Phasors in Modeling and Analysis of Unbalanced Polyphase Ac Machines," *Power Engineering Review, IEEE*, vol. 22, pp. 58-58, 2002.
- [32] P. Vas, "Generalized analysis of saturated AC machines," *Electrical Engineering (Archiv Fur Elektrotechnik)*, vol. 64, pp. 57, January, 1981.
- [33] J. E. Brown, K. P. Kovacs and P. Vas, "A Method of Including the Effects of Main Flux Path Saturation in the Generalized Equations of A.C. Machines," *Power Apparatus and Systems, IEEE Transactions on*, vol. PAS-102, pp. 96-103, 1983.
- [34] J. M. F. de Jesus, "A model for saturation in induction machines," *Energy Conversion, IEEE Transactions on*, vol. 3, pp. 682-688, 1988.
- [35] J. C. Moreira and T. A. Lipo, "Modeling of saturated AC machines including air gap flux harmonic components," *Industry Applications, IEEE Transactions on*, vol. 28, pp. 343-349, 1992.
- [36] E. Levi, "A unified approach to main flux saturation modelling in D-Q axis models of induction machines," *Energy Conversion, IEEE Transactions on*, vol. 10, pp. 455-461, 1995.
- [37] D. Bispo, L. Martins, Neto, J. T. de Resende and D. A. de Andrade, "A new strategy for induction machine modeling taking into account the magnetic saturation," *Industry Applications, IEEE Transactions on*, vol. 37, pp. 1710-1719, 2001.
- [38] Tang Ningping, Wu Hanguang and Qiu Peiji, "A saturation model of induction machine by space vector," *Electrical Machines and Systems, 2001. ICEMS 2001. Proceedings of the Fifth International Conference on*, vol. 1, pp. 85-88, 2001.

- [39] S. Nandi, "A detailed model of induction machines with saturation extendable for fault analysis," *Industry Applications, IEEE Transactions on*, vol. 40, pp. 1302-1309, 2004.
- [40] H. M. Jabr and N. C. Kar, "Effects of main and leakage flux saturation on the transient performances of doubly-fed wind driven induction generator," *Electr. Power Syst. Res.*, vol. 77, pp. 1019-1027, 6, 2007.
- [41] H. M. Jabr and N. C. Kar, "Leakage flux saturation effects on the transient performance of wound-rotor induction motors," *Electr. Power Syst. Res.*, vol. 78, pp. 1280-1289, 7, 2008.
- [42] S. Moulahoum, O. Touhami, R. Ibtouen and M. Fadel, "Induction machine modeling with saturation and series iron losses resistance," in *Electric Machines & Drives Conference, 2007. IEMDC '07. IEEE International*, 2007, pp. 1067-1072.
- [43] L. Lupsa-Tataru, "A Flux-Based Expression of Induction Machine Magnetizing Inductance," *Energy Conversion, IEEE Transactions on*, vol. 25, pp. 268-270, March, 2010.
- [44] J. Arrillaga and N. R. Watson, "Power System Harmonics (2nd Edition)," 2003.
- [45] S. R. Sanders, J. M. Noworolski, X. Z. Liu and G. C. Verghese, "Generalized averaging method for power conversion circuits," in *Power Electronics Specialists Conference, 1990. PESC '90 Record., 21st Annual IEEE*, 1990, pp. 333-340.
- [46] P. Kundur, N. J. Balu and M. G. Lauby, *Power System Stability and Control*. New York: McGraw-Hill, 1994.
- [47] D. W. Novotny and T. A. Lipo, *Vector Control and Dynamics of AC Drives*. New York: Oxford University Press Inc., 1996.

- [48] J. M. Aller, A. Bueno and T. Paga, "Power system analysis using space-vector transformation," *Power Systems, IEEE Transactions on*, vol. 17, pp. 957-965, 2002.
- [49] P. C. Krause, O. Wasynczuk and S. D. Sudhoff, *Analysis of Electric Machinery and Drive Systems*. New Jersey: John Wiley & Sons, Inc., 2002.
- [50] C. Ong, *Dynamic Simulation of Electric Machinery using MATLAB / SIMLINK*. New Jersey, USA: Prentice-Hall, Inc, 1998.
- [51] The MathWorks, "Simulink Product Documentation," 2012, .
- [52] E. Levi and V. A. Levi, "Impact of dynamic cross-saturation on accuracy of saturated synchronous machine models," *Energy Conversion, IEEE Transactions on*, vol. 15, pp. 224-230, 2000.
- [53] F. Therrien, L. Wang, J. Jatskevich and O. Wasynczuk, "Efficient Explicit Representation of AC Machines Main Flux Saturation in State-Variable-Based Transient Simulation Packages," *Submitted to Energy Conversion, IEEE Trans on*, August, 2012.
- [54] Liwei Wang, J. Jatskevich and S. D. Pekarek, "Modeling of Induction Machines Using a Voltage-Behind-Reactance Formulation," *Energy Conversion, IEEE Transactions on*, vol. 23, pp. 382-392, 2008.
- [55] Liwei Wang, J. Jatskevich and S. C. Foroosh, "A VBR induction machine model implementation for SimPowerSystem toolbox in matlab-simulink," in *Power and Energy Society General Meeting - Conversion and Delivery of Electrical Energy in the 21st Century, 2008 IEEE*, 2008, pp. 1-6.

- [56] M. Chapariha, Liwei Wang, J. Jatskevich, H. W. Dommel and S. D. Pekarek, "Constant-Parameter -Branch Equivalent Circuit for Interfacing AC Machine Models in State-Variable-Based Simulation Packages," *Energy Conversion, IEEE Transactions on*, vol. 27, pp. 634-645, 2012.
- [57] Liwei Wang and J. Jatskevich, "Approximate Voltage-Behind-Reactance Induction Machine Model for Efficient Interface With EMTP Network Solution," *Power Systems, IEEE Transactions on*, vol. 25, pp. 1016-1031, 2010.
- [58] Liwei Wang and J. Jatskevich, "Including Magnetic Saturation in Voltage-Behind-Reactance Induction Machine Model for EMTP-Type Solution," *Power Systems, IEEE Transactions on*, vol. 25, pp. 975-987, 2010.
- [59] J. Jatskevich, "EECE 549 Assignment Material," 2010.

Appendices

Appendix A - 500 HP Induction Machine Parameters

Table A.1 500hp induction machine parameters [49]

Rating: 500 HP		
Line-to-Line Voltage: 23 kV		
Poles: 4		
Rated Speed: 1773 rpm		
Rated Torque: 1980 N · m		
Inertia of rotor: $J = 11.06 \text{ kg} \cdot \text{m}^2$,		
Machine circuit parameters:		
$L_M = 0.143 \text{ H}$		
$r_s = 0.262 \Omega$		$r_r' = 0.187 \Omega$
$L_s = 3.199 \text{ mH}$		$L_r' = 3.199 \text{ mH}$

Appendix B - Saturation Data of 500 HP Induction Machine

Table B.1 Saturation data for 500hp induction machine [59]

λ_m (Wb)	i_m (A)	λ_m (Wb)	i_m (A)	λ_m (Wb)	i_m (A)	λ_m (Wb)	i_m (A)
-5.99537	-630.7	-5.62692	-254.3	5.377846	122.1	5.866186	498.5
-5.98555	-620.6	-5.61711	-244.2	5.411003	132.2	5.876	508.6
-5.97574	-610.4	-5.60703	-234	5.444425	142.4	5.885815	518.8
-5.96539	-600.2	-5.59695	-223.8	5.477583	152.6	5.89563	529
-5.95558	-590	-5.58713	-213.6	5.497477	162.8	5.905975	539.2
-5.94576	-579.9	-5.57732	-203.5	5.524268	172.9	5.915789	549.3
-5.93595	-569.7	-5.56406	-193.3	5.543897	183.1	5.925604	559.5
-5.9256	-559.5	-5.5439	-183.1	5.564057	193.3	5.935949	569.7
-5.91579	-549.3	-5.52427	-172.9	5.57732	203.5	5.945763	579.9
-5.90597	-539.2	-5.49748	-162.8	5.587134	213.6	5.955578	590
-5.89563	-529	-5.47758	-152.6	5.596949	223.8	5.965393	600.2
-5.88582	-518.8	-5.44443	-142.4	5.607029	234	5.975738	610.4
-5.876	-508.6	-5.411	-132.2	5.617108	244.2	5.985552	620.6
-5.86619	-498.5	-5.37785	-122.1	5.626923	254.3	5.995367	630.7
-5.85584	-488.3	-5.34495	-111.9	5.636738	264.5		
-5.84603	-478.1	-5.3118	-101.7	5.647083	274.7		
-5.83621	-468	-5.27837	-91.6	5.656897	284.8		
-5.82613	-457.8	-5.14548	-81.4	5.666712	295		
-5.81605	-447.6	-5.01258	-71.2	5.676792	305.2		
-5.80624	-437.4	-4.8468	-61	5.686871	315.4		
-5.79642	-427.3	-4.58128	-50.9	5.696686	325.5		
-5.78634	-417.1	-4.31549	-40.7	5.7065	335.7		
-5.77626	-406.9	-3.78444	-30.5	5.71658	345.9		
-5.76645	-396.7	-2.98256	-20.3	5.72666	356.1		
-5.75663	-386.6	-1.49128	-10.2	5.736475	366.2		
-5.74629	-376.4	0	0	5.746289	376.4		
-5.73647	-366.2	1.491282	10.2	5.756634	386.6		
-5.72666	-356.1	2.982564	20.3	5.766449	396.7		
-5.71658	-345.9	3.784439	30.5	5.776263	406.9		
-5.7065	-335.7	4.315486	40.7	5.786343	417.1		
-5.69669	-325.5	4.581275	50.9	5.796423	427.3		
-5.68687	-315.4	4.846799	61	5.806238	437.4		
-5.67679	-305.2	5.012585	71.2	5.816052	447.6		
-5.66671	-295	5.145479	81.4	5.826132	457.8		
-5.6569	-284.8	5.278374	91.6	5.836212	468		
-5.64708	-274.7	5.311796	101.7	5.846026	478.1		
-5.63674	-264.5	5.344954	111.9	5.855841	488.3		